LA-UR-98-5355

NUCLEAR FUELS TECHNOLOGIES

FISCAL YEAR 1998 RESEARCH AND DEVELOPMENT

SUMMARY OF TEST RESULTS

Kenneth Chidester
Project Leader, Nuclear Fuels Research and Development

D. P. Butt, P. Chodak, S. F. Demuth, S.L. Eaton, R. J. Hanrahan, G. J. Havrilla, C. L. Haertling, C. A. James, D. G. Kolman, A. D. Neuman, Y. Park, C. A. Smith, M. Stan, S. A. Talachy, J. G. Teague, H. R. Trellue, and C. J. Worley

Los Alamos National Laboratory

November 30, 1998

LA-UR-98-5355

NUCLEAR FUELS TECHNOLOGIES

FISCAL YEAR 1998 RESEARCH AND DEVELOPMENT

SUMMARY OF TEST RESULTS

Los Alamos National Laboratory

_____ Kenneth Chidester, Project Leader, Nuclear Fuels Research and Development	Date:
_____ David Alberstein, Project Leader, Nuclear Fuels Technologies	Date:

CONTENTS

TABLES

FIGURES

LA-UR-98-5355

NUCLEAR FUELS TECHNOLOGIES
FISCAL YEAR 1998 RESEARCH AND DEVELOPMENT
SUMMARY OF TEST RESULTS

ABSTRACT

In FY98, many research and development activities occurred at Los Alamos National Laboratory in support of the Department of Energy Office of Fissile Materials Disposition (DOE-MD) program for the irradiation of excess weapons-grade plutonium as MOX fuel (i.e., reactor-based disposition). The primary purpose of these activities was to conduct studies involving feed qualification, as well as supporting fuel fabrication and analytical methods development. The research focused on four main areas of research: feed qualification/supply, fuel fabrication development, analytical methods development, and the gallium removal system.

The purpose of feed qualification/supply was to define and develop the processes, equipment, and specifications for producing the UO_2 and PuO_2 feeds needed to qualify MOX fuel. The fuel fabrication and development activities included identifying and possibly resolving technical issues associated with applying the large experience base obtained by making MOX fuel with recycle reactor-grade plutonium to the fabrication of MOX with surplus weapons plutonium. The analytical methods tasks were designed to continue the development of analytical techniques in conjunction with the fabrication of MOX fuel. Finally, the purpose of the gallium removal system activities was to study ways to remove and the effects of gallium in preparing weapons-grade plutonium for use in MOX fuel.

This report summarizes the progress made in FY98 in each of these areas of research.

1.0. INTRODUCTION

This document summarizes the results of the research and development (R&D) activities that were conducted during Fiscal Year (FY) 1998 (98) by the Nuclear Fuels Technologies project team at Los Alamos National Laboratory (LANL) for the Department of Energy (DOE) Office of Fissile Materials Disposition (MD). This work is a continuation and extension of experimental activities conducted in support of the disposition program and focuses on the use of surplus weapons plutonium in the fabrication of mixed oxide (MOX) nuclear fuel for reactor-based disposition. This work provides information leading toward the resolution of technical issues associated with the use of surplus-weapons plutonium in the fabrication and use of MOX fuel in commercial light-water reactors (LWRs). Not only do the activities described in this plan directly support plutonium oxide (PuO_2) preparation and analytical improvements, as well as other ongoing Nuclear Fuels Technologies efforts, but the

results are expected to support the procurement process for MOX fuel fabrication and irradiation services. In addition, these results will be significant to the selected commercial fuel fabricator by providing a technical basis on which to build, thereby reducing the amount of development time and effort required for implementation of the MOX disposition mission.

Although fabrication of MOX fuel using reactor-grade plutonium is a well-developed, industrialized process, several differences between reactor-grade and surplus weapons plutonium generate technical issues that must be resolved. These differences include (1) variations in powder characteristics because the weapons material may be converted using a dry pyrochemical process as opposed to a chemical dissolution and precipitation process, which is used in spent-fuel reprocessing facilities; (2) the presence of gallium in the weapons material; and (3) the variation in plutonium isotopics between the reactor-grade and surplus weapons material. All of the experiments outlined in this report address one or more of these issues, and Table 1-1 summarizes which issues each task addresses.

The R&D activities performed during FY98 were divided into four major areas: (1) feed qualification/supply, (2) fuel fabrication development, (3) analytical methods development, and (4) gallium removal. These four areas are discussed briefly below. The proposed work for FY98 was described in Ref. 1-1, and results from each section appear in this document.

The feed qualification and supply activity (Section 2.0) covered several issues associated with the identification, acquisition, and characterization of both plutonium dioxide (PuO_2) and uranium dioxide (UO_2) feed materials. This included the creation and utilization of a feed characterization database, the acquisition of required feed materials, publication of a draft PuO_2 feed specification, interactions with pit disassembly and conversion activities, and evaluations of PuO_2 aqueous polishing.

The fuel fabrication development activity (Section 3.0) focused on the baseline development work necessary to use a new UO_2 feed material. This included establishing process parameter ranges for powder preparation, pressing, and sintering to fabricate high-density cylindrical pellets. The process parameter ranges then were used to develop baseline parameters for the fabrication of MOX fuel pellets. In addition, fabrication studies were performed with alternate sources of PuO_2 to study their effects on processing and final pellet characteristics. The effects of gallium on the sintering process also were studied, and phase diagram evaluation activities were continued from FY97.

The analytical methods development activity (Section 4.0) involved upgrading and improving several analytical measurement techniques needed to support other R&D and test fuel fabrication tasks and provided valuable information for the selected commercial fuel fabricator. The methods studied include MXRF to measure the spatial distribution and concentration of gallium and a laser-induced breakdown spectroscopy (LIBS) system to measure gallium on-line during processing. A small effort also was

TABLE 1-1. RELATIONSHIP BETWEEN PROPOSED TASKS AND TECHNICAL ISSUES

Applicable Section	Task	Difference in PuO_2 Characteristics	Presence of Ga[a]	Isotopic Differences
2.1	Feed Characterization Database	X	X	X
2.2	Feed Acquisition	X	X	
2.3	PuO_2 Feed Specification	X	X	X
2.4	Plutonium Stockpile and Oxide Sampling / Character-ization	X	X	X
2.5	MOX Fuel Aqueous Polishing Flowsheet	X	X	X
3.1	Feed Materials Baseline Development	X		
3.2	Ga Sintering Study		X	
4.1	MXRF[b] Development		X	
4.2	O / M[c] Measurement Technique Evaluation	X		
4.3	LIBS Capability / On-Line Ga Measurement		X	
4.4	Autoradiography Development			X
5.1	Chemistry / Physical Characteristics		X	
5.2	On-Line Ga Measurement		X	
5.3	Ga Removal Process Development		X	
5.4	Ga Removal Prototype Design and Testing		X	
5.5	Cold Prototype Testing		X	

[a]Ga=gallium.
[b]MXRF=micro x-ray fluorescence.
[c]O / M=oxygen to metal.

applied to studying alternate O/M ratio measurement techniques, with the goal of improving efficiency and accuracy.

Finally, the gallium removal system activity (Section 5.0) included the tasks planned for the first year of a 2.5-year effort to develop and integrate a gallium removal system into the Pit Disassembly and Conversion Facility (PDCF) design and the Phase II Advanced Recovery and Integrated Extraction System (ARIES) demonstration line. The primary activities for FY98 included developing a process to establish the gallium removal system design requirements, performing materials compatibility tests, and studying surrogate (CeO_2) fuel in the "cold" laboratory.

2.0. FEED QUALIFICATION/SUPPLY

The intent of this activity was to define and develop the processes, equipment, and specifications for producing the PuO_2 and UO_2 feed material needed to fabricate and qualify MOX fuel. These efforts ultimately are intended to support the award of a contract for private industry to perform the plutonium disposition mission. When this contract is awarded, the information produced here (on the characteristics of the feed materials and how these characteristics affect MOX fuel fabrication) will be used by the selected fabricator. Programmatically, this information was also desirable in understanding the potential classification issues associated with surplus weapons PuO_2 (WPu) feed, if future experimental results indicate this to be a problem. This activity is performed in close conjunction with pit disassembly and conversion activities currently in progress. The main tasks associated with this activity include a weapons-grade plutonium MOX feed database architecture, feed acquisition, PuO_2 feed draft specification, plutonium stockpile and oxide sampling and characterization, and MOX fuel aqueous polishing.

As well as supporting the procurement process, each of these tasks also supported several other R&D and MD programmatic tasks in FY98, including both fuel fabrication and thermally induced gallium removal (TIGR) R&D (see Sections 3.0 and 5.0, respectively), and test fuel fabrication for irradiation in the Advanced Test Reactor (ATR) at Idaho National Engineering and Environmental Laboratory (INEEL). In addition to the specific tasks listed above, this activity included overall interactions between the Nuclear Fuels Technologies and Pit Disassembly and Conversion projects, as well as participation in material declassification and inventory assessment and management activities as necessary. The results of these efforts are not discussed explicitly in the following sections. However, it should be noted that a material declassification action was submitted in September to the Office of Declassification for approval.

2.1. Weapons-Grade Plutonium MOX Feed Database Architecture

The differences between typical commercial (reactor-grade) PuO_2 (RPu) and WPu are significant enough to warrant development of a WPu–MOX-specific PuO_2 feed database (Ref. 2-1). This database supplements the existing commercial RPu MOX feed database to ensure that the WPu MOX is suitable for LWR use. In addition to building a licensing basis, the database also serves as an R&D tool. Central collection of R&D data facilitates the correlation of results and identification of additional data requirements, thereby helping to guide the direction of ongoing R&D studies.

2.1.1. Database Overview

The WPu MOX database provides a means of tracking WPu from its weapons source through processing (see Fig. 2-1) to post irradiation examination (PIE) of the MOX fuel. The specific process parameters used for each process and the sample data generated from each material product form are stored electronically in a Microsoft Excel database to enable material properties and process parameters to be correlated with fuel characteristics and performance. Material at any point in the fabrication process is clearly traceable to its weapon source and, for blended materials, its UO_2 source.

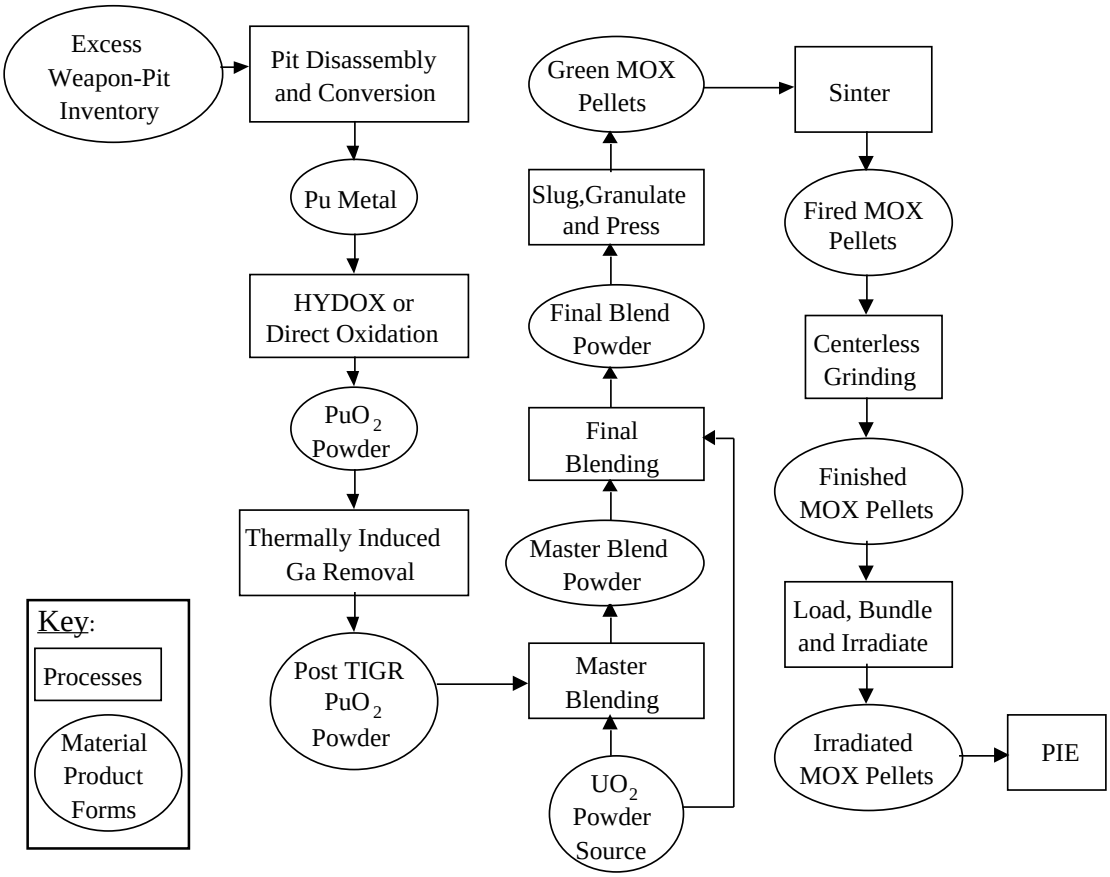

Fig. 2-1. Sample MOX fabrication R&D process diagram.

This traceability requires developing a record for each unique batch of fuel. A unique batch of fuel uses all plutonium from the same weapons source, uses the same UO_2 source, and uses material that has all undergone identical processing. A single record contains all data associated with the characterization and processing of a unique batch of fuel. The process of creating one record often involves the development of several different records from a single plutonium metal source. For example, a single record for PuO_2 powder produced from the same weapons source and undergoing the same metal-to-powder conversion process is split into two or more different records if the subsequent PuO_2–Ga removal processing parameters vary for different portions of the original batch. For this example, the different records are identical up to the step of gallium removal. It is understood that records are filled in as the data are collected. In addition, some powder used in R&D fabrication efforts may not be processed completely to produce fuel pellets, and not all fuel fabricated is irradiated or undergoes PIE. Thus, some records are incomplete but await further processing data, and some are never completed.

2.1.2. Method

The data associated with each of the numerous processing steps depicted in Fig. 2-1 will be generated by several organizations. Consequently, correlating the results at any point in the overall process with any individual or combined processing steps necessitates compiling a single record containing all data associated with each unique batch of fuel. Thus, copies of all data generated should be provided to those responsible for maintaining the database. It is envisioned that as the R&D effort develops, data analysis and reporting requirements will become better defined. Once centrally collected and electronically stored, the format of the data record now can be changed readily to meet these developing needs.

The first page excerpted from an individual data record is shown in Fig. 2-2. Column 1 lists specific attributes associated with the data to the right. Specific analysis methods are identified in Column 2 as appropriate. Columns 3 through 6 then list the WPu MOX specification for each attribute. This specification, including a definition of the analytical techniques associated with each value, is currently under development (see Section 2.3). The rest of the columns to the right contain unique batch-specific data. Each column represents data from a specific step in the process. The PuO_2, post-TIGR PuO_2, and UO_2 refer to powder products. Changes in properties caused by each processing step are viewed by moving horizontally in a row. All of the material characteristics present after an individual processing step are seen by moving vertically in a column. The record identification (ID) number at the top of each batch-specific data column identifies each batch uniquely. A separate master database document also is kept that correlates an individual analysis sample and weapon ID numbers with the record ID number. The comments, process, and description rows contain pertinent, amplifying information as necessary. Not all specifications are applicable to each product form. For instance, green density is specific to pellets; thus, no value for this characteristic is found in the PuO_2 column. Consequently, not all data slots are filled in, even for a complete record.

After the architecture was developed, an appropriate naming scheme was derived such that every filename indicates detailed information about what processing steps the associated material underwent. Then information about specific powders and fuel was entered into the main database. In FY98, this included the Cameco UO_2 powder, two-step PuO_2 powder from LANL, and various data obtained throughout the process of combining these two powders into MOX fuel pellets for the Parallex project.* More data involving other materials currently are being entered, including ammonium uranyl carbonate (AUC)-derived UO_2, three-step Lawrence Livermore National Laboratory (LLNL) PuO_2 powder, and MOX fuel developed for the Advanced Test Reactor (ATR) average power test.* Additional data will be entered as they are received.

---

* The Parallex project (Parallel Experiment) was performed for the DOE-MD program with the intent of placing MOX fuel fabricated from weapons-grade plutonium here in the United States (US) and in Russia in the Atomic Energy of Canada, Ltd. (AECL)-owned test Canadian deuterium-uranium (CANDU) reactors. Although the logistics of the Parallex program still are being negotiated with Russia and Canada, many MOX pellets were produced by LANL for this program.

* After the Parallex project was started for the joint disposition of Russian and US plutonium, efforts also were begun in the US to perform sample MOX fuel irradiations in an LWR. The ATR project involves the fabrication of MOX fuel from weapons-grade plutonium at LANL and irradiation of the fuel in the ATR at INEEL.

Classified /	Specification				Record Identification Number:						
Unclassified	Analysis Method	PuO_2	UO_2	MOX Pellet	Metal	PuO_2	Post-TIGRPuO$_2$	UO_2	Master Blend	MOX Pellet	Post Irrad
Reference(s)											
Weapon #											
Comments/											
Process											
Description						Time:	Time:				
						Temp:	Temp:				
U Assay - Powder	Davies-Gray										
&Pellet	Titration										
Pu Assay - Powder	Coulometry										
Pellet	IDMS										
O / M	Modified										
	Lyon'sMethod										
Loss On Ignition	Thermal										
	Treatment										
Green Density	Geometric										
	Calculations										
Immersion Density	Archimedes										
	Method										
Particle Size	LAB-TEC										
Distribution	LAB-TEC										
Surface Area	BET Surface										
	Area Analyzer										
Moisture Content											
Sieve											
Sinterability											
Fission Product											
Activity											

Fig. 2-2. First page of a sample data record.

2.2. Feed Acquisition

This task covered all efforts associated with the acquisition of PuO_2 and UO_2 feed materials for planned research, development, and testing activities. The existing sources of material were integrated with the schedules and requirements for other planned R&D and test fuel fabrication tasks to determine additional feed material needs.

In FY97, the MD Program selected a single UO_2 source for use in fuel fabrication R&D activities. Accordingly, in early March, ~115 kg of depleted, AUC-derived UO_2 powder was obtained from ABB-Sweden. In mid-March, after measurements were verified and the required materials control and accountability activities were completed, the powder was split into smaller lots and transferred to the Plutonium Facility (PF-4). By March 23, AUC powder lots had been released for fuel-fabrication-process development activities. However, this powder was not made available for surrogate testing until July. Just

under 1 kg of AUC-derived UO_2 was used in baseline development experiments (see Section 3.1). Four kilograms of AUC UO_2 was used for gallium removal studies and ATR fuel fabrication. At the end of FY98, ~110 kg of AUC UO_2 remained.

Additionally, sources of PuO_2 powder were needed for fuel fabrication and TIGR R&D activities, as well as for ATR test fuel fabrication. Potential sources of material included PuO_2 powder created at LLNL by the three-step (hydride-nitride-oxidation) method, PuO_2 directly oxidized from metal ingots on hand, and PuO_2 powder aqueously processed. In February, PuO_2 supplies required for ATR test fuel fabrication in FY98 and for TIGR R&D were identified. Five hundred grams of LLNL three-step PuO_2 was used for TIGR R&D. Another 30 g of PuO_2 (10 g LLNL three-step PuO_2, 10 g of LLNL two-step PuO_2, and 10 g of aqueous PuO_2) were used in the alternative PuO_2 fabrication experiments (see Section 3.2). An additional 350 g of LLNL three-step PuO_2 was used for ATR fuel fabrication. The remaining PuO_2 holdings at the end of FY98, including the aqueously processed batches, are shown in Table 2-1.

TABLE 2-1. LANL PuO_2 INVENTORY AS OF OCTOBER 1, 1998*

PuO_2 Source Process	Quantity (g)	Commitment	Chemistry	Morphology
LLNL Two-Step	900	None	LLNL Data	None
LLNL Three-Step	360	ATR Hi Power	Complete	Complete
LLNL Three-Step TIGR'd	293	TIGR R&D [a]	Complete	Complete
LLNL Three-Step UnTIGR'd	287	TIGR R&D	Complete	Complete
LANL IX [b,c]	592	None	Complete	None
LANL IX - Exhaustive Wash [d]	1000	ATR	F,Cl, Fe, C	None
LANL IX	2000	TBD	None	None
LANL SX [e]	1000	TBD	None	None
LANL DMO [f]	2000	None	None	None

*With the exception of the LLNL two-step material, chemistry samples have been taken and results are pending. Also, LANL MD holds sufficient PuO_2 to meet all current R&D and fuel fabrication requirements.

a. 100 g of TIGR'd material is set aside in reserve for the ATR high-power test.

b. IX = Ion exchange.

c. This was 94-1 material, was processed only to test gallium removal potential, and is high in fluorine, chlorine, boron, and silicon.

d. 1000 g of the IX material was put through exhaustive washing to minimize the potential for trace impurities.

e. SX = Solvent extraction.

f. DMO = direct metal oxidation.

g. DMO material is produced under conditions more likely to be prototypic of a potential final ARIES design. Significant quantities of DMO material will be produced in FY99 as part of the ARIES demonstration.

2.3. PuO_2 Feed Draft Specification

The main interface between pit disassembly and conversion and MOX fuel fabrication efforts for the MD program is through the PuO_2 feed specification. This specification details the physical characteristics of the material, including the maximum acceptable impurity levels, and serves as a major negotiating point between the government (the DOE) and the selected fuel fabricator. The government will agree to a specification to represent its commitment of what the PDCF product will look like. The selected vendor will agree to the specification knowing that feed material meeting the specification should fabricate acceptable MOX fuel. As such, a draft specification is needed by both sides as a starting point for negotiations. This task was intended to produce such a draft, using all available resources of feed material characterization to determine individual limits and included historical data, finger ingot analyses, and data as they were received from ongoing activities. A separate report was to be published detailing this draft specification.

The project plan originally directed development of a MD PuO_2 feed specification by June 15, 1998. By direction, this task was accelerated to support release of the procurement activity request for proposals (RFP) in February 1998 (Ref. 2-2). The results of the ensuing efforts to arrive at a PuO_2 specification were presented to the DOE in a meeting on January 14, 1998. At this meeting it was agreed that because chemical characterization of the plutonium metal to be converted to PuO_2 feed is substantially incomplete, it was not yet practical to define a specification. Instead, the projected worst-case PuO_2 feed characteristics were to be included in the RFP as presented at the January 14 meeting, with the exception of increasing the lead to 200 ppm; however, the results were not published as a separate report. Table 2-2 lists potential powder characteristics, and Table 2-3 presents maximum impurity values in parts per million.

2.4. Plutonium Stockpile and Oxide Sampling and Characterization

Plutonium feedstock characterization is required to identify any potential impurity problems and to ensure that ARIES processing ultimately delivers PuO_2 feed suitable for MOX fabrication. In FY98, a plutonium feed sampling plan was issued, sampling activities were begun, and an initial characterization report was issued.

TABLE 2-2. POTENTIAL PuO_2 POWDER CHARACTERISTICS

PuO_2 Powder Characteristic	Potential Value
Lot Size (kg)	To be determined
Plutonium Content (wt %) {(Pu/PuO_2) X 100)}	86–88.2
^{240}Pu min. wt % (fabrication criticality)	Reported
^{241}Am (wt % with respect to Pu)	<0.5
Surface Area (m^2/g)	Reported
Particle Size (μm)	1. >95% <44 2. 99–100% <100

TABLE 2-3. MAXIMUM POTENTIAL IMPURITY LEVELS

Impurity	Level (μg/g Pu)	Impurity	Level (μg/g Pu)
Ag	100	**Mn**	100
Al	150	**Mo**	100
B	10	**N**	300
Be	100	**Na**	300
Bi	100	**Nb**	100
C	500	**Ni**	200
Ca	500	**P**	100
Cd	10	**Pb**	200
Cl	(+Fl < 250)	**S**	250
Co	100	**Si**	200
Cr	100	**Sm**	2
Cu	100	**Sn**	100
Dy	1.0	**Ti**	100
Eu	1.0	**Th**	100
F	(+Cl < 250)	**U**	5000
Fe	500	**V**	300
Ga	200	**W**	200
Gd	3	**Zn**	100
In	20	**Zr**	50
K	100	**Boron Equivalent**	10
Li	100	**Total Impurities**	5300
Mg	500		

2.4.1. FY98 Sampling Plan for Metal and Oxide

A sample plan was drafted in May 1998 to characterize plutonium feedstock impurities systematically. The characterization plan called for collecting samples from the ARIES demonstration feed material. The sampling plan was to be completed in FY98; however, delays in the start of the ARIES demonstration program resulted in the bulk of the sampling plan being carried out in FY99. A summary of the plan follows.

2.4.1.1. Objective

The intent of the plan is to ensure that a sufficient amount of plutonium from pits is sampled to establish a statistically significant database of impurities levels found in metal from weapons and to verify the accuracy of the data found in the ingot databases. This database will increase the confidence level associated with the impurity levels likely to be found in PuO_2 from weapons. This information also is needed for

negotiations with the perspective vendors for MOX fuel fabrication and for PDCF Title I design activities. However, it should be stressed that the scope of the FY98 plan covered only 7 of the approximately 40 pit types. To increase the confidence level, sampling must continue for several years and/or until all pit types bound for disposition have been sampled. A more detailed description of the sampling activities is given below.

2.4.1.2. Sampling

Sampling will occur three times during the proposed PDCF process: (1) after bisection, (2) after hydride/dehydride (H/D), and (3) after conversion to oxide. First, a sample of metal will be collected from each hemishell after pit bisection. This sample must be removed from the hemishell either by cutting or punching. Options for sample acquisition have been and are being investigated. Techniques for acquiring samples from most pit types have been developed and tested in the cold (non-plutonium) laboratory. Second, a sample of metal will be collected from each button after the H/D process. This sample will be removed from the button using established technology at LANL. Finally, a sample will be taken from the oxide produced from each hemishell. Table 2-4 outlines the numbers of samples from each activity and phase of ARIES. Approximately 10 g of material will be taken each time, and in the case of pits, a sample will be taken from each hemishell.

2.4.1.3. Archives

To conserve resources without sacrificing needed data, some of the metal samples will be archived pending results from the oxide samples. This will involve fabrication of containers for storage of 5 to 10 samples in a controlled atmosphere, placement of samples in these containers, and placement of those containers in storage. If the oxide samples contain unexpected impurities, the metal samples will be analyzed to determine if the impurities came from the pits or the processing. Table 2-4 outlines the number of samples that may be archived.

2.4.1.4. Analysis

All oxide samples will be analyzed. In addition, all of the metal samples taken from the pits or H/D before the demonstration will be analyzed. This analysis will utilize several standard techniques, including inductively coupled plasma mass spectrometry (ICP-MS) or inductively coupled argon plasma atomic emission spectrometry (ICP-AES) for determining metal impurities, ion chromatography for determining halide and nitrogen levels, and analyses for determining carbon and hydrogen. Table 2-5 lists the elements for which concentrations will be determined, the lower limit capable of being detected, and the associated certainty. In addition, particle morphology (particle size, shape, and surface area) of a sample from each oxidation methodology and each set of operating parameters will be examined. The particle size will be determined by sieving, the shape by scanning electron microscopy (SEM), and the surface area by the Brunauer, Emmett, and Teller (BET) technique. Table 2-4 outlines the number of samples that may be analyzed. Not all of each sample will be sent for analysis; a portion of the sample will be archived pending receipt of the analytical results.

2.4.2. Plutonium Feed Initial Characterization Report

The bulk of the characterization work will be completed in FY99; however, an initial characterization report was delivered in September 1998 (Ref. 2-2), with a more substantial report due in FY99.

During the ARIES demonstration, several pit types intended to be representative of the disposition inventory will be processed. Consequently, the plutonium metal characterization plan calls for collecting samples from the ARIES demonstration feed material. Delays in the start of the ARIES demonstration program resulted in the bulk of the sampling plan being deferred to FY99.

TABLE 2-4. ARCHIVAL SAMPLE INVENTORY

Activity/Stage	# Sampled	# Archived	# Analyzed
FY97 R&D activities (LLNL)			
14 oxide samples from oxidation (7 dwarfs)	**14**		**14**
5 metal samples bound for oxidation (7 dwarfs)	**5**		**5**
FY98 R&D (LLNL)			
26 metal samples bound for oxidation	**26**		**26**
26 oxide samples from oxidation	**26**		**26**
Pre-demo (startup) activities (LANL)			
28 metal samples bound for oxidation or H/D	**28**		**28**
5 metal samples from H/D	**5**		**5**
20 oxide samples from oxidation	**20**		**20**
Demonstration (LANL)			
80 metal samples bound for oxidation or H/D	**80**	**80**	
35 oxide samples from hydride oxidation (HYDOX)	**35**		**35**
13 metal samples from H/D bound for oxidation	**13**	**13**	
22 metal samples from H/D	**22**	**22**	
Totals	274	115	159

TABLE 2-5. TRACE ELEMENT LIST

Element Abbr.	Element Name	Level Required	Technique
Ag	Silver	10 ppm (±1)	ICP-MS
Al	Aluminum	100 ppm (±10)	ICP-AES
Am	Americium	100 ppm (±10)	ICP-MS
Au	Gold	100 ppm (±10)	ICP-MS
B	Boron	1 ppm (±0.1)	ICP-MS
Be	Beryllium	1 ppm (±0.1)	ICP-MS
Bi	Bismuth	10 ppm (±1)	ICP-MS
C	Carbon	100 ppm (±10)	LECO
Ca	Calcium	100 ppm (±10)	ICP-AES
Cd	Cadmium	1 ppm (±0.1)	ICP-MS
Cl	Chlorine	10 ppm (±1)	IC
Co	Cobalt	10 ppm (±1)	ICP-MS
Cr	Chromium	100 ppm (±10)	ICP-MS
Cu	Copper	100 ppm (±10)	ICP-MS
Dy	Dysprosium	0.5 ppm (±0.1)	ICP-MS
Eu	Europium	0.5 ppm (±0.1)	ICP-MS
F	Fluorine	10 ppm (±1)	IC
Fe	Iron	100 ppm (±10)	ICP-AES
Ga	Gallium	1 ppm (±0.1)	ICP-MS
Gd	Gadolinium	0.5 ppm (±0.1)	ICP-MS
H	Hydrogen	1 ppm (±0.5)	LECO
Hf	Hafnium	10 ppm (±1)	ICP-MS
In	Indium	10 ppm (±1)	ICP-MS
K	Potassium	10 ppm (±1)	ICP-AES
Li	Lithium	10 ppm (±1)	ICP-MS
Mg	Magnesium	10 ppm (±1)	ICP-MS
Mn	Manganese	10 ppm (±1)	ICP-MS
Mo	Molybdenum	10 ppm (±1)	ICP-MS
N	Nitrogen	100 ppm (±10)	IC
Na	Sodium	10 ppm (±1)	ICP-AES
Nb	Niobium	10 ppm (±1)	ICP-MS
Ni	Nickel	100 ppm (±10)	ICP-MS
P	Phosphorus	10 ppm (±1)	ICP-AES
Pb	Lead	10 ppm (±1)	ICP-MS
S	Sulfur	10 ppm (±1)	IC
Si	Silicon	100 ppm (±10)	ICP-MS
Sm	Samarium	1 ppm (±0.1)	ICP-MS
Sn	Tin	10 ppm (±1)	ICP-MS
Ta	Tantalum	100 ppm (±10)	ICP-MS
Th	Thorium	10 ppm (±1)	ICP-MS
Ti	Titanium	10 ppm (±1)	ICP-MS
U	Uranium	1000 ppm (±100)	ICP-MS
V	Vanadium	10 ppm (±1)	ICP-MS
W	Tungsten	100 ppm (±10)	ICP-MS
Zn	Zinc	10 ppm (±1)	ICP-AES
Zr	Zirconium	10 ppm (±1)	ICP-MS

In the absence of the planned ARIES sample feed stream, samples were taken from other ongoing LANL PF-4 activities, including pit surveillance and DMO work. The results of four metal samples were received in FY98. Table 2-6 compares metal sample chemical analysis results with the PuO_2 draft specification; circled values exceed the specification value, and shaded elements were not analyzed. Gallium results were not reported because of classification concerns. Several elements for which there were no specifications also were analyzed. Sulfur, fluorine, and potassium contents were above specification and warrant observation as more sample information is gathered. It was not possible to draw any conclusion based on the scant data available, but the initial data do not reveal any major unforeseen impurity concerns.

2.5. MOX Fuel Aqueous Polishing Flowsheet

In support of the DOE-MD program, integrated flow sheets were developed for the aqueous separation of impurities from plutonium in a nitrate-salt solution by ion exchange (IX) and solvent extraction (SX) techniques. The integrated flow sheets consist of dissolution, separations, precipitation, and calcination unit operations. The intent of the demonstrations was to (1) verify the separations feasibility for preparation of PuO_2 to be used as feed for MOX fuel fabrication, and (2) evaluate the HF/HNO_3 dissolution of PuO_2 derived from direct oxidation, ARIES three-step PuO_2, and ARIES three-step PuO_2 plus TIGR.

The integrated flow-sheet tests were conducted as planned with PuO_2 derived from the direct oxidation of retired weapons parts and dissolved by way of HF (hydrofluoric acid) in HNO_3. IX was conducted with Reillex HPQ polyvinylpyridine anion resin, and SX was based on a tri-butyl phosphate (TBP) solvent in a dodecane diluent. Pu^{III+} oxalate precipitation then was followed by calcination at 600°C to 650°C for 6 h. Purity of the final oxide was within the current MD PuO_2 specifications, including ~3 ppm gallium for IX, where $\leq$200 ppm gallium is the feed specification for MOX fuel, and was 87.13–87.31 wt % plutonium, which corresponds to approximately $PuO_{2.2}$ and is also within the specification.

Midway through this test program, it was decided to focus the dissolution evaluations only on electrolytic dissolution of PuO_2. Consequently, evaluation of HF/HNO_3 dissolution of PuO_2 derived from the various methods was discontinued. However, because dissolution by HF/HNO_3 for the integrated flow sheets was completed before its exclusion and because the method of dissolution should not affect the separations efficiency significantly, the integrated flow sheets were demonstrated as planned. A literature review, which completed the evaluation of electrolytic dissolution, indicated satisfactory dissolution independent of the PuO_2 preparation technique.

TABLE 2-6. COMPARISON OF METAL SAMPLE CHEMICAL ANALYSIS RESULTS AND PuO_2 DRAFT SPECIFICATION

Impurities	PuO_2 Specification	Metal Sample #200057158	Metal Sample #200057142	Metal Sample #200057133	Metal Sample #200057138
Ag	100	0.1	0.1	0.1	4
Al	150	25	36	80	89
As	none	10	10	10	10
Am-241	none				
Au	none	0.4	0.4	0.4	0.5
B	10	2	2	2	2
Ba	none	0.06	0.06	0.05	0.06
Be	100	0.2	0.9	0.7	63
Bi	100	6	0.4	0.4	0.4
C	500				
Ca	500	20	22	8	8.9
Ca+Mg	none	70	42	23	34.9
Cd	10	0.08	0.2	0.05	5
Ce	none	0.07	0.07	0.07	0.07
Cl	(+F < 250)	88	121		
Cl+F	250	356	527		
Co	100	0.5	1	0.04	1.8
Cr	100	30	35	1.5	49
Cs	none	0.02	0.02	0.02	0.02
Cu	100	9	30	8	21
Dy	1	0.04	0.04	0.04	0.04
Er	none	0.04	0.04	0.04	0.04
Eu	1	0.02	0.02	0.02	0.02
F	(+Cl < 250)	268	406		
Fe	500	350	280	12	297
Ga	200				
Gd	3	0.06	0.06	0.05	0.06
Ge	none	0.2	0.2	0.2	0.2
H	none				
H-3	none				
Hf	none	0.04	0.04	0.05	0.04
Hg	none	2	2	2	2
Ho	none	0.01	0.02	0.01	0.02
In	20	0.02	0.09	0.02	0.1
Ir	none	0.09	0.1	0.2	0.4
K	100	70	80	104	115
La	none	0.05	0.05	0.05	0.05
Li	100	0.4	0.4	0.4	0.4
Lu	none	0.02	0.02	0.02	0.04
Mg	500	50	20	15	26
Mn	100	13	9	0.3	10
Mo	100	3	1.7	1.1	3
N	300				
Na	300	9	10	9	10
Nb	100	0.4	0.4	0.8	0.4
Nd	none	0.04	0.04	0.04	0.04
Ni	200	20	70	8	108
Np	none				
P	100	40	40	88	98
Pb	200	1.5	5.5	1	20
Pd	none	0.04	0.04	0.04	0.1
Pr	none	0.02	0.02	0.02	0.02
Rb	none	0.06	0.06	0.05	0.06
Re	none	0.2	0.25	0.2	0.2
Ru	none	0.04	0.04	0.04	0.04
S	250				
Sb	none	0.4	0.4	0.4	0.4
Se	none	2	2	2	2
Si	200	60	95	80	89
Sm	2	0.04	0.04	0.04	0.04
Sn	100	1.9	6.9	0.7	6
Sr	none	0.04	0.04	0.04	0.04
Ta	none	0.3	5	1	6
Tb	none	0.02	0.02	0.02	0.02
Te	none	0.8	0.4	0.2	0.4
Th	100	0.12	0.4	0.08	0.3
Ti	100	2.7	0.9	0.07	2.6
Tl	none	0.06	0.06	0.05	0.06
U	5000				
V	300	20	160	20	14
W	200	2.2	5	16	6
Y	none	0.01	0.01	0.2	0.02
Yb	none	0.01	0.02	0.01	0.02
Zn	100	10	10	10	10
Zr	50	0.02	0.1	0.02	0.1
Total Impurities	5300	882	1028	230	670

3.0. FUEL FABRICATION DEVELOPMENT

The purpose of the fuel fabrication development activities was to identify and, if possible, resolve technical issues associated with applying the large experience base (existing mainly in Europe) created by those making MOX fuel with recycled reactor-grade plutonium to those fabricating MOX using surplus weapons plutonium. More specifically, the fabrication of MOX fuel using a new baseline of AUC-derived UO_2 and various PuO_2 sources and processing parameters was required to establish a database used in supporting the selection of a private firm to carry out fuel fabrication activities in the disposition mission. Furthermore, in support of contract negotiations, the gallium sintering studies helped determine the impact of residual gallium levels on fuel fabrication process parameters and equipment, with specific attention being paid to the impact of residual gallium levels on the sintering process.

The first two tasks in this activity involved developing fabrication processing parameters for use with the new AUC UO_2 feed material. It has been determined through previous efforts that a certain amount of development work is necessary when new feed materials are introduced into an established fabrication process. The first task attempted to establish the parameters by which MOX fuel would be fabricated with the AUC UO_2. The second task examined the effect of varying sources of PuO_2 on the fabrication process. These tasks are combined into Section 3.1.

The third main task was the gallium sintering studies. Previous R&D experiments performed at LANL have demonstrated that the gallium found in WPu volatizes in a reducing atmosphere. Because the sintering of MOX fuel occurs in a reducing atmosphere, this behavior could lead to significant sintering furnace degradation, especially in larger-scale processing of surplus weapons MOX fuel. A more detailed description of all of the fuel fabrication development activities and their results can be found in Refs. 3-1 and 3-2.

3.1. Feed Materials Baseline Development

The efforts described in this section were performed in support of the DOE-MD Program. There were two main tasks included in this effort:

1. Develop baseline MOX fuel-fabrication processing parameters for the AUC-derived source of UO_2 feed material, using both surrogate CeO_2 and prototypic PuO_2 powders.

2. Fabricate MOX fuel using the baseline fabrication processing parameters, the new source of UO_2 feed material, and an alternative source of PuO_2 feed material.

The experiments performed and results obtained from these feed materials baseline development activities are described in the following sections and in Ref. 3-1.

3.1.1. UO_2 Development Results

Approximately 115 kg of depleted, AUC-derived UO_2 powder was received at LANL in early March 1998. The original estimated date of receipt was mid-January, but the schedule slipped as a result of a 6-week delay in receiving the cost estimate for the

material from the supplier. Once received, the powder was repackaged into containers suitable for use in the glovebox line and transferred into PF-4. ABB-Sweden provided a complete characterization of the material, and it was decided that the only comparison analyses needed were for particle size and surface area. A comparison of these results from the ABB data package and LANL analyses is shown in Table 3-1. Results also are shown for characterization performed at a different point in the fabrication process (after mixing in a Turbula® mixer). These results are presented here together to facilitate comparison but will be discussed further in the appropriate section.

Several experiments were performed to understand the AUC-derived powder's ability to make MOX fuel according to predetermined specifications. Table 3-2 shows the variables examined and the parameters used for the experiments performed to date. Each batch utilized 200 g of material, which yielded ~14 pellets (and 14 corresponding data points). However, the additional experiments described in Section 3.1.3 were on the order of only seven pellets to increase throughput. A description of each experiment as well as many of the results obtained are provided below; however, a complete summary of the results can be found in Ref. 3-1.

TABLE 3-1. CHARACTERIZATION RESULTS FOR AUC UO_2 AND MOX POWDERS

Analysis	ABB UO_2	LANL As-Received UO_2	LANL Turbula Mixed UO_2	LANL Turbula Mixed MOX
Particle Size (μ)	Not available	12.5 10.6	15.5 9.7	10.7 15.4
Surface Area (m^2/g)	5.31	5.1402 5.6118 5.2436	1.8265 2.1493	Not available

TABLE 3-2. BASELINE DEVELOPMENT EXPERIMENTAL VARIABLES AND PROCESSING PARAMETERS

Experiment	PuO_2 (g)	UO_2 (g)	Lubricant	Blending	Slug and Granulation	Pressing (ksi)	Sintering
1697-8ST1	None	200	None	None	None	28.8–86.5	1750°C for 7 h
1697-8ST2	None	200	None	None	None	28.8–57.7	1750°C for 7 h
1697-8ST3	None	199.6	0.4 g zinc stearate	Turbula 5 min	None	40.4–69.2	1750°C for 7 h
1697-8ST4	None	190+10	None	Turbula 15 min	None	40.2–54.8	1750°C for 7 h
1697-8ST5	10 g 3-step	190	None	Turbula 15 min	None	40.4–57.7	1750°C for 7 h

The first experiment, labeled 1697-8ST1, was performed to obtain powder flowability and pellet shrinkage information. This first test was performed by pressing the as-received UO_2 powder at various pressing pressures without additives, additive removal, or precompaction. The order of the pellets was inadvertently mixed up after sintering of the fuel; thus, only flowability was determined from this test. In general, it was determined that the powder had good flow properties. The sintered density was not determined because the identity of the pellets with respect to the pressing variables was lost after sintering.

The second experiment, labeled 1697-8ST2, was performed to obtain the shrinkage data not available from the first experiment. Again the powder was pressed as received, without additives. In general, the pellets fabricated in this experiment showed increasing density with increasing pressure. Several of the pellets (pressed at >~43 ksi[1]) were within the predetermined specification of 95% (±1%) of theoretical density. One pellet (pressed at 52 ksi) actually exceeded the specification at 96.8% of theoretical density. The shrinkage values decreased with increasing pressing pressure, ranging from ~19%–23%.

The third experiment, labeled 1697-8ST3, was performed to determine the effects of the addition of a lubricant. Zinc stearate (0.2 wt %) was added to the UO_2 powder before pressing. The remaining processing parameters were held constant. The pellets had almost linear sintered densities with increasing pressure. The pellets pressed at <~50 ksi were within the predetermined specification of 95% (±1%) of theoretical density. The shrinkage values again decreased with increasing pressing pressure, ranging from ~17%–20%.

The fourth experiment, 1697-8ST4, was performed to determine the effects of making a primary blend with a Turbula® mixer, but using only UO_2. The master blend consisted of 95 wt % UO_2 and 5 wt % UO_2 (as a substitute for PuO_2) to simulate a MOX fuel master blend. The powder was blended with the Turbula® for 15 min and pressed as blended, without any additives. A sample of the Turbula® mixed powder was analyzed for particle size and surface area characterization; the results are shown in Table 3-1. The particle size remained roughly the same after mixing, but the surface area appeared to decrease. This decrease possibly was caused by agglomeration during mixing; however, this has not been fully determined yet. The mixed powder showed good flowability properties and pressed without problems. The pellets showed a slightly increased density with increased pressure. Only pellets pressed at >~52 ksi were within the predetermined specification of 95% of theoretical density (±1%). The shrinkage values decreased slightly with increased pressing pressure. The shrinkage of the pellets ranged from ~19% to 21%. The pellets exhibited a rough, "blistered" diametral surface, and some pellets were "hourglassed." This probably was caused by insufficient die lubrication and could have been an indication of a rough die surface. Prepressing and granulation, although not normally required for AUC-derived material, could alleviate these problems and improve the sintered pellet densities.

The fifth experiment, labeled 1697-8ST5, was the first MOX batch made using the AUC-derived UO_2 and PuO_2 powders. The three-step PuO_2 powder processed by LLNL was

[1] ksi = 1000 psi.

used for this experiment. This experiment was performed exactly as the fourth (1697-8ST4), except that 5 wt % PuO_2 powder was used to create a true MOX blend. Samples of the blended powders were sent for particle size and surface area characterization. Table 3-1 also shows the particle size characterization results for this MOX blend. However, the surface area results were unavailable when this report was prepared. The MOX powder showed good flowability properties and pressed without problems, indicating that adding the PuO_2 has no detrimental effect on pressing behavior. The pellets showed an increased density with increased pressure. None of the pellets were within the predetermined specification of 95% of theoretical density (±1%), but all were >91% of theoretical density. The shrinkage values decreased slightly with increased pressing pressure, ranging from ~19%–20%. A pellet sample was submitted for SEM and autoradiograph analyses, but results were unavailable when this report was prepared. Again, the pellets exhibited a rough, "blistered" diametral surface, and some pellets were "hourglassed."

3.1.2. Alternative PuO_2 Fabrication Results

The second specific task under the baseline development effort was to identify alternative PuO_2 sources for fabrication purposes. The majority of FY98 and past PuO_2 experiments used three-step LLNL material. Two other sources of PuO_2 powder became available for this task in FY98: the two-step hydride-oxidation material created by LLNL and an aqueously derived source processed at LANL. Although it is not currently anticipated that the two-step process will be selected as the method for PuO_2 conversion, it was hoped that the material would behave similarly to the three-step material. This would allow its use as an additional source of feed for future experiments because there is little inventory of the three-step material currently left available. MOX pellets were fabricated using these two sources and the same parameters used for experiment 1697-8ST5 (see Section 3.1.1). For each batch, the AUC powder was blended with 5 wt % PuO_2 (with no additives) in a Turbula® mill for 15 min. Batch number 1697-8ST7 refers to the pellets made with the two-step material, and batch number 1731-T1 refers to the pellets made with the aqueously derived source.

This activity compared these results directly with those obtained using the three-step PuO_2 (experiment 1697-8ST5). Figure 3-1 shows the comparison of the green densities for the three batches, whereas Fig. 3-2 shows the comparison of the final sintered densities. None of these sintered densities for the three-step and two-step batches met the 95% (±1%) of theoretical density (TD) specification. However, the aqueous batch met the density specification at ~52- and 55-ksi pressing pressures. Figure 3-3 compares the shrinkage values for the three batches.

Because so few of the pellets actually met the predetermined specification, new batches using the three sources of PuO_2 powder (three-step, two-step, and aqueously derived) were fabricated in an attempt to increase the sintered density results. The new batches are designated by 1697-8ST9 for the three-step material, 1697-8ST10 for the two-step material, and 1731-T3 for the aqueously derived material. A single pressing pressure of 52 ksi was used for all pellets in all batches because that pressure created higher-quality pellets in the initial batches. The main difference in the original and new batches was

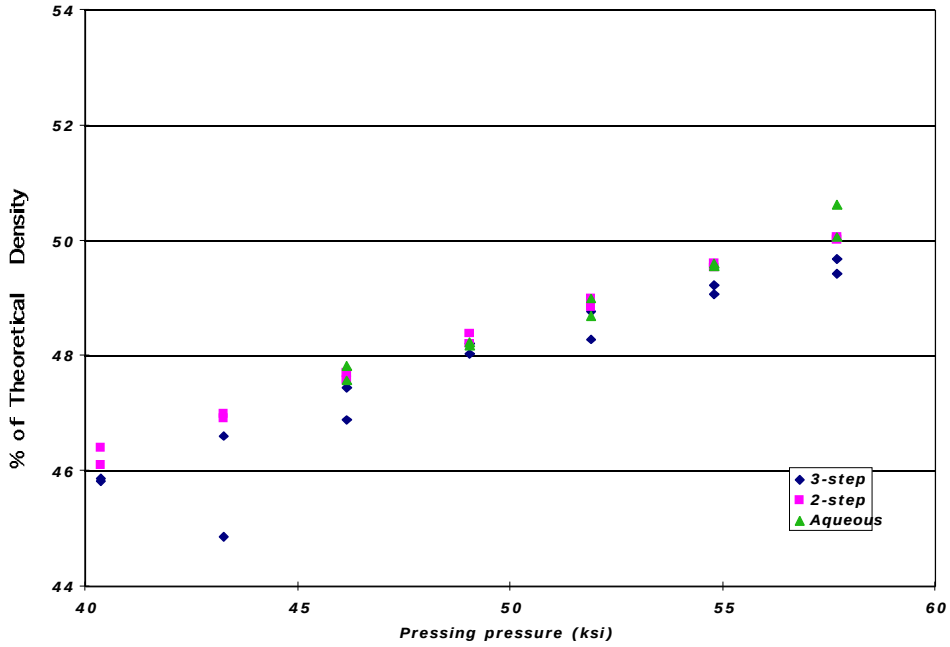

Fig. 3-1. Comparison of green densities as a function of pressure.

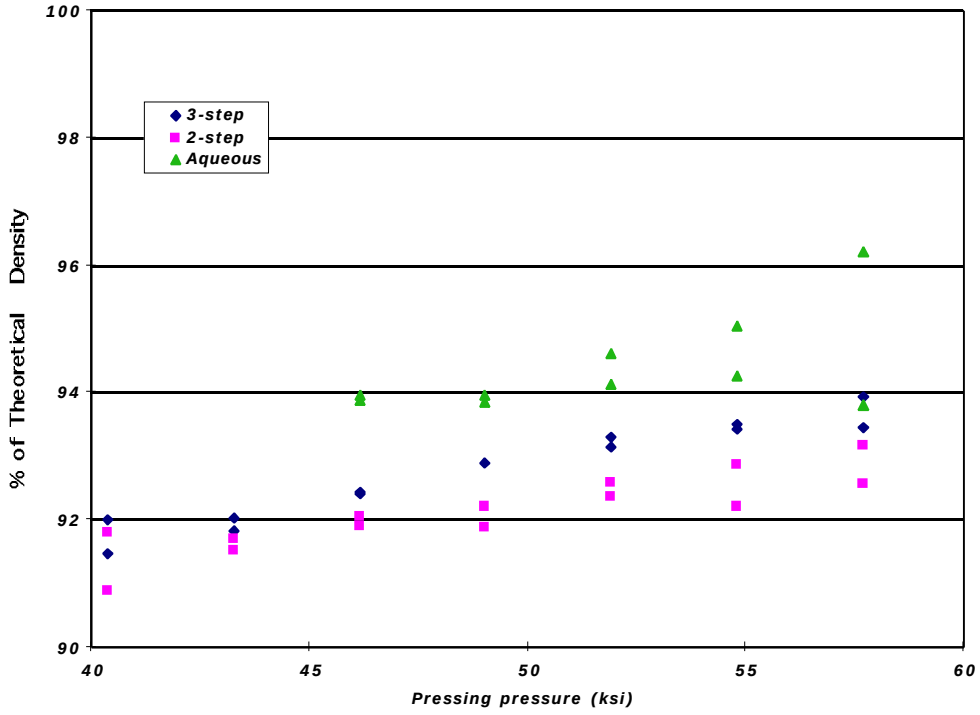

Fig. 3-2. Comparison of sintered densities as a function of pressure.

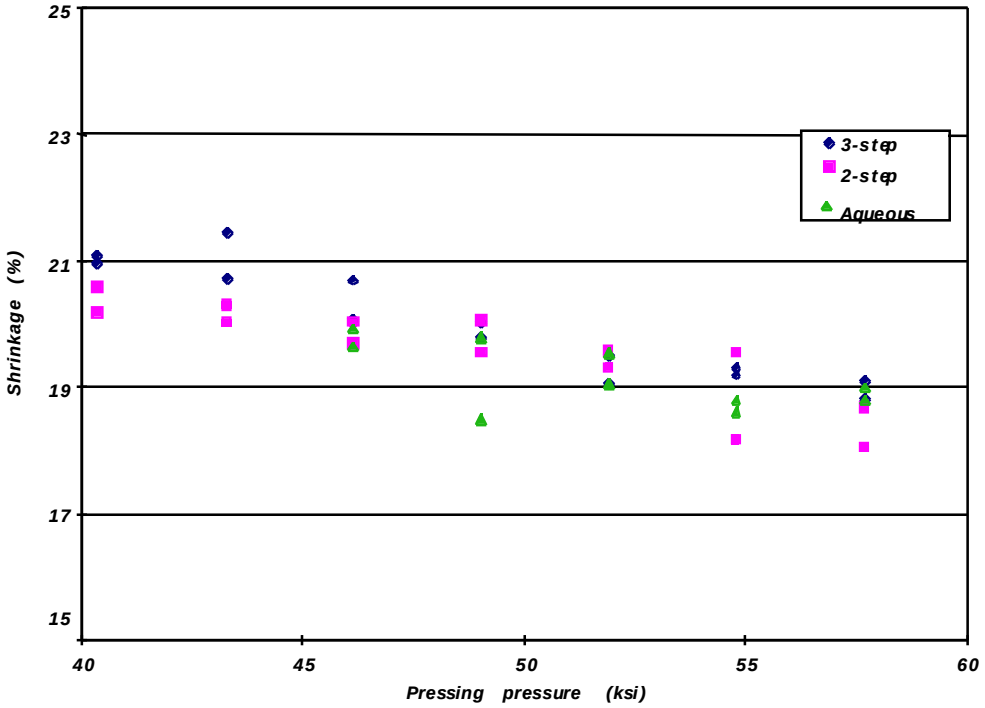

Fig. 3-3. Comparison of shrinkage values as a function of pressure.

the addition of zinc stearate to the new batches. Table 3-3 provides a summary of the green and sintered density and shrinkage data from the original batches and compares that summary with the results obtained from the new batches. The new three-step batch had approximately the same green density as the original three-step batch, but lower sintered densities and shrinkage values. The same trends also were seen with the two-step and aqueously derived batches. Overall, the aqueous batches had the highest sintered densities, although they were still below the desired specification. Therefore, adding the zinc stearate did not have the desired effect of increasing the sintered densities.

3.1.3. Additional Baseline Development Experiments

A few additional experiments not specified in the original test plan were performed in the course of the development activities. Fabrication tests were performed at constant pressures to determine if constant pellet lengths and sintered densities could be achieved (Batch 1697-8ST6). Tests also were initiated to determine the effect of varying the sintering temperature on the final pellets (Batch 1697-8ST8). Table 3-4 shows the parameters used and the results obtained for each experiment. Each of the three experiments shown in Table 3-4 used a single pressing pressure, and the desired results of constant pellet lengths and sintered densities were obtained. However, only Batch 1697-8ST6 met the sintered density specification at 94.1% TD. Decreasing the sintering temperature (1697-8ST8B) increased the sintered density by half a percent.

TABLE 3-3. COMPARISON OF ORIGINAL AND NEW PuO_2 VARIABILITY STUDY RESULTS

PuO_2 Source	Parameter	Original Value(s)	Original Values at 52 ksi	New Value(s) (at 52 ksi)
THREE-STEP	Green density (% of TD)	45.9–49.7	48.3, 48.8	48.0–48.8
	Sintered density (% of TD)	91.4–93.9	93.1, 93.3	90.1–91.6
	Shrinkage (%)	18.8–21.4	19.5, 19.0	17.7–18.9
TWO-STEP	Green density (% of TD)	46.1–50.1	48.9, 49.0	48.6–49.3
	Sintered density (% of TD)	90.9–93.2	92.4, 92.6	90.8–91.5
	Shrinkage (%)	18.0–20.6	19.6, 19.3	17.4–18.8
AQUEOUS	Green density (% of TD)	47.6–50.6	48.7, 49.0	48.7–49.8
	Sintered density (% of TD)	93.8–96.2	94.6, 94.1	91.8–92.8
	Shrinkage (%)	18.5–19.9	19.5, 19.0	17.6–19.3

TABLE 3-4. ADDITIONAL EXPERIMENTAL VARIABLES AND PROCESSING RESULTS

Batch Number	Feed	Blending	Pressing (ksi)	Sintering	%TD	Length (in.)
1697-8ST6	UO_2 + zinc stearate	Turbula 5 min	52	1750°C for 7 h	94.1 (±0.2)	0.404 (±0.010)
1697-8ST8A	UO_2 + zinc stearate	Turbula 5 min	58	1750°C for 7 h	91.9 (±1.2)	0.405 (±0.011)
1697-8ST8B	UO_2 + zinc stearate	Turbula 5 min	58	1600°C for 7 h	92.4 (±0.2)	0.414 (±0.039)

3.1.4. Baseline Development Summary

The experiments performed to date have completed much of the development work needed to perform other activities, including providing shrinkage data to determine appropriate punch and die sizes for ATR fuel fabrication. Overall, these experiments showed that the AUC powder has good flow properties. Pellets were fabricated to almost 94% of theoretical density, which was just outside the required specification. Future experiments still are planned to develop more fully the ability to make quality MOX fuel using the AUC powder. These experiments will be geared toward obtaining specification densities and examining other variables in the set of parameters described in the draft test matrix. Most of the tests will be performed using only UO_2 powder because the small amount of PuO_2 powder currently available for this program is required for other tasks. Further PuO_2 variability experiments will be performed as new sources of PuO_2 powders become available. Experiments not completed in FY98 should

be completed early in FY99 to finish the complete characterization of the AUC feed material.

3.2. Gallium Sintering Study

The main thrust of the sintering studies was to fabricate MOX pellets containing varying amounts of Ga_2O_3, sinter the pellets under a wide range of conditions, then characterize the sintered pellets to determine what effects, if any, the gallium had on the sintering process. Studies were performed first in the cold (without plutonium) laboratory using surrogate materials and were intended to be performed in PF-4 with plutonium. (However, these plutonium studies were not performed because fabrication personnel were assigned to other, higher-priority MD efforts.) A separate activity in this task was the continuation of the phase relations assessment begun as part of the FY97 R&D activities (Ref. 3-3). Limited results from both of these activities are reported here; the rest are included in Ref. 3-2.

3.2.1. Surrogate Sintering Studies

Surrogate materials are used to examine more easily a wide range of experimental variables at a lower cost than can be achieved using plutonium-bearing materials. For this particular activity, CeO_2 was used as a surrogate for PuO_2 in all experiments.

For the surrogate studies, the feed materials were put through an initial fabrication process to obtain a homogeneous mix. Two powder-pressing methods were used for these experiments. The first was a one-step process, and the second was a two-step process. The two-step process was intended to achieve a more uniform distribution of gallium and to saturate the CeO_2 with gallium, thereby creating conditions thermodynamically similar to PuO_2–Ga_2O_3. A more complete description of the fabrication process and the surrogate sintering studies in general is found in Ref. 3-2.

3.2.1.1. Cerium-Gallium

A sintering study using CeO_2 and CeO_2 + 2 wt % Ga_2O_3 (1.37 mol % gallium) was performed initially without UO_2 to evaluate the relevance of CeO_2-Ga_2O_3 as a surrogate system for PuO_2-Ga_2O_3. Furthermore, to evaluate the effects of gallium in a ternary system (CeO_2–Ga_2O_3–UO_2), an understanding first is needed of the effects in the binary system. (The results of these particular studies also support the gallium removal task currently underway and discussed in Section 5.0.) This study investigates the product formed from commercial CeO_2 powder using various processing conditions.

Figure 3-4 shows SEM micrographs of CeO_2 pellets (produced by the two-step process) sintered at 1650°C for 2 h and 6 h. With increased sintering time, the porosity (dark phase) appears to be coalescing to create fewer, larger pores, and the sintered grains appear to increase in size. The same scenario is evident for the CeO_2 + 2 wt % Ga_2O_3 pellets, as seen in the micrograph in Fig. 3-5. The micrograph also shows a third phase present at grain boundaries. Wavelength-dispersive spectroscopy (WDS), shown in Fig. 3-6, shows that the grain boundary phase contains gallium compounds.

Some porosity in the CeO_2 + 2 wt % Ga_2O_3 pellets may have formed from vaporization of gallium compounds at high firing temperatures. A loss of ~50% gallium in CeO_2 + 2 wt % Ga_2O_3 pellets has been observed after sintering (Ref. 3-4). The majority of the

porosity in the pellets is in a spherical shape. However, a few circular structures are filled. Energy-dispersive spectroscopy (EDS) of the filled circular structures indicated a chemical composition of cerium with minute amounts of gallium. A gallium-rich phase is not indicated.

The sintering trends for CeO_2 + 2 wt % Ga_2O_3 and CeO_2 also were studied. For the CeO_2 pellets, volume shrinkage and density increased with increasing sintering temperature and time. The density decreased slightly between sintering times at 1650°C, potentially because of gallium compound vaporization. The CeO_2 + 2 wt % Ga_2O_3 pellets showed greater volume shrinkage and density than the CeO_2 pellets. In the oxidizing environment used in these studies, the gallium may act as a sintering aid by forming a liquid. Micrographs show a coalescing of pores and increased grain size of the CeO_2 matrix with increased sintering temperatures/times. WDS analysis of CeO_2 + 2 wt % Ga_2O_3 shows that gallium migrates selectively to grain boundaries.

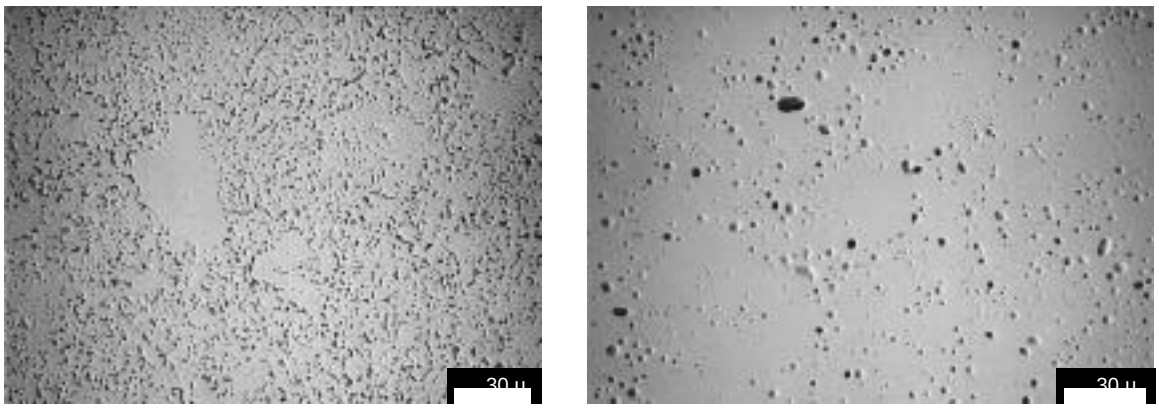

Fig. 3-4. SEM micrographs for 2-h (left) and 6-h (right) sintering times in CeO_2 sintered at 1650°C.

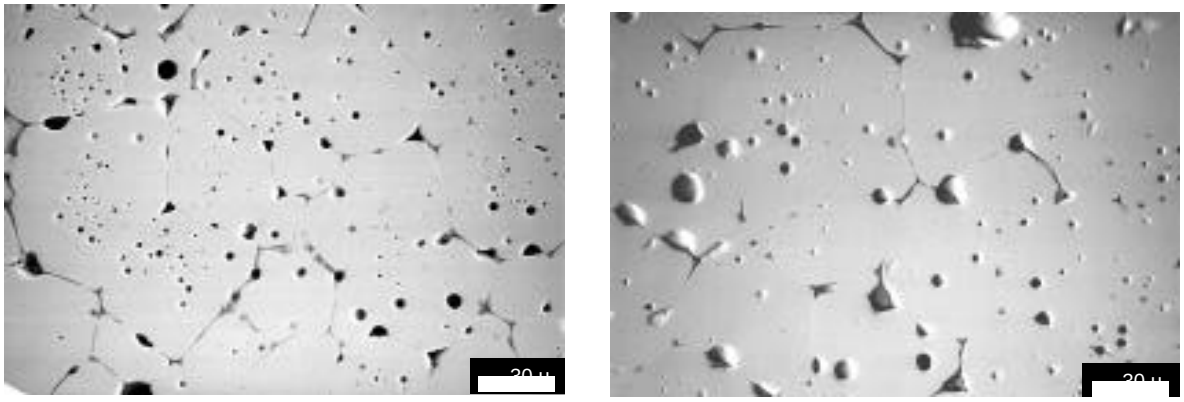

Fig. 3-5. SEM micrographs for 2-h (left) and 6-h (right) sintering times in CeO_2 + 2 wt % Ga_2O_3 sintered at 1650°C.

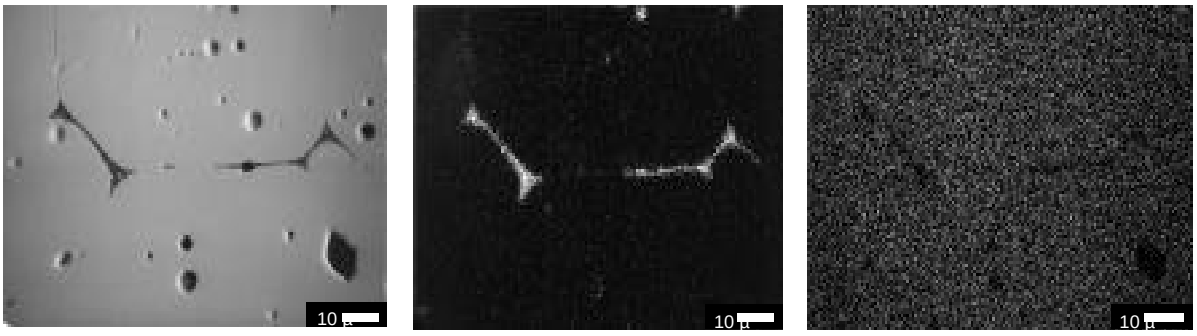

Fig. 3-6. Elemental mapping by WDS of CeO_2 + 2 wt % Ga_2O_3 sintered at 1650°C for 6 h: (left) SEM of scanned area; (middle) distribution of gallium; (right) distribution of cerium.

3.2.1.2. Cerium–Gallium with Cameco UO_2

To accomplish the sintering studies, it was necessary first to obtain the proper feed materials. If AUC-derived UO_2 feed had been obtained early enough in the fiscal year, these studies would have been performed using only that material. Because the AUC powder was not available, a limited matrix of tests was conducted with the Cameco UO_2 powder already on hand. The AUC powder currently is being tested with the compositions in weight percent given in Table 3-5. The Cameco material was used to produce annular pellets for the Oak Ridge National Laboratory (ORNL)/Texas A&M Phase III gallium-clad interaction study. The tests discussed here were limited in scope to determining the sintering parameters necessary to produce pellets acceptable for use in this experiment. The sample compositions are given in Table 3-6.

TABLE 3-5. COMPOSITIONS BLENDED FOR SINTERING STUDIES WITH AUC UO_2

wt % UO_2	wt % CeO_2	wt % Ga_2O_3	Comments
100	0	0	Sieved, binder then added
97	3	0	No gallium
97	2.94	0.06	Commercial powder
97	2.94	0.06	Ce–2% Ga alloy converted to oxide by HYDOX route

TABLE 3-6. COMPOSITION OF CAMECO UO_2–Ga TEST PELLETS

wt % UO_2	wt % CeO_2	wt % Ga_2O_3	Comments
100	0	0	Sieved, binder then added
96	3	1	“High” gallium
97	2.94	0.06	“Low” gallium

One of the objectives of the Phase III test plan was to investigate the effects of gallium at the highest level achievable. Therefore, a 1% Ga_2O_3 blend was prepared in an attempt to achieve this goal. As discussed below, this ultimately proved futile because practically all of the gallium escaped from the pellet as Ga_2O during sintering. Nonetheless, this series of experiments was valuable because trends that are suggested by the effects of gallium at low concentrations are clearly visible in samples tested at the higher concentrations.

Most of the experiments were performed at temperatures from 1400°C to 1700°C and at times from 5 to 15 h. This study ultimately resulted in a processing schedule of 10 h at 1600°C for the production of the annular pellets for the Phase III experiments. In all of the experiments conducted with the pellets containing gallium, the ultimate density was limited to <92%. The solid pellets containing a starting composition of 1 wt % Ga_2O_3, 3% CeO_2 (to balance the UO_2) always sintered to a significantly lower density than the otherwise identically processed UO_2 pellets. Two different initial gallium levels were used for the production of the annular pellets, 1 wt % (blend A) and 0.06 wt % (blend B). Although neither of these compositions reached the sintered density of pure solid UO_2 pellets under the same conditions, the pellets having the lower gallium content (blend B) reached slightly higher densities than did those with the higher gallium content (blend A).

Samples of both batches of pellets were analyzed at ORNL to determine the gallium content relevant to the Phase III effort. Surprisingly, both batches came out with approximately the same gallium level (~10 ppm), in spite of starting concentrations of 1 wt % and 0.06 wt %. Clearly, the gallium was volatilized during sintering, but this does not explain completely the relatively low densities obtained in the gallium-doped pellets.

Microstructural analysis showed that the pellets that initially contained gallium developed very coarse closed porosity that could not be removed by further sintering. This effect is illustrated in the two micrographs shown in Fig. 3-7 that compare the microstructure of UO_2 with that of the UO_2–CeO_2–Ga_2O_3 blend after sintering for 10 h at 1600°C. Essentially all of the CeO_2 went into solution in the UO_2.

At this point, all of the planned work on the Cameco powder has been completed. This work involved sintering at temperatures from 1400°C to 1700°C for periods of up to 15 h. Although some additional work could be performed, the trends are clear, and it is planned that future efforts will focus instead on the AUC material. The microstructure in samples containing gallium at the 1 wt % level show clear evidence of transient liquid phase sintering. Apparently, the Ga_2O_3 melts internally to the pellet before it is all vaporized. The residual level of 10 ppm suggests that the ultimate gallium level in the ternary system may be limited by a factor other than the reduction of Ga_2O_3 and transport of Ga_2O from the pellet.

3.2.2. Phase Relations Studies

FY98 efforts for phase relations included evaluating the Pu-Ga perovskite stability and continuing to assess the solubility of gallium in PuO_2 as well as Ga_2O_3 (see Ref 3-2 for information on the solubility). Based on the dependency of the partial pressure of

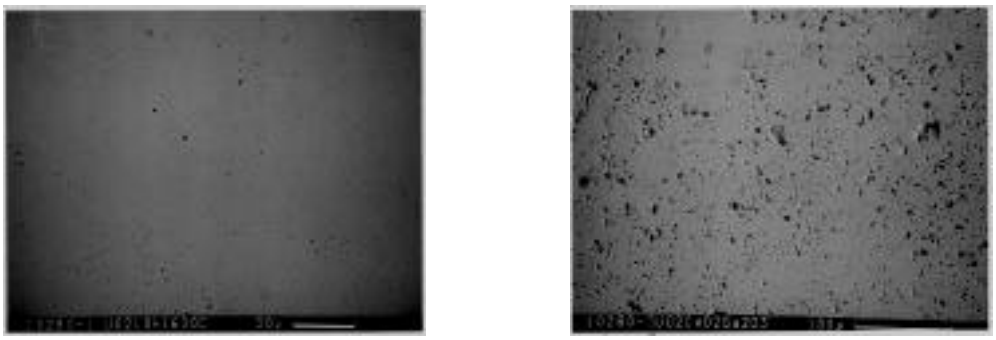

Fig. 3-7. UO_2 sintered 10 h at 1600°C, 500 X (left); UO_2–3%CeO_2–1%Ga_2O_3 sintered 10 h at 1600°C, 250 X (right).

oxygen on the temperature, at thermodynamic equilibrium the limits of stability for the $Pu(Ce)O_3$ perovskites can be calculated. The stability diagram shows very similar limits for both $PuGaO_3$ and $CeGaO_3$. This is an additional argument supporting the use of cerium oxides as surrogates for the plutonium oxides. The perovskite structures cannot be obtained (at reasonable temperatures) in normal conditions of atmospheric oxygen pressure (in air). If the partial pressure of oxygen is 10^{-10} atm, then both compounds are stable between 715 K and 1250 K. For a partial pressure of oxygen of 10^{-20} atm, the stability limits are 1100 to 1825 K for $CeGaO_3$ and 1175 to 1825 K for $PuGaO_3$. Therefore, the likelihood of generating the perovskites is proportional to the severity of the reducing atmosphere.

3.2.2.1. Phase Diagrams

If the conditions of obtaining the perovskite are achieved, then in the Pu(Ce)-Ga-O system, the phase diagram should include a compound of composition Pu(Ce)–GaO_3 placed on the Ga_2O_3–Pu_2O_3 line (see Ref. 3-2, Fig. 21). As a result of the previous calculations, the compound can be in equilibrium with the metallic gallium and with PuO_{2-x} for certain values of x. Figure 3-8 shows the superimposed phase diagrams of the Ga_2O_3–Pu_2O_3 and Ga_2O_3–Ce_2O_3 systems under reducing conditions.

3.2.2.2. Theoretical X-Ray Pattern

A systematic experimental study has revealed the difficulties of isolating a stable perovskite phase. Because there is no known standard for the x-ray pattern of the $CeGaO_3$ phase, this study is intended to provide a model for the structure and a theoretical x-ray pattern.

Synthesis of $CeGaO_3$ by arc melting recently has been reported in Ref. 3-5. The authors argue that the structure is tetragonal (space group P4/mmm) with lattice parameters at a = b = 3.873, and c = 3.880 Å. Table 3-7 shows the predicted x-ray pattern of the $CeGaO_3$ phase in this model.

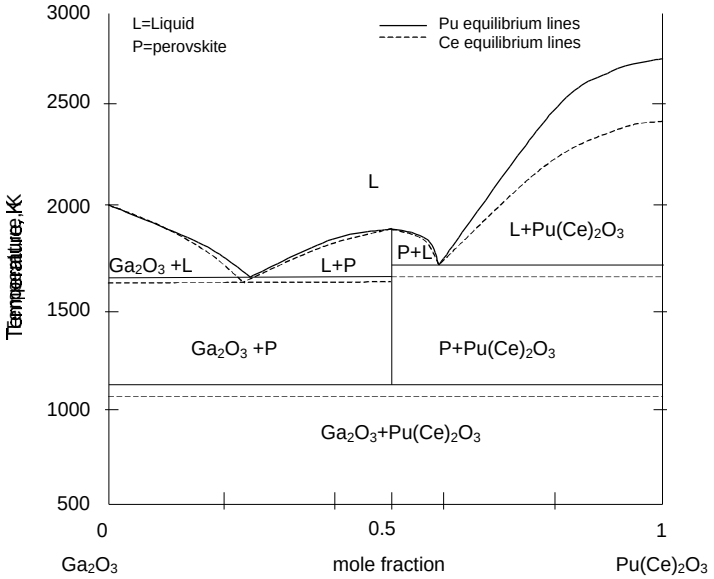

Fig. 3-8. Superimposed phase diagrams of Ga_2O_3–Pu_2O_3 and Ga_2O_3–Ce_2O_3 systems in reducing conditions (partial pressure of oxygen of 10^{-10} atm.)

TABLE 3-7. CALCULATED X-RAY PATTERN OF $CeGaO_3$

d_{hkl}	Int	h k l	2θ ($\lambda_{Cu\alpha1}$)
3.880	11.8	0 0 1	22.90
3.873	23.1	1 0 0	22.94
2.741	100.0	1 0 1	32.64
2.739	49.9	1 1 0	32.67
1.940	15.0	0 0 2	46.79
1.936	29.8	2 0 0	46.88
1.583	17.1	1 1 2	58.23
1.582	34.1	2 1 1	58.29

When sintered in a pure argon environment, initial x-ray analysis results showed that CeO_2 and Ga_2O_3 are present when starting with the perovskite composition of powders. The samples sintered in an inert atmosphere showed CeO_2 and Ga_2O_3 but also contained some unindexed lines that matched the predicted pattern for the perovskite phase. The samples are bluish, indicating nonstoichiometric CeO_{2-x} (i.e., an oxygen deficiency). The samples fired in an Ar-6% H_2 environment also show the formation of a new phase at 1000°C and 2000°C. This again appears to be the perovskite phase. At temperatures as high as 1400°C, CeO_2 and Ga_2O_3 are present with a few unindexed lines that might be trace amounts of this third phase.

In conclusion, it has been demonstrated that the perovskite phase, previously predicted by the theoretical phase diagram effort in the CeO_2-Ga_2O_3 system, can be produced

under conditions relevant to the processing and operation of MOX fuel. It reasonably can be extrapolated that the analogous compound may be present at low concentrations in the weapons-grade PuO_2 powder. Because this compound is a solid at the temperatures where gallium removal or pellet sintering is conducted, it therefore may control the ultimate gallium removal obtainable under a particular set of conditions. The perovskite phase also may affect the sintering mechanism in the pellets processed with high initial gallium levels because the gallium appears to segregate to grain boundaries in these samples.

3.2.3. Gallium Sintering Summary

Most of the gallium sintering studies planned for FY98 were completed using the surrogate materials. CeO_2 pellets were fabricated with and without gallium and sintered under various conditions. The pellets were characterized for density and shrinkage, and results were compared to determine the effect of gallium on the sintering process. The pellets also were characterized for microstructure and elemental analysis. No pellets that incorporated the AUC-derived UO_2 feed powder were fabricated because of its late availability. However, UO_2–CeO_2–Ga_2O_3 pellets were fabricated using the Cameco feed material, and similar characterization and comparisons were performed. The sintering studies proposed using actual plutonium feed material were not completed this FY because fabrication personnel were assigned to other MD activities; however, they are expected to be completed in FY99. Finally, the phase diagram studies, both theoretical and experimental, were continued.

Although there is much more work to be done to quantify fully the effect of gallium on the sintering kinetics of MOX fuel, the trend so far is fairly clear. In the high-temperature reducing environment typically used to sinter UO_2-based ceramics, almost all of the gallium initially present is volatilized. Even if none of the gallium were removed from the starting powder, residual gallium levels in the fuel would not be much greater than 10 ppm. Therefore, removing as much of the gallium from the powder as is practical before fuel production is required. At the higher gallium levels in the UO_2–CeO_2–Ga_2O_3 experiments, transient liquid phase sintering is clearly evident, which results in coarse intergranular porosity that cannot be removed by further sintering. Therefore, it is still necessary to reduce the gallium level, particularly the amount of Ga_2O_3 present, before the powders are blended. At this stage, it is not easily discernable what, if any, effect residual amounts of gallium below the 500- to 1000-ppm level may have on the sintering kinetics; however, this question should be answered by the AUC sintering study now underway.

The studies to date have demonstrated further the value of studying the thermodynamics and phase relationships in the Pu–Ga–O and Ce–Ga–O systems. It appears likely that the limiting phase controlling the removal of gallium from the starting powders, as well as the ultimate form of the gallium in the fuel, may be the perovskite Pu (Ce) GaO_3, which before this work had not been identified under the conditions used in the sintering or operation of nuclear fuels.

4.0. ANALYTICAL METHODS DEVELOPMENT

The continued development of analytical techniques used in conjunction with the fabrication of MOX fuel was considered necessary for several areas in FY98. The technical tasks included in this activity were to

- continue development of an MXRF system to measure the spatial distribution and bulk concentration of gallium in PuO_2 feedstock, unsintered MOX fuel, and sintered fuel pellets;
- continue development and implementation of O/M measurement techniques;
- assess the ability to measure gallium concentrations using the existing LIBS capability in TA-55; and
- complete implementation of autoradiography measurement techniques.

These techniques directly supported other ongoing MD program activities in FY98, including R&D and test fuel fabrication efforts. The MXRF and LIBS techniques were needed in the TIGR R&D efforts, whereas the O/M and autoradiography measurements were needed for both the R&D fuel fabrication and ATR test fuel fabrication. In addition, these techniques and the results obtained from their analyses this year ultimately supported the successful fabrication of MOX fuel for the plutonium disposition mission (i.e., the ATR average power test fuel).

4.1. MXRF Development

As work has progressed in ongoing R&D efforts, a need has been demonstrated for a sensitive, spatially resolved method of gallium detection. The goal of this task then was to develop the MXRF system further to measure the spatial distribution and bulk concentration of gallium in PuO_2 feedstock, unsintered MOX fuel, and sintered fuel pellets. This task was a continuation of past efforts, where MXRF demonstrated its unique ability to provide rapid elemental information that could not be obtained with any other analytical method in elucidating the movement of gallium in surrogate MOX fuel pellets under reducing conditions. In addition to being nondestructive and requiring minimal sample preparation, MXRF offers many other advantages over conventional electron microprobe techniques for acquiring elemental distributions from a sample, including higher sensitivity, greater penetration depth, the ability to operate in air, and large area sample analysis. Studies performed with MXRF include (1) elemental detection capabilities of the technique, including spatial resolution, (2) demonstration of phase identification abilities, and (3) developmental work for MXRF as a more widely known measurement technique, especially for gallium in MOX fuel surrogates.

MXRF was used in FY97 to study MOX surrogate pellets consisting of a CeO_2 matrix with 2% gallium oxide as a starting material. These studies demonstrated that gallium aggregates along grain boundaries of the matrix material and the surrogate pellet exterior when the pellet is exposed to a reducing atmosphere. In FY98, research on method development improved the MXRF gallium sensitivity, which should aid in

detecting gallium aggregates in real MOX pellets. The improved sensitivity for gallium was due to four factors described below. A discussion of studies regarding the phase of gallium in surrogate pellets also is provided.

4.1.1. Hardware Improvements

During FY98, a high-powered 100-W x-ray tube was installed in the Kevex Omicron MXRF system (the same instrument used for the FY97 studies), which replaced the 50-W tube and provided twice the power. The 100-W source, at a voltage of 20 kV, gave elemental peak intensities from a National Institute of Standards and Technology Standard Reference Material 1643c dried residue sample about three times the intensity obtained using the 50-W tube. This increase was due to a factor-of-three increase in current at 20 kV for the 100-W tube compared to the maximum current obtainable with the 50-W tube.

A monolithic polycapillary optic was installed in the Kevex MXRF instrument in FY97 to enhance the gallium sensitivity. This sensitivity improvement was possible because the optic provided a much higher flux of x-rays to spatially shape the primary beam than the small pinhole apertures did. The polycapillary actually focuses the x-rays to a spot with a diameter of a few hundred microns or less. In addition, the high-power x-ray source can be used in conjunction with the capillary for even better gallium sensitivity. During the FY97 studies, only a moderate improvement in gallium sensitivity was achieved over using a pinhole beam collimator because of inherent instrument geometric constraints. The capillary was designed to be shorter than its ideal length to fit into the Kevex unit, and this short length hindered its high-energy x-ray transmission efficiency. Although the gallium sensitivity improved, the result was a poorer gallium signal than would be obtained using a longer ideal optic. However, by aligning the optic very precisely with the source and using an x-ray filter on the detector, the gallium sensitivity improved significantly over the aperture optic.

X-ray transmission is sensitive to the alignment of the capillary, and movement of <100 μm in the x or y direction results in a severe loss in signal. A reproducible method of aligning the capillary was established using shims, which allowed incremental movements as small as 20 μm in the x and y directions. Plans currently are being pursued to modify the capillary stage with micromanipulator screws for even more optimal and reproducible alignment.

Another important parameter in using the capillary is the focal spot size because this determines the MXRF image lateral resolution. Also, focusing the x-ray beam to a small spot allows better gallium sensitivity from the microdomains that are observed in MOX surrogate pellets (and potentially in real MOX pellets). Higher-energy x-rays >17 keV were found to penetrate the capillary optic without being focused. If the operating voltages are >~24 kV, then significant beam spreading occurs, and poor image lateral resolution is the result. Based on these observations, the source is operated at 20 kV when using the capillary.

The capillary focal spot size was determined by moving a tungsten-foil knife edge across the x-ray beam. The distance between the optic and sample then was varied, and focal spot sizes were determined at each distance. A minimum focal spot width of 36 μm full width at half maximum was achieved for the tungsten Lα line (8.4 keV). This

is actually slightly larger than the effective spot size for exciting the gallium K line (atomic emission is represented in terms of K and L lines) at the 9.2-keV line. This is due to the inherent change in spot size as a function of x-ray energy through the polycapillary. Thus, the capillary provides the capacity to detect gallium inclusions significantly smaller than 100 µm in diameter.

4.1.2. Sensitivity Improvements

The elemental sensitivity performance of the capillary was determined by analyzing a NIST SRM 1833 silica-based glass thin film, which contained silicon, potassium, titanium, iron, zinc, and lead at concentrations of a few weight percent each. Spectra acquired from the sample using the capillary were compared with spectra obtained using a 50-µm aperture source collimator because the focal spot using this aperture was closest in size with the capillary spot size. A capillary intensity gain of ~350 was observed for the low-energy silicon and potassium Kα lines vs using the 50-µm aperture. However, because of the low transmission efficiency of the capillary for higher-energy x-rays, the intensity gain at the higher-energy lead L line (10.5 keV) was considerably less (~18). A gain of 18 is still a marked improvement over using the aperture. Spectra also were acquired from Plexiglas using the capillary and the 50-µm aperture. A spectrum from Plexiglas actually shows the source emission profile due to the source x-rays scattering off the sample rather than inducing fluorescence. The intensities from the Plexiglas spectrum acquired using the capillary were divided by those from the aperture spectrum and plotted as a function of energy (see Fig. 4-1).

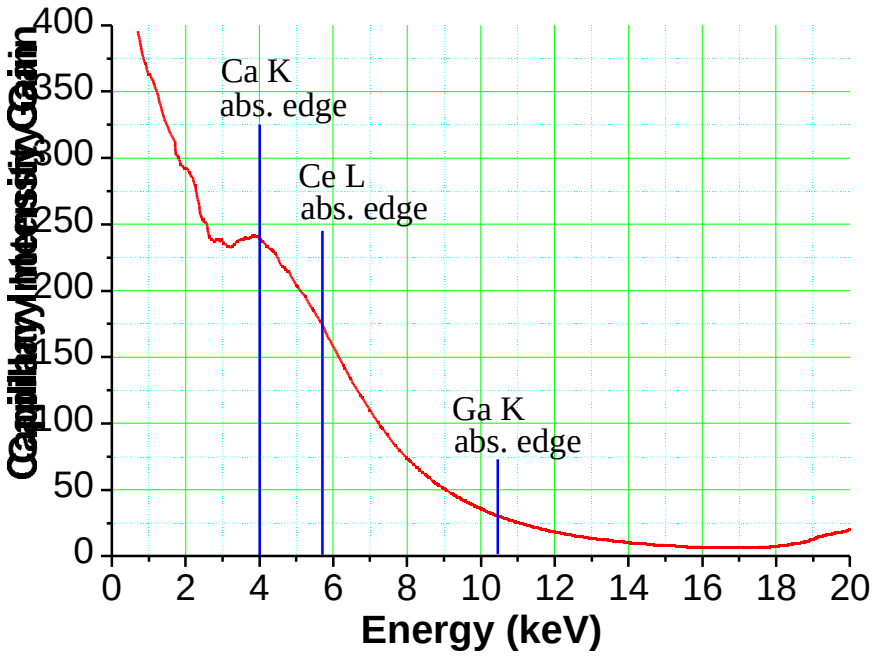

Fig. 4-1. Intensity gain curve using polycapillary for excitation of a Plexiglas specimen.

Gains as high as 400 were seen in the low-energy regime; even at the higher-energy Ga–K absorption edge, a gain of ~30 was obtained.

To improve the capillary high-energy analyte line sensitivity (gallium and other elements), a $CaCO_3$ filter was placed over the instrument detector, which attenuated the cerium signal in the MOX surrogate samples. This allowed the source current to be increased without saturating the detector electronics. This resulted in boosting the gallium peak intensity because the filter did not attenuate gallium as substantially as cerium. To date, the most optimized filter resulted in an increase of 3.2 in the gallium peak intensity when compared with using the capillary without the filter. Using the capillary and filter with the source at 20 kV provided a gallium peak intensity 5.4 times greater than using the 50-µm aperture at 50 kV and 15.1 times greater than using the aperture at 20 kV. Figures 4-2a and 4-2b show a comparison of the gallium images acquired from a surrogate pellet reduced at 1000°C. Figure 4-2a was acquired using the 50-µm pinhole collimator and the 50-W source, and Fig. 4-2b shows the substantial improvement in gallium sensitivity obtained by using the capillary, detector filter, and 100-W source. The mean gallium pixel intensity from the image acquired with the capillary and filter is ~12 times greater than the image obtained using only the aperture. The thickness of the filter could be tailored further to attenuate the gallium peak less, which would result in an even stronger gallium signal.

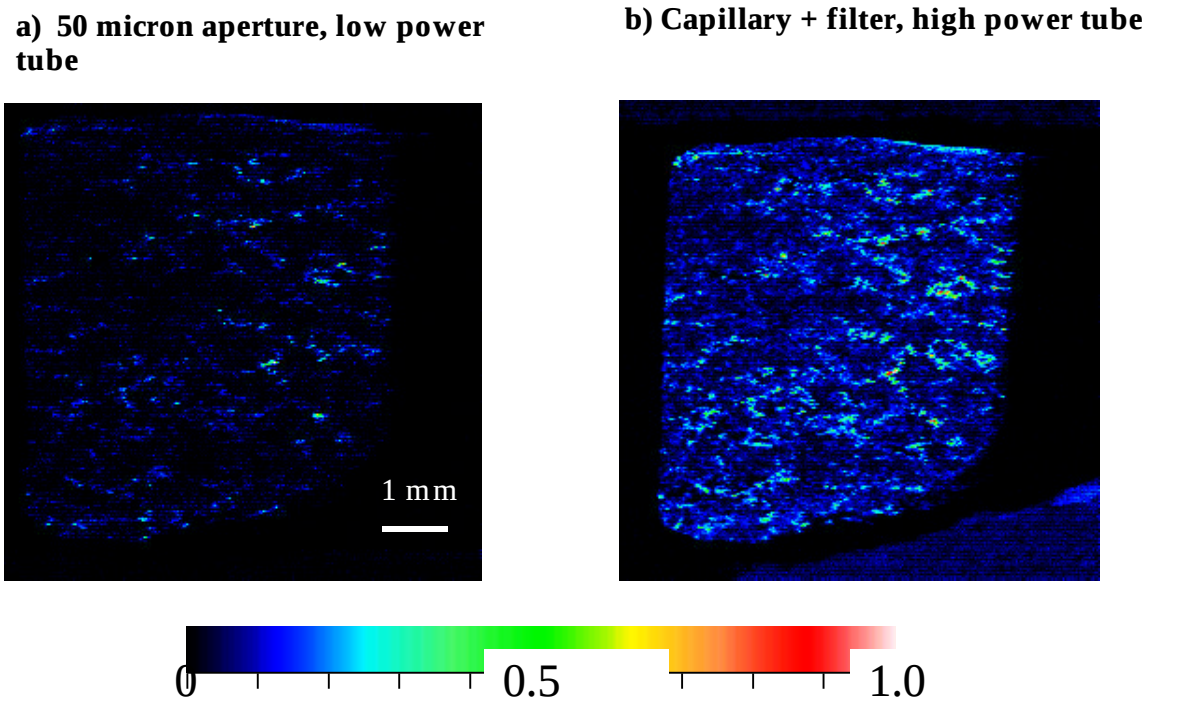

Fig. 4-2. MXRF gallium images of 1000°C MOX feed surrogate under two excitation conditions.

4.1.3. Ideal Capillary Comparisons

Studies were performed comparing the high-energy x-ray throughput of the short optic (29 mm long) to a longer (73 mm), more ideal polycapillary optic. These studies were performed at X-Ray Optical Systems (XOS), the company that manufactured the capillary. Because the longer 73-mm optic would not fit into the Kevex system, comparison studies were performed at the XOS company site in Albany, New York. A dried-spot residue was prepared from NIST SRM 1643c. The limit of detection (LOD) for the iron Kα line from this sample using the 73-mm optic at 50 kV was 227 ppt, whereas the iron LOD using the shorter optic at 20 kV was 1.1 ppb (approximately five times worse than with the longer optic). The short optic spectrum was not obtained at 50 kV because above 20 kV, the capillary focal spot was not focused and widened significantly.

A 50% Ga_2O_3 and 50% CeO_2 sample 200 µm in diameter was prepared to compare the gallium sensitivity in a cerium matrix using the two optics. All of the spectra were acquired using a source current of 0.1 mA, which was the maximum available current using the XOS system. Figure 4-3 is an overlay comparison of the gallium and cerium peaks using the 29- and 73-mm-length optics at different voltages. The gallium peak intensity using the XOS optic at 50 kV is 20 times greater than that using the LANL optic in the Kevex Omicron system at 20 kV.

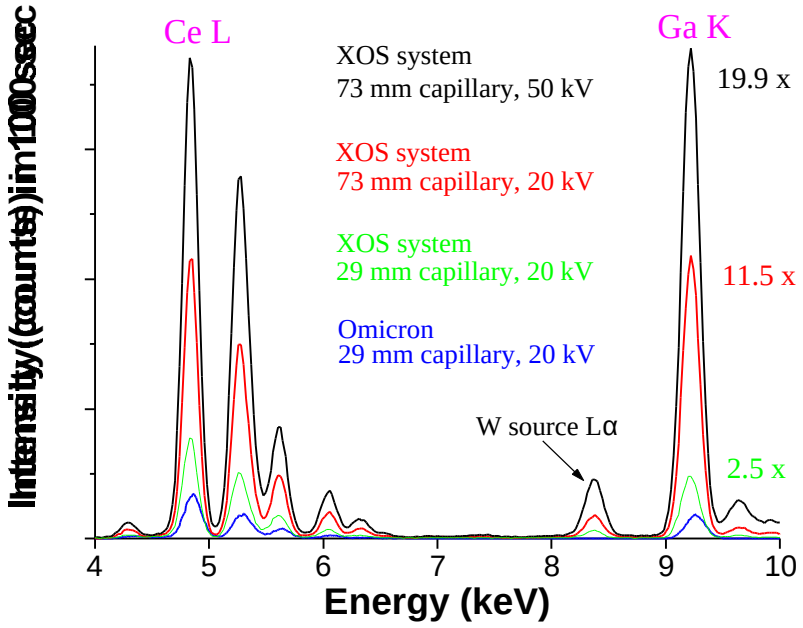

Fig. 4-3. Comparison of polycapillary optics and excitation voltages, which shows a gain in intensity for MOX surrogate elements.

4.1.4. Quantitative Imaging

All MXRF images acquired with the Kevex system spatially display the relative intensity differences (relative concentration differences) for a given elemental line. Only regions higher in concentration for a particular element relative to the rest of the sample can be determined directly from these images. Absolute intensity and concentration information is not directly available. Thus, true quantification of these images cannot be performed directly on the raw images. However, during FY98, a protocol was developed for determining actual pixel intensity values from an image by importing the raw image into an image processing program (Fortner Research's Transform). This program converts the image pixel colors into numeric values, which then can be translated into intensities and ultimately into concentration values using standards. Using the transform program, histograms of an image also can be prepared showing the number of pixels corresponding to a given concentration over a range. This preliminary work has demonstrated that quantitative imaging is feasible; however, the work is still in progress and requires additional development.

4.1.5. Identification of Gallium Phases in Reduced Surrogate Pellets

Although MXRF is capable of detecting gallium in the surrogate pellets, the phase of the gallium remains unknown. A small effort involving several collaborators was initiated to determine the gallium phase and explore potential analytical methods for measuring the gallium phase in real MOX pellets.

Collaborative efforts were pursued to study MOX CeO_2–Ga_2O_3 surrogates using Auger spectroscopy. A reduced surrogate pellet, with observable gallium inclusions shown by MXRF, was imaged using Auger spectroscopy, as shown in Fig. 4-4. A 9-to-1 Ce-to-Ga peak intensity ratio was observed from several gallium inclusions. Because Auger is a highly sensitive surface method, there was no possibility of the bulk material contributing to the cerium signal. Three points (1, 2, and 4) were within a white gallium-rich inclusion and two points (3 and 5) were in the cerium matrix. Representative spectra from points 1 and 3 are shown in Fig. 4-5. Only the white area shows a gallium signal. The carbon was cleaned off the surface with ion beam sputtering and still showed similar intensity ratios for the gallium and cerium. The point of interest in the lower spectrum of the white inclusion (point 1) is that both gallium and cerium were present in the spectrum, indicating a mixed elemental phase. Further support of a mixed gallium phase is evident in the Auger images shown in Fig. 4-6. These images of cerium, oxygen, and gallium cover the white inclusion. Although the cerium image is dark in the gallium region, there is still a cerium signal present in the gallium-rich region. The same applies for the oxygen map. These Auger data suggest a mixed Ce-Ga phase with a Ce-to-Ga ratio of 9 to 1. Although there are no known mixed cerium gallates, this work is important in understanding what possible phases might form when plutonium and uranium are the matrix materials.

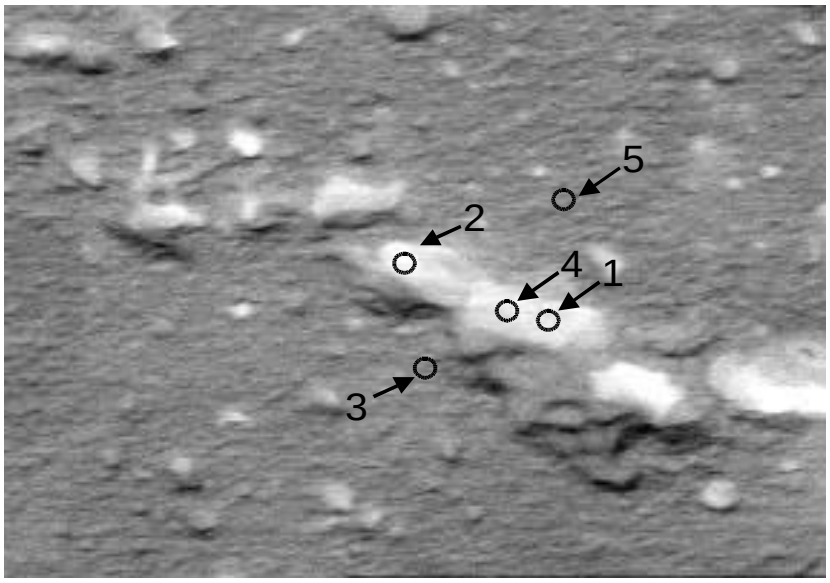

Fig. 4-4. An Auger image of MOX-feed surrogate-pellet gallium inclusions. The labeled points indicate Auger spectra locations.

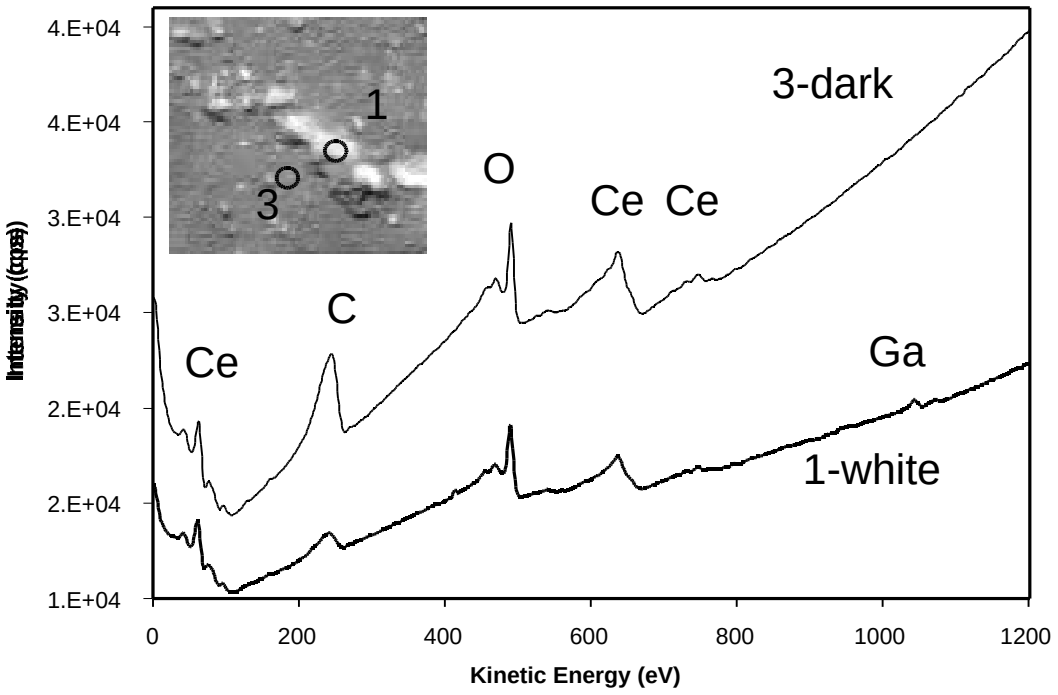

Fig. 4-5. Auger spectra from points 1 and 3, both on and off the gallium region.

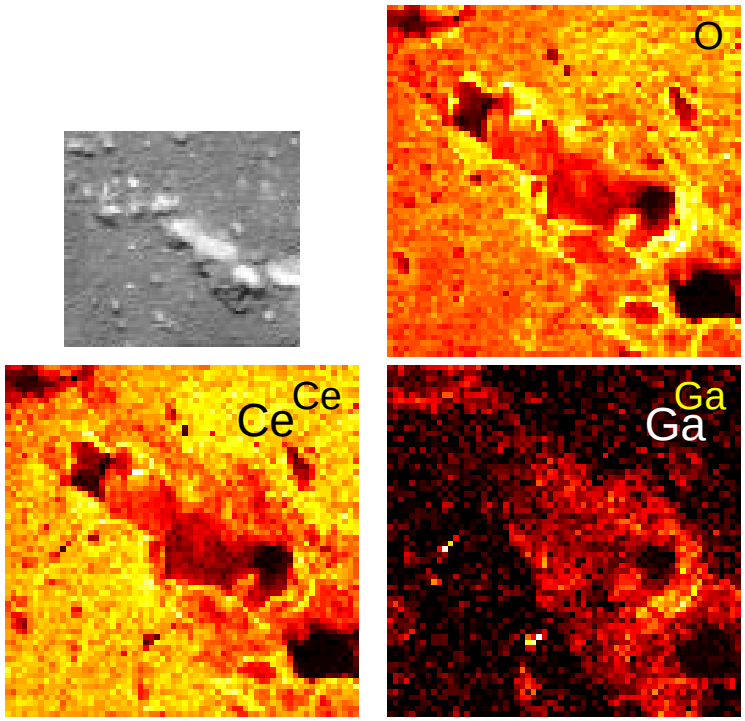

Fig. 4-6. Auger elemental maps over the gallium inclusion.

Collaborative work also was undertaken with ORNL to examine surrogate pellets using SEM, electron diffraction, and micro-x-ray diffraction. Figure 4-7 shows an SEM image of the cerium grains. The elemental maps showed that gallium resided in the grain boundaries. However, all attempts to obtain diffraction patterns for possible phase identification were unsuccessful. This means that the mixed Ce–Ga phase appears to be amorphous and will not be detected by crystallographic methods.

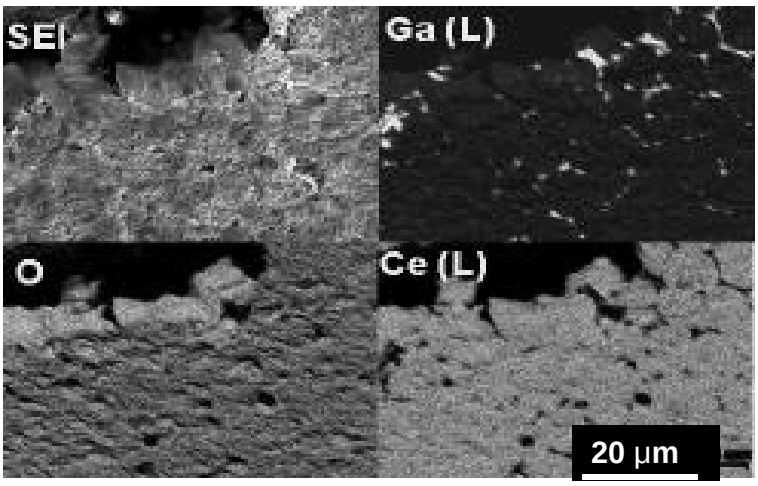

Fig. 4-7. SEM backscatter image and elemental images of MOX feed surrogate pellet.

Because the diffraction methods were unsuccessful in identifying or at least obtaining a spectrum, the surrogate pellets were analyzed by Raman imaging and Raman spectroscopy. The spectra of the gallium inclusions, along with a pure gallium oxide, are shown in Fig. 4-8. It is clear that the gallium-rich inclusions are not gallium oxide. Figure 4-9 shows different images of the grain boundary material. This figure shows the CeO_2 grains with some material between the grains. The Raman image in the center shows the cerium matrix as white and the gallium-rich grain boundaries as black. This shows that there appears to be a Raman active phase in the grain boundary of the cerium matrix. Figure 4-10 shows the Raman image, as well as spectra from the two regions of the grain and grain boundary. The presence of the peak at 461 cm^{-1}, which is assigned to the CeO_2 matrix, confirms the presence of a mixed Ce–Ga phase in the white grain boundary areas. The difficulty lies in identifying this mixed phase. Extensive analytical studies and molecular orbital calculations need to be performed on the white inclusions to identify the composition of this mixed phase. It appears that Raman spectroscopy and imaging can be used to identify this mixed phase, but additional efforts are needed to fabricate reference materials and determine positive phase identification. More information on this and other analytic R&D activities can be found in Ref. 4-1.

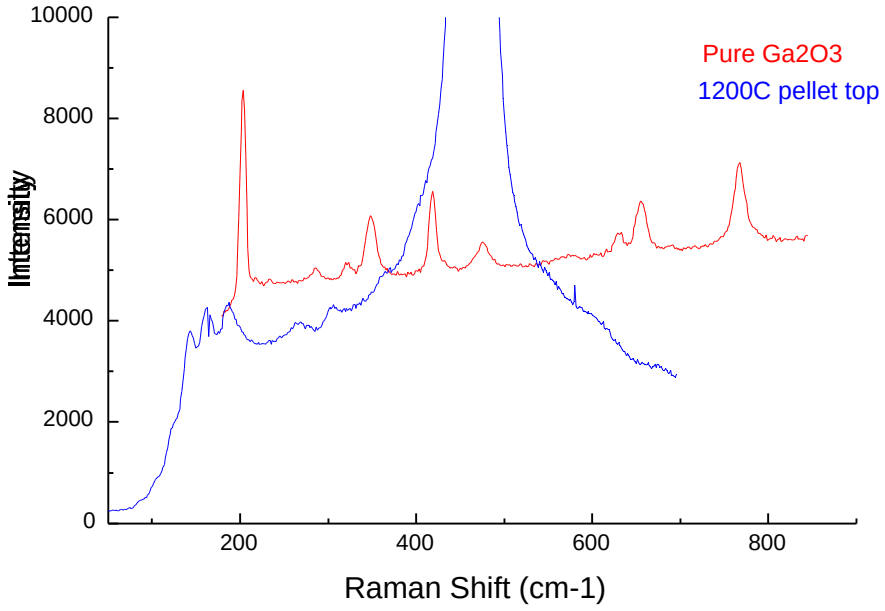

Fig. 4-8. Raman spectra of gallium-rich inclusion and gallium oxide powder. The large peak in the gallium-rich inclusion is due to CeO_2.

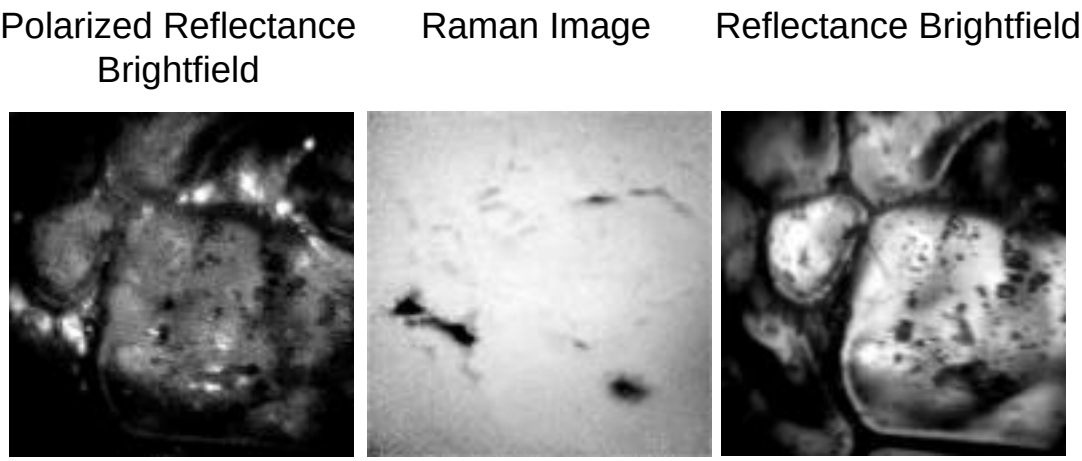

Fig. 4-9. Brightfield images and Raman image of CeO_2 grains and grain boundary gallium-rich material.

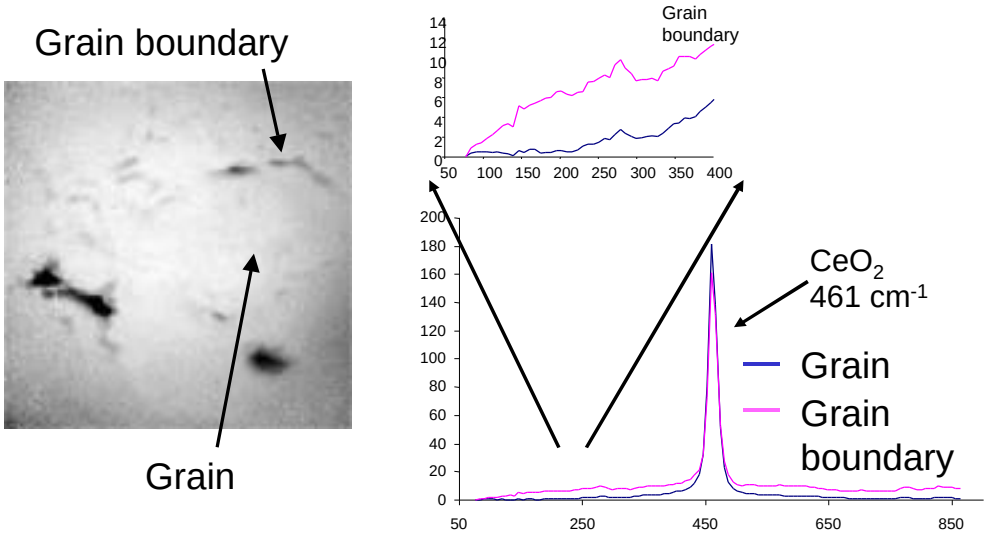

Fig. 4-10. Raman spectra from the CeO_2 matrix grain and grain boundary gallium-rich region.

4.2. O/M Measurement Technique Evaluation

This fiscal year, efforts were undertaken to identify potential O/M measurement techniques for eventual use in PF-4. Although the existing O/M measurement technique is sufficient for current activities, it is time consuming, and it is likely that future efforts may require more accurate measurements. In FY98, a comprehensive survey of the literature of all the different methods used to determine the O/M ratio

was completed, and it is in the final editing stage (Ref. 4-2). This is a very comprehensive survey citing over 1200 references and comprising over 200 pages. The report will be completed in early FY99 at no additional cost to the DOE-MD.

4.3. LIBS Capability/On-Line Gallium Measurement

This task continued to develop an on-line method for determining trace gallium concentration in PuO_2 in real time as the product is treated for gallium removal. Preliminary investigations suggested that LIBS is the best candidate for on-line analysis because (1) critical LIBS components can remain external to the glovebox, and (2) the technique was already in the early stages of setup in the plutonium facility. Thus, this system was installed in PF-4 and demonstrated for gallium and plutonium analyses. Gallium and plutonium standards also were developed for use with the system. The ultimate use for this technique was as a real-time measurement system for TIGR R&D activities (see Section 5.0). This effort will continue into FY99 and be funded directly under the TIGR R&D task. As such, all efforts associated with this task will be integrated with the TIGR R&D activity, and plans will be developed concurrently for the system's implementation into the Phase II ARIES demonstration line.

The LIBS technique uses a focused, pulsed laser source to generate high-energy densities needed for plasma formation. Light emitted by the laser-induced plasma contains emission line spectra characteristic of plutonium and all other elements present in the sample. A high-resolution spectrometer is employed to resolve these emission lines and their intensities spectrally. Elemental composition and quantitative information are obtained through careful analysis of the spectra. LIBS can be performed on metals, compressed powders, and even liquid solutions.

The LIBS has been developed for use in PF-4 for the quantitative analysis of gallium in PuO_2. LIBS supports TIGR to provide a rapid turnaround time and on-line quantitative analysis for gallium in PuO_2. Although not new technology, published LIBS spectra for plutonium and plutonium compounds do not exist in the literature. Additionally, the capability to perform LIBS in PF-4 did not exist before this project.

4.3.1. Experimental Description and Results

The current LIBS system installed in PF-4 utilizes a pulsed neodymium/yttrium aluminum garnet laser operating at its fundamental infrared wavelength of 1064 nm. This laser emits 5-ns pulses and is rated at 420 mJ/pulse at 20 Hz. The 6-mm-diam beam is focused to a spot size of <100 μm and generally is attenuated to <25 mJ/pulse. This pulse generates an energy density of ~10^{11} W/cm^2 and easily exceeds the breakdown threshold for all samples analyzed to date. The resultant flash of light is focused onto the entrance slit of a spectrometer, and the dispersed light is imaged onto a two-dimensional intensified charge-coupled device (CCD) camera. The image consists of 384 vertical by 576 horizontal pixels. A fast-delay generator provides high-speed gating for the intensified CCD (ICCD) so that the temporal evolution of the plasma plume can be followed. Spatial information is preserved, and the spatial evolution of the plasma also can be followed. Additionally, the sample is enclosed in an evacuated chamber so that the buffer gas composition and pressure can be varied. All data presented here were collected using 100-torr helium as the buffer gas.

The first several months of FY98 were spent installing the LIBS system in PF-4. This consisted of many crafts jobs, including seismically mounting the optical table, connecting the gas and electrical services, moving necessary instrumentation into PF-4 from cold laboratories, and obtaining approval for the experimental procedure. The first plutonium LIBS spectrum was collected in early March 1998.

Cold experiments revealed that gallium has two principal emission lines of high intensity, 403.299 and 417.204 nm. Because the emission spectrum of plutonium contains more than 32,000 lines in the wavelength range of 200 to 2000 nm, resolution became of paramount importance. Currently, the LIBS system employs a 1-m focal length spectrometer utilizing a 3600-g/mm grating and has a resolution >0.02 nm. The gallium line at 417.204 nm was found to be the most intense and best suited for LIBS analysis. Table 4-1 contains a list of plutonium emission lines in the region of interest.

These eight lines in a spectral region of <2 nm constitute the current region chosen for analysis. Spectral dispersion across the 576-pixel horizontal span of the ICCD is 1.87 nm, or 0.00325 nm/pixel. Normally, a minimum of five pixels are required to define a line shape. This definition would produce a resolution of ~0.016 nm. Several features concerning Table 4-1 should be noted. First, all lines are resolved adequately by the current spectrometer configuration, with the exception of the weak plutonium line at 417.20541 nm that interferes with gallium at 417.204 nm. This wavelength difference of 0.001 nm may be resolved using a higher resolution spectrometer, but it is on the order of the $^{239}Pu/^{240}Pu$ isotopic splitting. Increased resolution may be hampered by observation of other plutonium isotopes. However, this plutonium emission line is so weak that very low detection limits for gallium are still possible. Second, the fact that some emission lines occur from neutral atoms and some from singly ionized atoms is important. At short delay times following the laser pulse (<100 ns), the plasma emission is dominated by ions. At later times, mostly atomic emission is observed. Because the

TABLE 4-1. PLUTONIUM EMISSION LINES IN THE REGION OF INTEREST

Element[a]	Intensity (relative)	Neutral (1) or Ion (2)	Wavelength
Pu	0	2	417.13088
Pu	2	unassigned	417.14646
Pu	5	2	417.16653
Pu	1	unassigned	417.18960
Ga	vs strong	1	417.204
Pu	1	unassigned	417.20541
Pu	7 (unsymmetrical)	1	417.24210
Pu	6	2	417.31072

[a]All plutonium positions are quoted from Ref. 4-3. These spectra were recorded on a 9-m-long photographic plate-type spectrograph and include data from 1962 to 1984. All line positions are for ^{239}Pu. Relative intensities are in half-log units ranging from 0 to 9. The gallium emission line is quoted from Ref. 4-4.

gallium emission is atomic, the strongest intensity (relative to plutonium) occurs at a relatively long delay time. Typically, a delay of 1 μs is used with a gate of 10 μs (the gate time represents the length of time that the CCD intensifier is opened, much as an electronic "shutter").

Although spectrally dispersed images of the plasma plume are collected on the two-dimensional ICCD array, the gallium and plutonium emissions generally are not well separated in space. The spatial evolution of plutonium and gallium emission within the plume is essentially the same. Thus, the 384 vertical pixels are typically "binned," or added together to create a conventional appearing spectrum of intensity vs wavelength (or horizontal pixel number). It is this spectrum that can be analyzed using off-the-shelf curve-fitting software to produce line intensities and integrated peak areas suitable for analytical comparison. Currently, a program called "PeakFit™" (Jandel Scientific) is being used to fit the spectral lines. Figure 4-11 shows a sample of output obtained from PeakFit™.

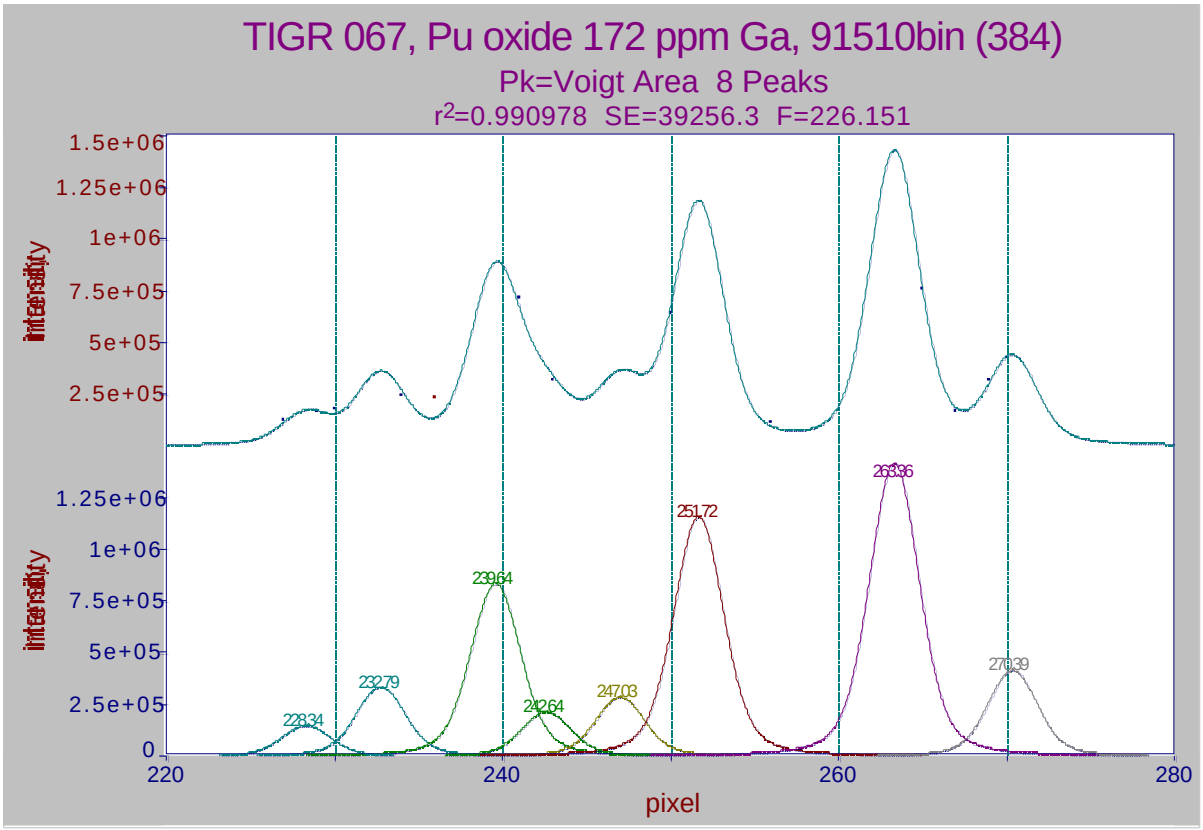

Fig. 4-11. A typical spectral line fit obtained from PeakFit.™

The spectral region spanned the eight peaks listed in Table 4-1. Gallium emission (417.204 nm) is seen at pixel 251.72. The actual binned (384 vertical channels) data from the ICCD were represented by the discrete points in the topmost plot. The bottom trace was the deconvolution by PeakFit™ using a Voigt Area algorithm. The sums of these Voigt curves formed the top trace through the data. Note that the plutonium line at pixel 263.36 corresponding to 417.24210 nm was most intense. Plutonium ionic lines at pixel 239.64 (417.16653 nm) and pixel 270.39 (417.31072 nm) were weaker but still visible at this long delay time of 1 μs. Thus, the plutonium peak at 417.24210 nm was chosen to ratio against the gallium line at 417.204 nm for preliminary analysis. In the initial fits, the linewidth (both Gaussian and Lorentzian components) for the Voigt algorithm were held constant so that either amplitude or integrated area ratios yielded the same result. A total of 12 PuO_2 samples were run under identical conditions as follows: laser energy ~20 mJ/pulse at 20 Hz and accumulations ranging from 2 to 20 s, 1-μs delay and 10-μs gate, and 100 torr helium as the buffer gas. All samples were products from small-scale TIGR runs, and portions had been analyzed by conventional destructive wet chemical techniques to yield gallium concentrations ranging from 34 to 8336 ppm. Table 4-2 summarizes these data, and Fig. 4-12 displays the results in the form of a calibration curve. From Fig. 4-12, it is noticeable that most of the data (10 of 12 data points) lie below 500 ppm and that the ratio of integrated area appears to become nonlinear at the highest concentrations. The plot appears scattered, but closer to linear, when only data <500 ppm is considered, as shown in Fig. 4-13.

TABLE 4-2. RESULTS OF GALLIUM CONCENTRATION MEASUREMENTS FOR SMALL-SCALE RUNS

Sample ID	ppm Ga[a]	Ga/Pu[b]
TIGR 076	34	0.45751
TIGR 010	40	0.47558
TIGR 034	43	0.28793
TIGR 108B1	82	0.57649
TIGR 007	112	0.53787
TIGR 073	121	0.61677
TIGR 516	127	0.49055
TIGR 092	136	0.36258
TIGR 067	172	0.81943
TIGR 031	414	2.6909
TIGR 037	2213	5.4055
TIGR 064	8336	9.9210

[a]Concentrations were reported by wet chemical analyses at the LANL Chemistry and Metallurgy Research Facility.
[b]These are ratios of the integrated area of the gallium line at 417.204 nm and the plutonium line at 417.24210 nm.

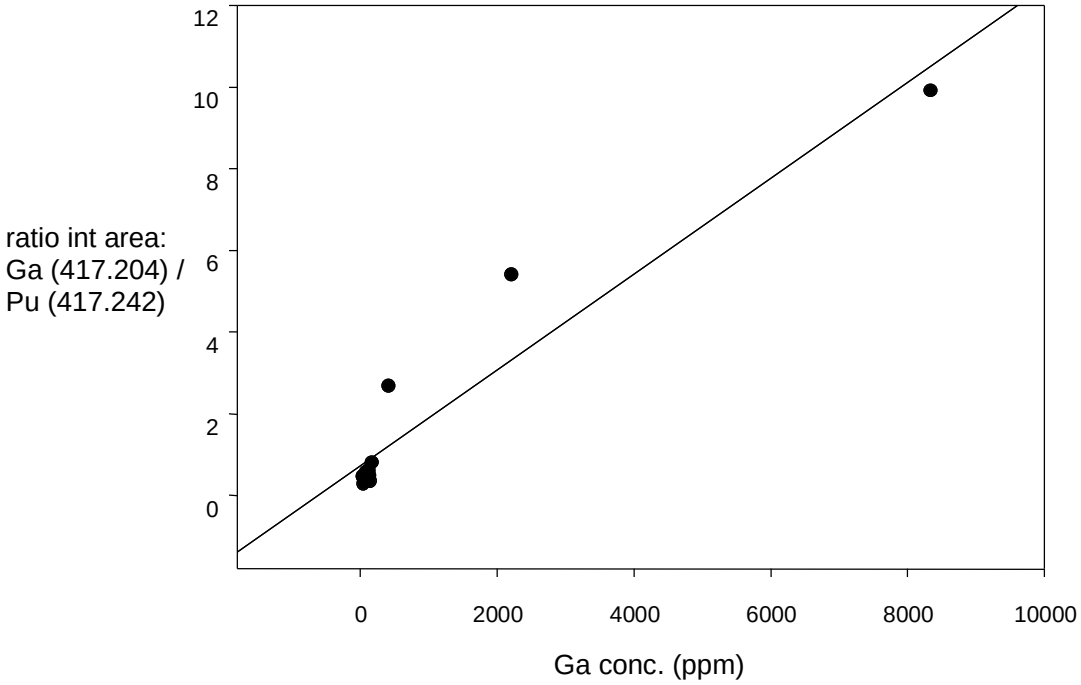

Fig. 4-12. Calibration curve for gallium concentrations.

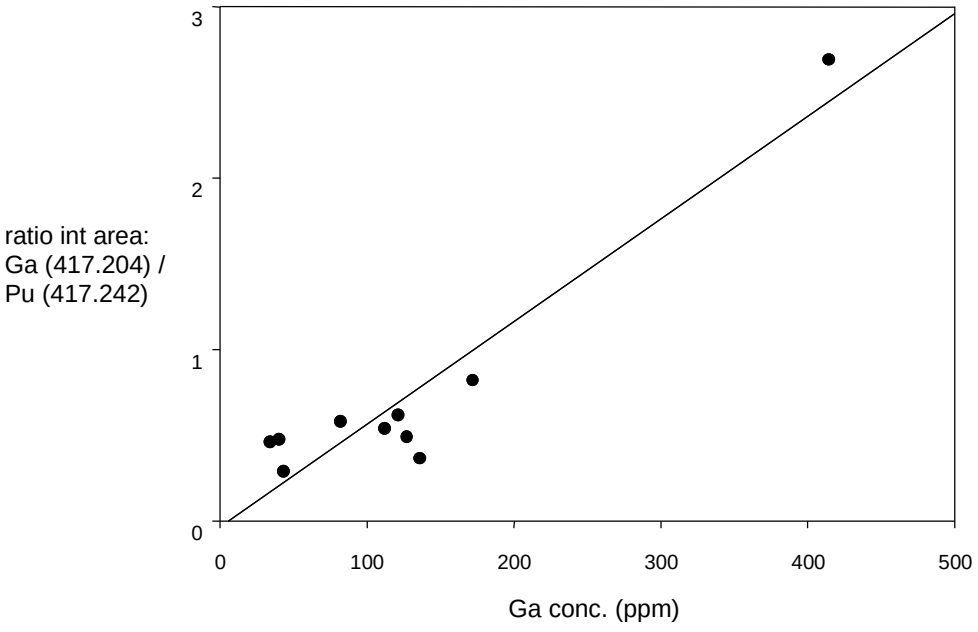

Fig. 4-13. Calibration curve for gallium concentrations <500 ppm.

All samples were prepared for LIBS analysis by being pressed into a thin layer at ~9.05E+04 psi, corresponding to 10,000 lb of hydraulic pressure acting on a 0.37-in.-diam pellet die. These data are to be regarded strictly as preliminary, and the scatter is to be treated with caution. Such scatter could be generated by irreproducibility in the LIBS technique, but it also could be due to the same irreproducibility in the wet chemical analysis of gallium content. An adequate set of dependable standards must be generated.

The nonlinearity of gallium emission intensity at high concentrations was expected. The concentration at which this saturation phenomenon is observed is element-specific and depends on adjustable experimental parameters, such as the laser energy, focused laser spot size, buffer gas composition and pressure, and delay time for the ICCD camera.

Plutonium metal samples appeared to yield similar peak area ratios for similar concentrations. The gallium/plutonium ratio for electrorefined plutonium (nominally 1 ppm gallium) remained larger than expected (one analysis yielded a ratio of 0.198). This result suggests that at very low gallium concentrations, the plutonium line at 417.20541 nm may have contributed to the apparent gallium intensity. This interference will limit the eventual lowest possible detection limit for gallium. However, it has been shown that a measurable integrated area ratio can be observed in the lowest gallium concentration TIGR sample analyzed to date, 34 ppm. Detection limits approaching 10 ppm should be possible in the near future.

4.3.2. Future Work

As part of the FY98 development plan, a fiberoptic laser delivery and emission light collection system was designed and built. This system adds a true in-line capability for LIBS because the fiber can be extended to any physical location in PF-4. Thus, when the full-scale TIGR system becomes operational, the PuO_2 can be analyzed in-situ without the need for excessive handling and resultant worker exposure. This fiberoptic system was installed on the PF-4 LIBS system in late FY98 and is currently fully operational. Future FY99 activities will work to enhance the emission light collection efficiency of this fiberoptic system. Currently, the system employs a single fiber for the laser delivery and light collection. It appears that a dual fiber configuration using a dedicated fiber for light collection will greatly increase the signal-to-noise ratio. Other parameters leading to increased light collection efficiency are the collection probe lens package diameter and F-number, type of fiber (i.e., bundled vs single, diameter, and material of composition), sample chamber mounting, and coupling to the spectrometer. Reference 4-5 provides more information about FY99 work activities.

4.3.3. LIBS Summary

LIBS has proven to be a very useful technique for the nearly nondestructive analysis of plutonium and plutonium compounds. The value of this technique rests in the rapid turnaround time, virtually no sample preparation, and essentially zero consumption of samples. LIBS data always will be highly matrix-dependent, and its utility critically depends on the generation of adequate standards for each matrix. The LIBS system in PF-4 was assembled and made functional during FY98 and has delivered all project milestones on time.

4.4. Autoradiography Development

This task evaluated improvements to the current autoradiography capability at LANL and provided information useful for a future MOX fabricator. A need has been identified to develop this in-house homogeneity measurement capability further for use with R&D and test fuel fabrication activities. The ultimate goal was to develop an autoradiograph technique for MOX fuel fabricated with surplus weapons plutonium that is semiquantifiable and quality-assurance certified as an effective homogeneity measurement technique. Although most of this work has been completed, it has not yet been reported. This will be done in early FY99 at no additional cost to DOE-MD.

5.0. GALLIUM REMOVAL SYSTEM

One of the critical steps in preparing weapons-grade plutonium for use in MOX fuel is the removal of gallium. At high concentrations, gallium can affect the sintering behavior of a ceramic such as PuO_2 and can result in damage to sintering furnace components. Therefore, to ensure consistent PuO_2 characteristics, it is important that the gallium concentration be as low as possible. In addition, gallium could react deleteriously with the zirconium-based fuel cladding. Consequently, it has been concluded that reducing the gallium concentration as low as possible before MOX fuel fabrication significantly reduces the risk of sintering and cladding failures. Two different processes for gallium removal have been examined: (1) TIGR by gallium vaporization and (2) classical aqueous processing such as ion exchange or solvent extraction. The TIGR process is a dry, low-cost, and low-waste method for removing gallium from the PuO_2 powder derived from the pit disassembly system.

The purpose of this task was to develop and design a dry gallium removal system based on the TIGR process for a system to be built and tested during FY98 through FY00. The TIGR process must be integrated directly with the PDCF; in particular, the ARIES/HYDOX (or equivalent) system and must satisfy the MOX fuel fabrication feed requirements. The effort during FY98 has been focused by way of (1) a TIGR R&D test plan (Ref. 5-1) and (2) a TIGR functional requirements document (Ref. 5-2). Midway through the fiscal year, the schedule was extended 6 months to be consistent with the latest schedule for ARIES development.

FY98 R&D activity was divided into five different tasks: (1) chemistry/physical characteristics, (2) development of a method for on-line gallium concentration measurement, (3) process development that leads to the prototypic design, (4) prototypic design and testing, and (5) cold prototype testing. Following feed fabrication development and validation, the surrogate feed material was used to verify furnace material compatibility and process material handling for the prototypic equipment. The PuO_2 feed material was used to demonstrate adequate gallium separation and to optimize process operating conditions. This entire activity is a 2.5-year effort, which will culminate in the final prototypic demonstration of the TIGR process. The results from the first year, FY98, are presented here.

5.1. Chemistry/Physical Characteristics

This activity included analyzing several samples in support of TIGR R&D activities; the results of these analyses appear throughout this and several other documents. As an on-going activity, samples were submitted for characterization of trace elements, anions, isotopic composition, assay, carbon, and water. Facility and instrumental problems delayed the processing of samples, but most analyses requested for FY98 were processed.

5.2. On-Line Gallium Measurement

During FY98, the on-line gallium measurement efforts in PF-4 were considered to be part of the analytical methods development area, and the results from their

development appear in Section 4.3 of this report. However, during FY99, the results will be reported as part of the TIGR process development.

5.3. Process Development

This task focused on several areas to demonstrate the adequacy of the TIGR process and aid in the selection of prototypic processing equipment and conditions. The goal of the work was to develop a dry process to reduce the gallium concentration of weapons-derived PuO_2 that can be integrated into the PDCF. A dry method for gallium removal is desirable for many reasons, including waste reduction and relative ease of facility licensing. A dry method for removing gallium from PuO_2 was thought to be possible based on initial calculations. It was theorized that a reducing gas could be passed over the powder, thereby reducing the solid Ga_2O_3 to Ga_2O gas using Eq. (1).

$$Ga_2O_{3(s)} + 2H_{2(g)} \rightarrow Ga_2O_{(g)} + 2H_2O_{(g)} \quad (1)$$

During FY97, tests incorporating CeO_2 surrogates and $Ar–H_2$ gas confirmed that such a process was viable.

TIGR process and prototype development was initiated at the start of FY98. Preliminary work included identifying and acquiring glovebox space; purchasing, installing, and testing equipment; and obtaining approvals for conducting TIGR experimentation. Experimental details and results to date of TIGR tests are discussed in the following sections.

5.3.1. Experimental Details

Process development efforts are described in four different areas: material characteristics, test procedure, analysis techniques, and reproducibility. Characterization efforts included gallium concentration and particle morphology (i.e., size distribution and surface area).

5.3.1.1. Material Characteristics

The process development tests incorporated surplus weapons PuO_2, which was produced using the three-step process at LLNL (see Section 3.1.2 for more information). Analysis of the powder indicated a bimodal particle size distribution, with a significant fraction of the powder comprising submicron particles (see Fig. 5-1). This powder was found to have a surface area of 6.4 m^2/g (+/- 0.3 m^2/g). Chemical analysis of this powder (using ICP-MS) indicated a gallium concentration of 0.87 wt % [8700 $\mu g/g$ (ppm)], or 1.1 at. %.

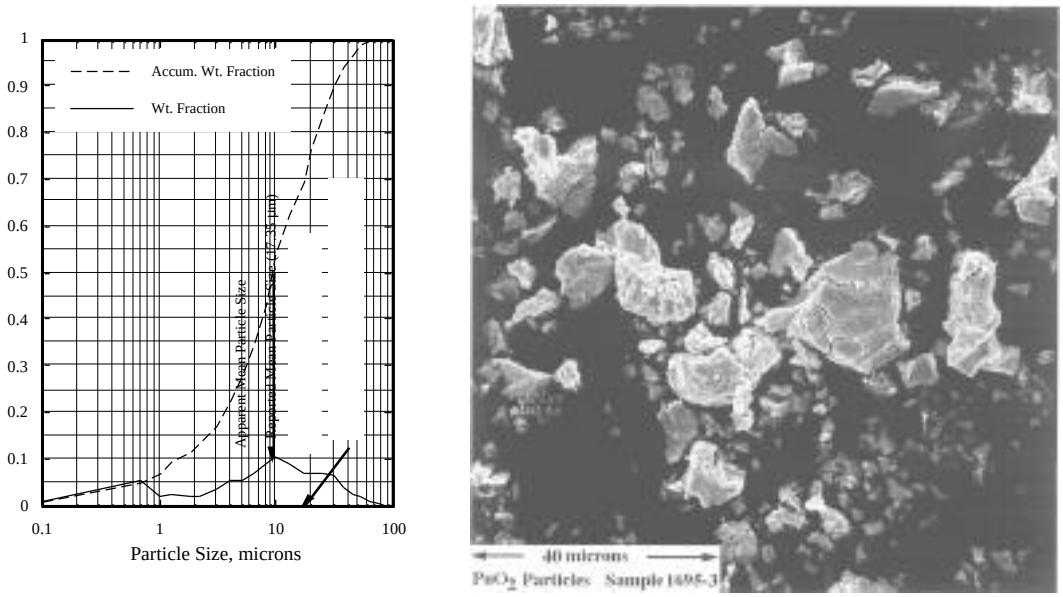

Fig. 5-1. Particle size distribution and micrograph of three-step PuO_2 powder.

5.3.1.2. Test Procedure

TIGR tests involved the exposure of PuO_2 to Ar–6% H_2 gas (O_2 < 8 ppm, H_2O < 0.7 ppm). PuO_2 samples (typically 0.3, 0.9, and 2.5 g) were weighed, placed in nonreactive alumina boats, and then reweighed, noting the gross weight of each boat. These small boats then were placed into a large alumina boat to facilitate handling. The large boat was inserted into the hot zone of a tube furnace (see Fig. 5-2). The temperature was ramped at a rate of 20°C/min until the temperature of interest was reached. The samples were held at that temperature for a fixed period of time. At the end of this period, the furnace was turned off, and the samples were allowed to furnace cool. Following cooling to nearly room temperature (<50°C), the samples were removed from the furnace, the gas flow was stopped, and the gross weight of the boats was recorded. Note that a sample exposed to a higher temperature for the same duration of time as one exposed to lower temperature is exposed to an elevated temperature for a longer period of time because of the increased ramp-up and ramp-down time. The temperature, time at temperature, sample mass, and gas flow velocity were varied in an effort to determine the rate limiting step and thus optimize gallium removal.

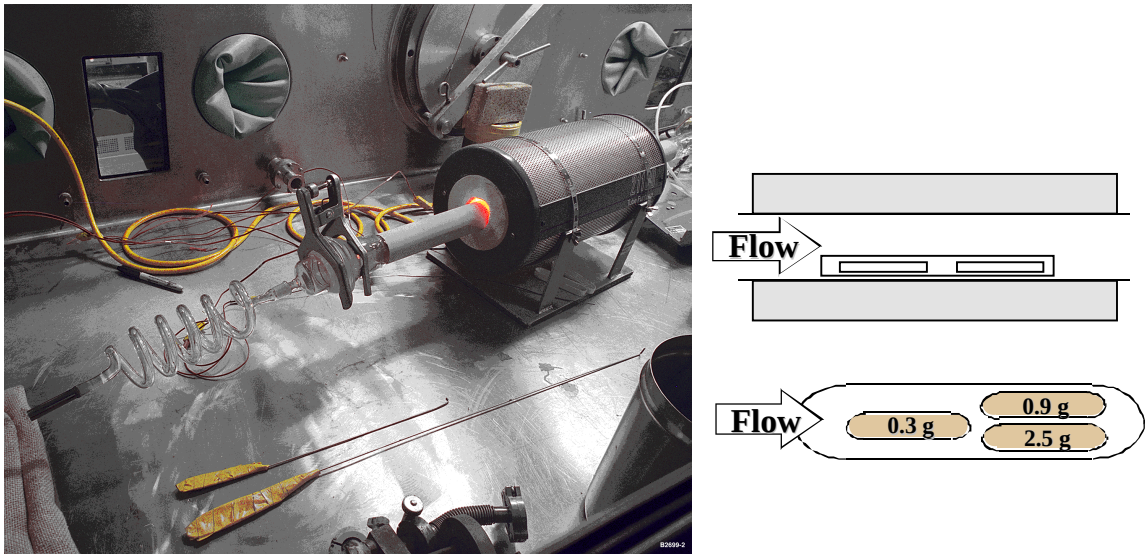

Fig. 5-2. Furnace setup (left); drawing of boat placement within furnace (top right); arrangement of small boats within the large boat (bottom right).

5.3.1.3. Analysis Techniques

The extent of gallium removal is determined best by chemical analyses following sample exposure. However, weight loss measurements also can be used to infer gallium removal. This technique is used when the gallium concentration has not been determined by chemical analysis. Figure 5-3 shows that weight loss measurements correlate well with the gallium loss. Thus, weight loss may be used as a predictor of gallium loss. Note that weight losses >2% are observed even though Ga_2O_3 comprises only 0.87 wt % of the starting material. This indicates that significant reduction of the PuO_2 occurs concurrently with Ga_2O_3 reduction / Ga_2O evolution.

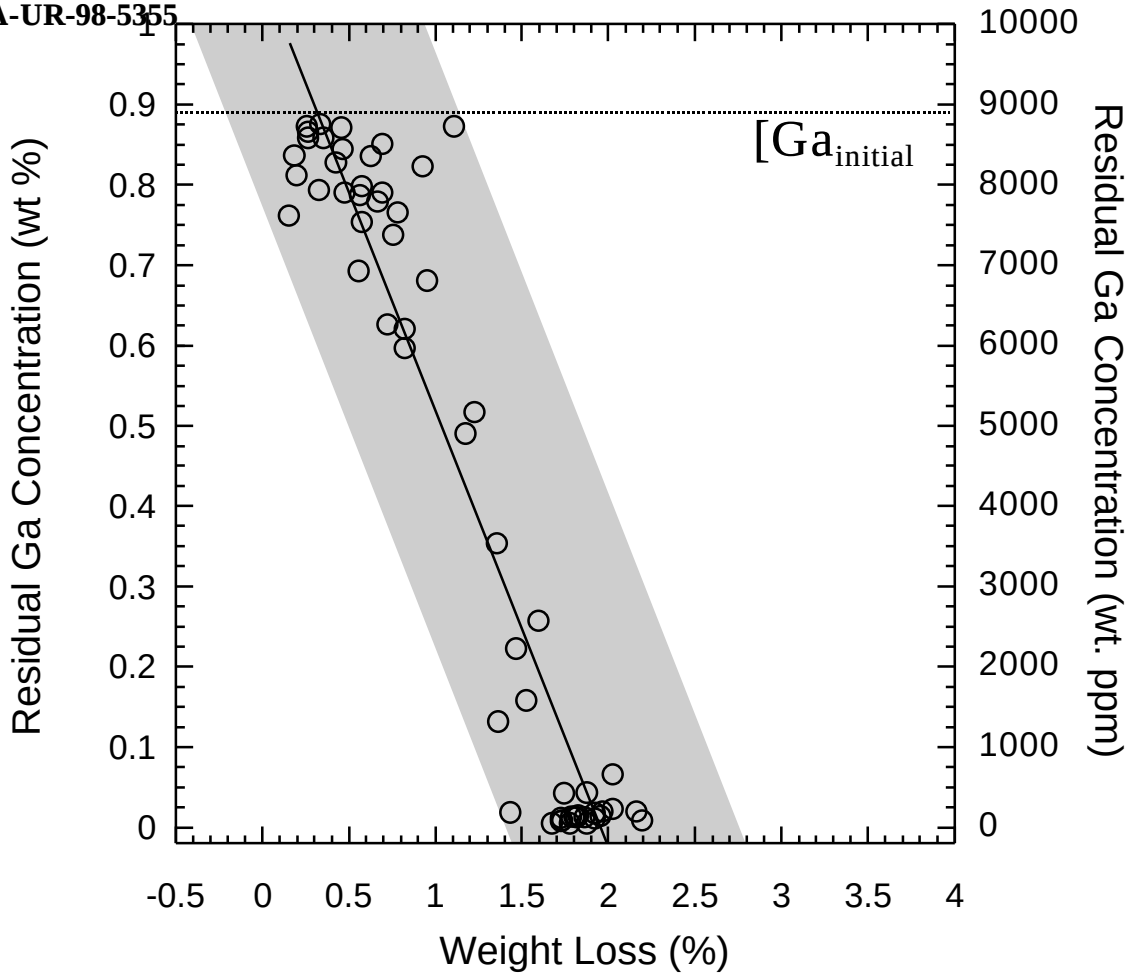

Fig. 5-3. Correlation of weight loss to remaining gallium concentration following exposure for various sample masses, exposure temperatures, durations, and gas flow rates.

5.3.1.4. Reproducibility

Weight loss measurements yielded superior reproducibility as compared with gallium concentration analyses. Weight loss measurements on four replicate tests (1200°C, 4 h, and 1.5-cm/s gas flow velocity) had standard deviations of 7.0%, 12%, and 7.6% for samples of 0.3, 0.9, and 2.5 g, respectively. Gallium measurements were less reproducible. Three replicate tests (1200°C, 4 h, and 1.5-cm/s gas flow velocity) yielded standard deviations of 29%, 8.9%, and 4.2% for samples of 0.3, 0.9, and 2.5 g, respectively. Some of the gallium measurement error may have originated from contamination of the samples. This is consistent with the larger standard deviations and gallium concentrations observed in smaller samples (i.e., 0.3-g samples).

5.3.2. Experimental Results

This section presents results obtained from the processing parameters studied, including temperature, time, sample mass, and flow rate (i.e., gas velocity). In addition, tests involving batch size currently are being performed.

5.3.2.1. Effect of Temperature

The gallium concentration and weight loss following exposure to different temperatures are shown in Fig. 5-4. Exposures of 0.5 h at 600°C and 800°C resulted in essentially no gallium removal, and exposures at 900°C resulted in only slight gallium removal. Figure 5-4 indicates that a temperature of at least 1000°C is required to obtain significant gallium removal. At 1200°C, the gallium concentration was reduced to ~150 ppm. Future work will include tests at higher temperatures.

Figure 5-4 also shows that there is significant weight loss at 800°C, even though there is little gallium evolution at this temperature. Thus, the majority of the weight loss at the lower temperatures is attributable to something other than gallium evolution (i.e., PuO_2 reduction). At higher temperatures, a significant fraction of the weight loss is attributable to gallium removal. The fraction of the weight loss attributable to gallium removal increases with increasing exposure temperature (see Fig. 5-5).

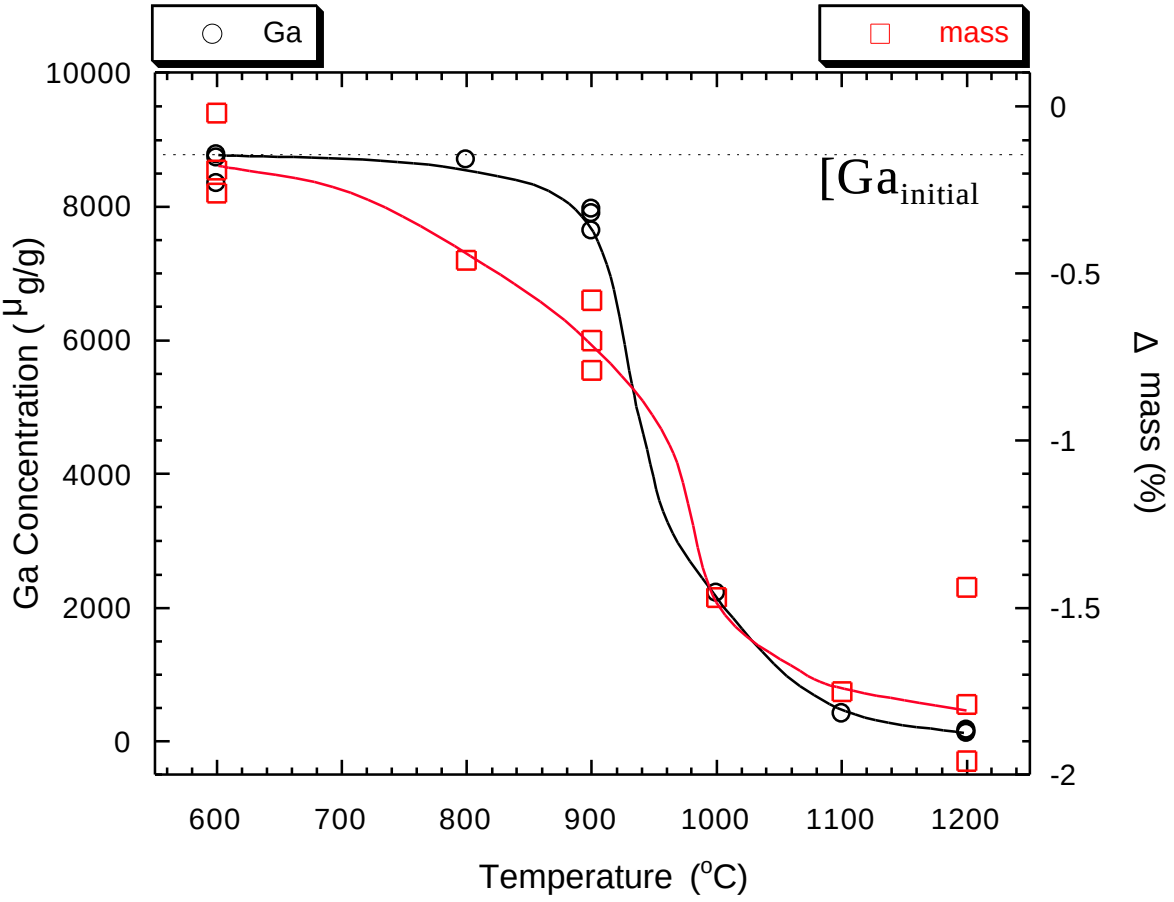

Fig. 5-4. Remaining gallium concentration and weight loss as a function of exposure temperature. Test duration: 0.5 h. Sample mass: 2.5 g. Flow velocity: 1.5 cm / s.

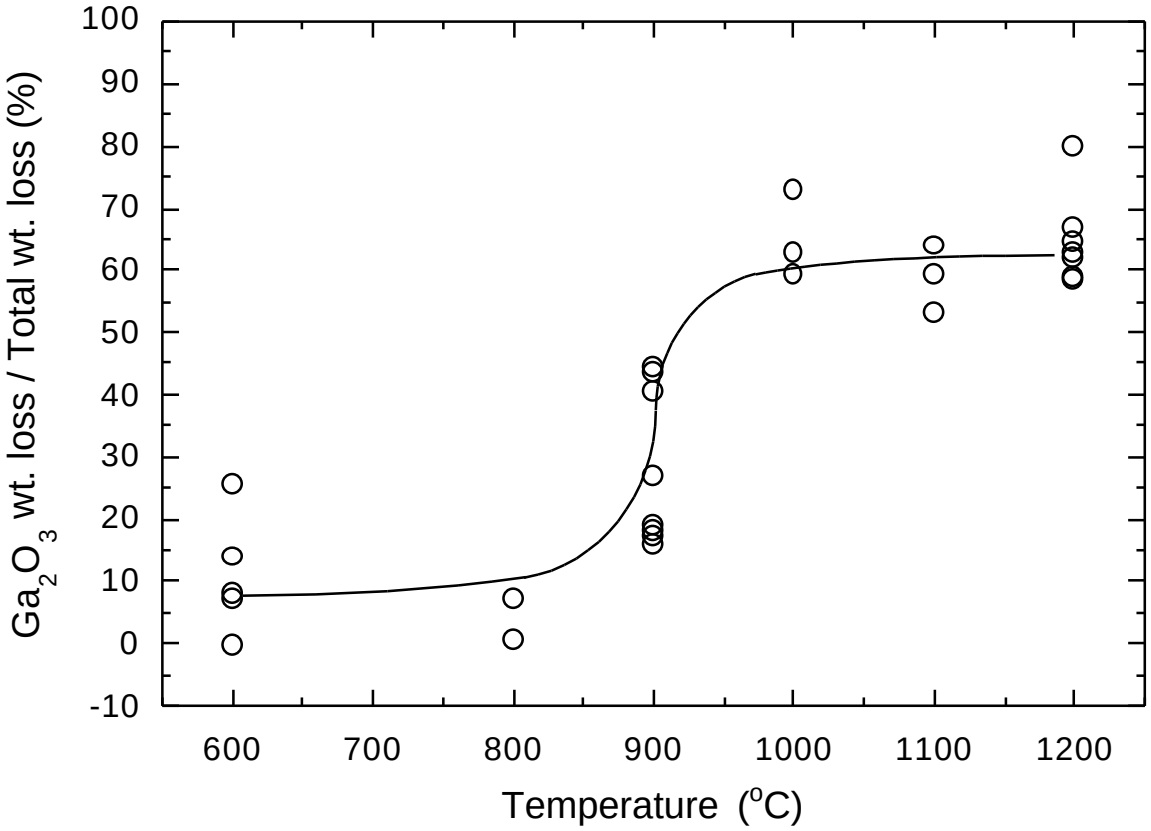

Fig. 5-5. Percentage of total weight loss attributable to Ga_2O_3 loss as a function of temperature.

5.3.2.2. Effect of Time

The effect of exposure duration on gallium removal is plotted in Fig. 5-6. It was observed that increasing exposure time produced diminishing returns in gallium removal. For the 8-h exposure, the gallium concentration was reduced by over two orders of magnitude (from 8700 to 34 ppm). However, the majority of the gallium was removed during the first 0.5 h, at which point the gallium concentration was 150 ppm. More tests are required before the asymptotic limit under these conditions can be determined.

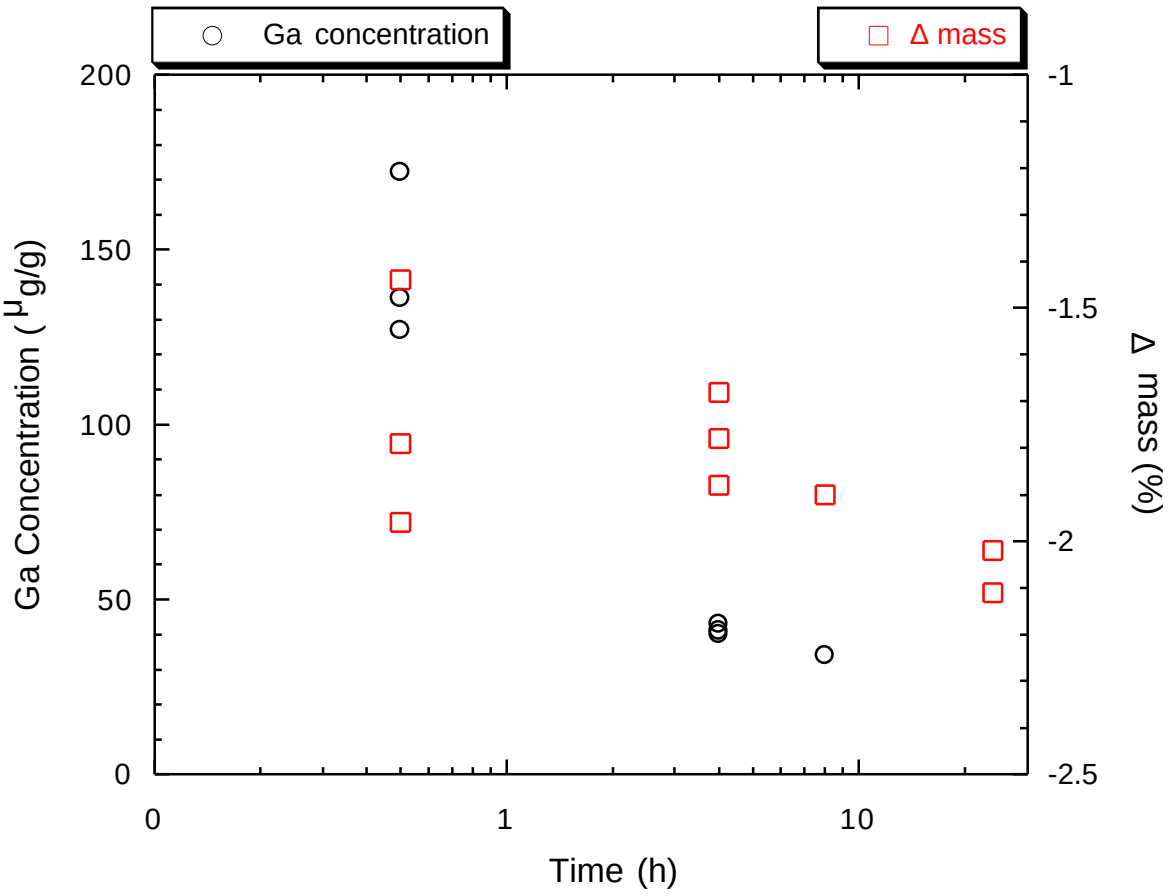

Fig. 5-6. Remaining gallium concentration and weight loss as a function of test duration. Temperature: 1200°C, sample mass: 2.5 g, flow velocity: 1.5 cm / s.

5.3.2.3. Effect of Sample Mass

It is important to understand the effect of sample mass for two reasons. First, during pit disassembly and conversion, it will be desirable to perform gallium removal using kilogram-size batches. Because the tests to date use gram quantities, it is imperative to understand any potential effects of scale-up. Moreover, an observed dependency on sample size may suggest mass transport limitation through the powder interstices. Enhanced mass transport during processing of kilogram batches then may be necessary to reduce the gallium to a desired level in a reasonable time. Enhancement may take the form of vessel rotation, fluidized bed, etc. Thus, understanding the effect of sample mass (or, more generally, the rate limiting step) is necessary to design a gallium removal system.

The effect of sample mass on gallium removal currently is unclear. Weight loss measurements suggested that increasing the sample mass decreases the percent weight loss with a confidence of >99% based on linear regression of the 0.3-, 0.9-, and 2.5-g

data. One test using 25 g of PuO_2 yielded a weight loss similar to the smaller samples (Fig. 5-7). Further, gallium concentration measurements suggested that sample mass had no statistically significant effect on gallium removal. However, the gallium concentration analyses of the samples are suspect because some of these samples may have become contaminated with the starting material following testing. The samples were placed back into containers that previously contained the starting material. For a given amount of contamination per sample, the largest percentage effect would be expected for the smallest samples and for samples that had the greatest incidence of gallium removal. When the data were examined, this appeared to be the case. Further tests will be performed using clean vials to ascertain whether there was any significant effect of contamination. In summary, the effect of sample size cannot be determined at this time.

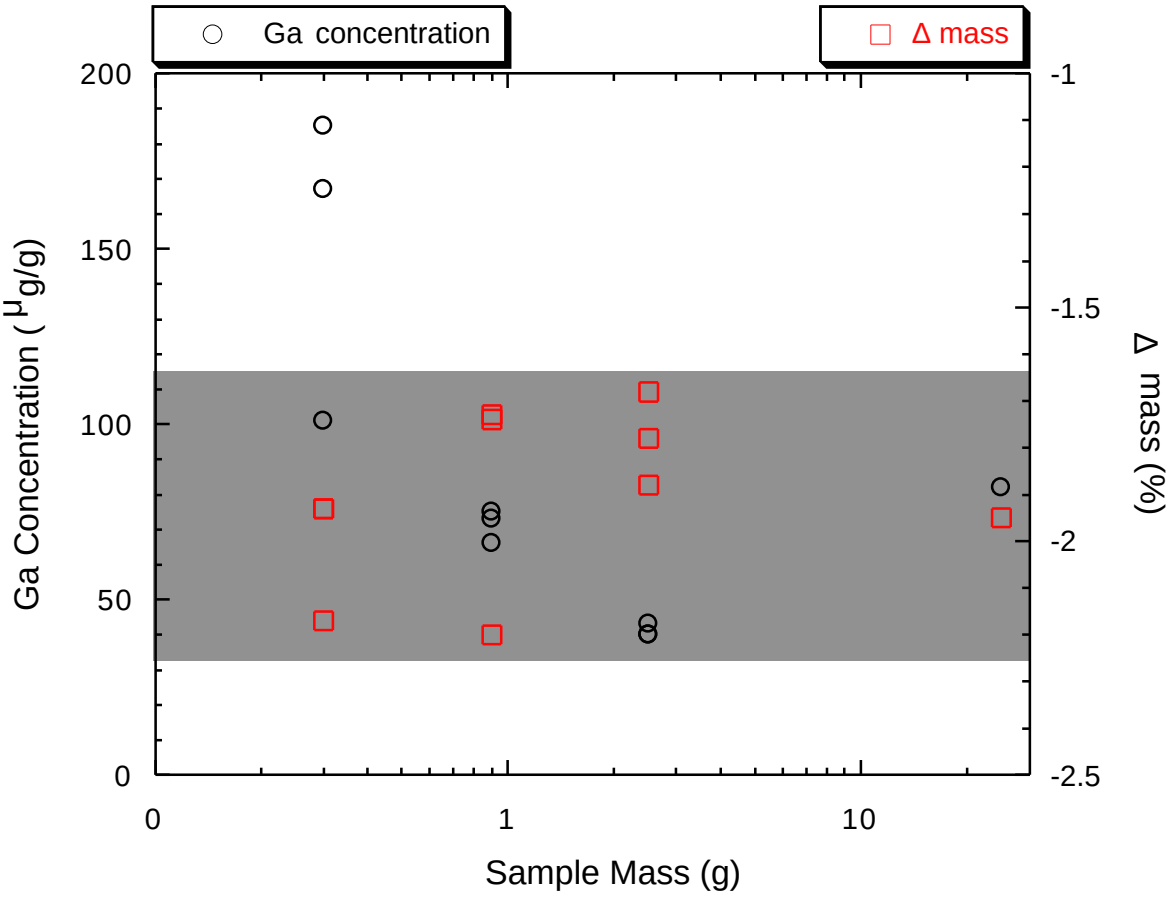

Fig. 5-7. Remaining gallium concentration and weight loss as a function of sample size. Temperature: 1200°C, test duration: 4 h, flow velocity: 1.5 cm / s.

5.3.2.4. Effect of Flow Rate

As with sample size, understanding the effect of flow rate is critical to determining the rate limiting step. As with sample mass, the effect of the gas flow rate cannot be determined unambiguously at this time. Initial experiments involving gallium removal used gas flow rates of 1.5 cm/s and 3.0 cm/s. Weight loss results from tests incorporating identical temperatures, times, and sample masses but different flow rates are compared in Fig. 5-8. There is no apparent difference in weight loss when the flow rate is doubled. That is, for every test condition where mass loss was larger for a faster flow rate, there was a different test condition where mass loss was larger for the slower flow rate. The same was observed when comparing gallium concentration data. Linear regression of the weight loss and gallium concentration data confirmed this observation. Thus, gallium evolution did not appear to be limited by the mass transport of Ga_2O_3 away from the boat to its deposition point downstream.

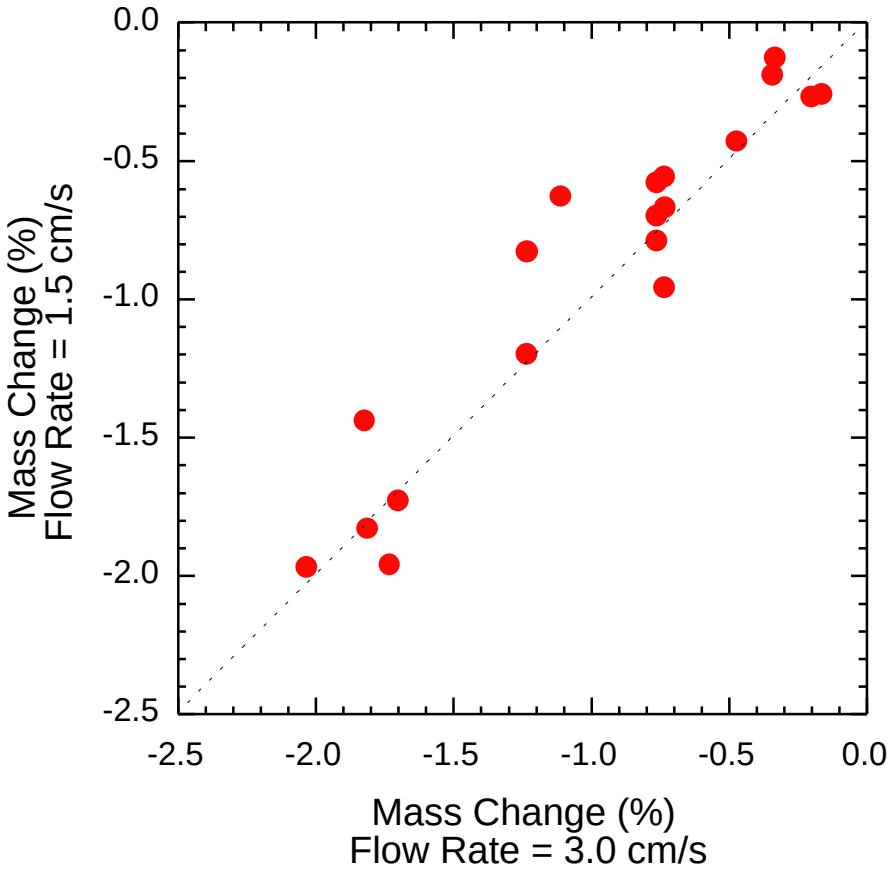

Fig. 5-8. Weight loss following exposure to a 1.5-cm/s gas flow velocity as compared with the weight loss following exposure to a 3.0-cm/s gas flow velocity. Various temperatures, test durations, and sample masses were analyzed. The diagonal dashed line represents the condition where the mass loss during the 1.5-cm/s flow rate is identical to that during the 3.0-cm/s flow rate.

Additional tests were run using much higher flow rates of 13 and 26 cm/s. Although it appeared that these higher flow rates may have enhanced gallium removal, the effect of flow rate cannot be concluded unambiguously at this time because of significant scatter in the data. More tests are required before the effect of flow rate can be determined.

The effect of flow rate on pure Ga_2O_3 also was determined (Fig. 5-9). For pure Ga_2O_3, doubling the flow rate from 1.5 to 3.0 cm/s increases the rate of gallium evolution. This indicated that gallium evolution was not reaction-rate limited but rather was limited by mass transport. Calculations indicate that in the event of mass-transport limitation, Ga_2O is the limiting species, as opposed to hydrogen or water (H_2O) (Fig. 5-10). Given that Ga_2O evolution is not reaction-rate limited for pure Ga_2O_3, evolution will not be reaction-rate limited for PuO_2. Because gallium evolution does not appear to be either kinetically limited or mass transport limited by transport away from the boat, there are only two other potential rate-limiting steps: mass transport within the PuO_2 particles themselves or mass transport within the interstices between the powder particles. Tests using a rotating tube should be able to determine whether the latter is the controlling step. These tests are planned for FY99.

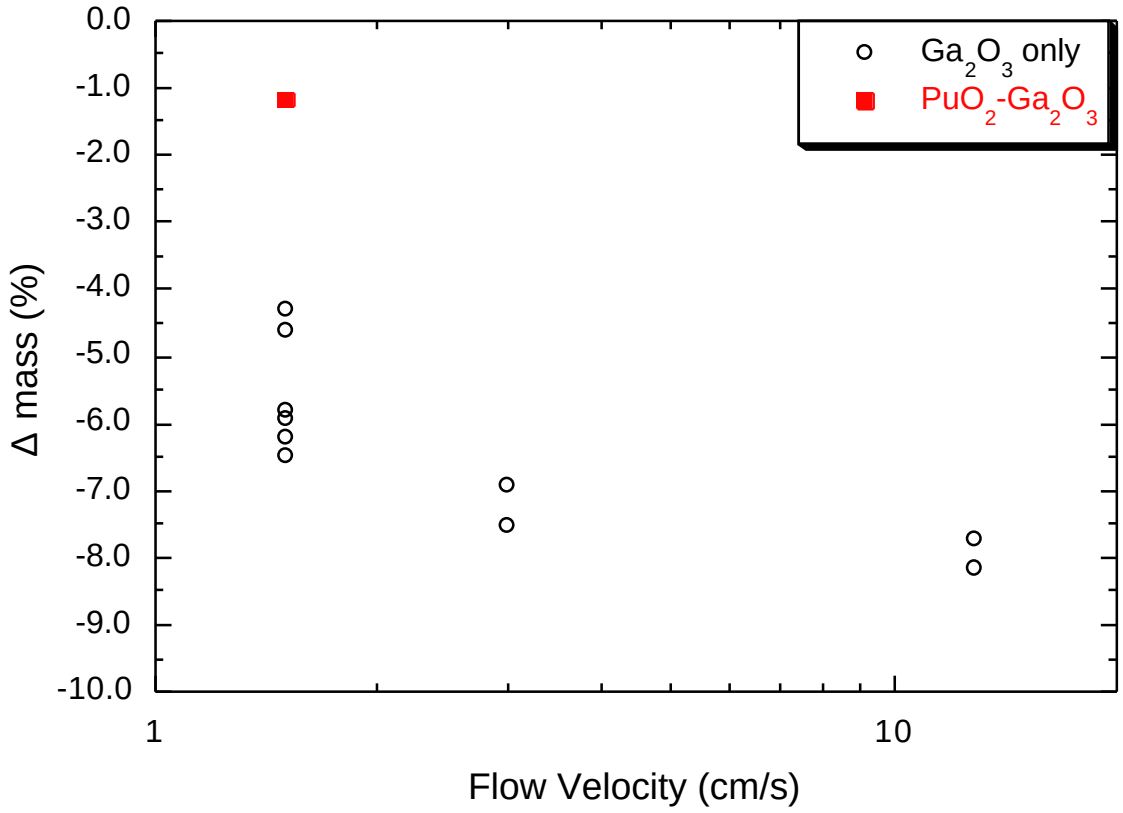

Fig. 5-9. Plot of mass change as a function of flow velocity for 2.5-g samples at 900°C for 4 h. Data for pure Ga_2O_3 and the three-step PuO_2 powder are shown.

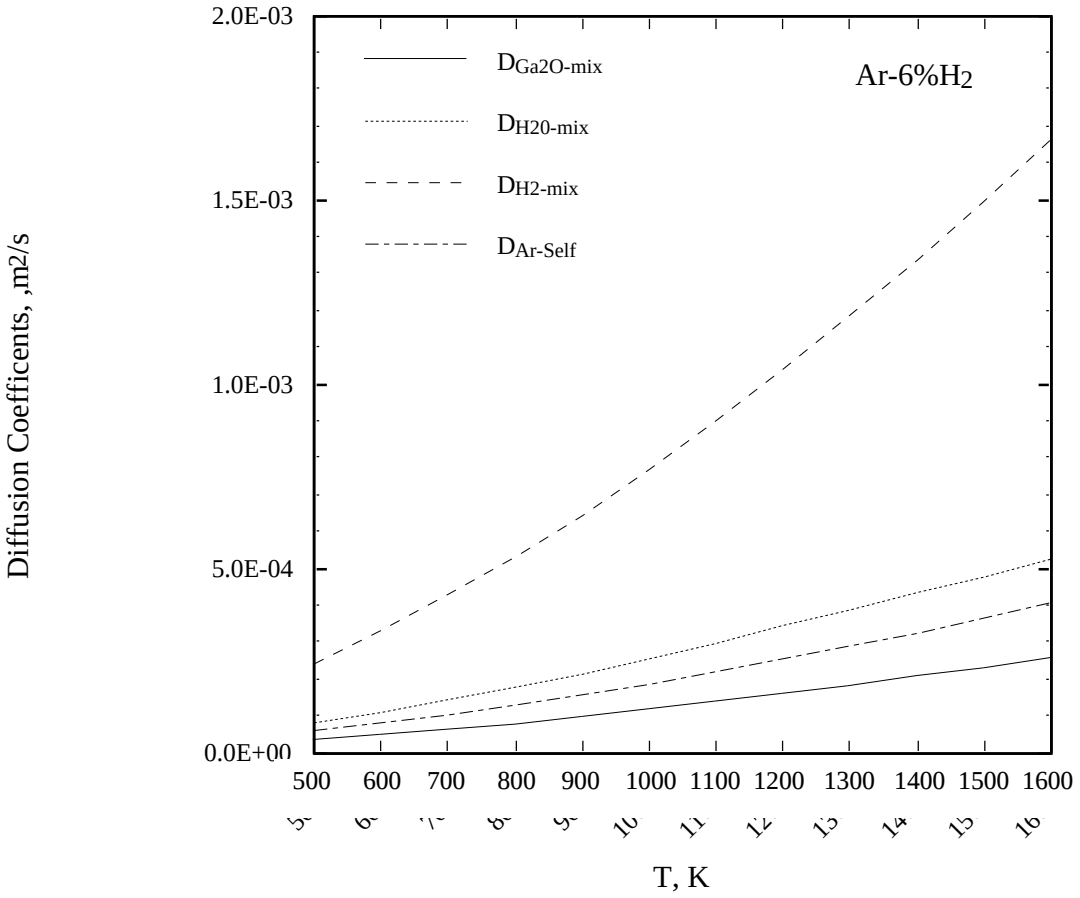

Fig. 5-10. Diffusion coefficients for relevant gas species as a function of temperature.

5.4. Prototype Design and Testing

Most of the prototype design and testing efforts were combined with the process design efforts, and thus, separate results are not published here. However, some materials compatibility tests were performed in this area and are included here. Further activities should culminate in FY99.

The environment for removing gallium must be very aggressive. The environment should be at a relatively high temperature (≥1200°C) and should contain hydrogen and Ga_2O (which are embrittling agents). If a rotating apparatus is required, the use of ceramics may be prohibited because of poor mechanical properties. Thus, metals may be required for furnace construction. However, materials selection is not trivial because there is little information in literature regarding the corrosion of metals exposed to these particular conditions. Thus, more experimentation is required to determine the suitability of candidate materials.

Two different types of tests have been initiated. The first type is the "short-term" test. This experiment involves placing three identical, well-polished samples of materials in different positions in a 1200°C furnace containing flowing Ar–6 % H_2 and Ga_2O_3 for 24 h (Fig. 5-11). These different positions represent different conditions within a hypothetical furnace. Short-term tests recently have been initiated following a few initial test runs, but they are being redone to verify results. The second type is the "long-term" test. This experiment involves the encapsulation of highly polished samples within an evacuated vial containing a mixture of gallium and Ga_2O_3 (Fig. 5-12). The vial then is placed in a furnace at 1100°C for 2 months. The high temperature allows the gallium and Ga_2O_3 to react and form Ga_2O, which is relatively volatile and reacts with the sample. These long-term tests are ongoing. Both short- and long-term tests will use a variety of surface science methods to determine the effect of gallium in the corrosion of different candidate metals.

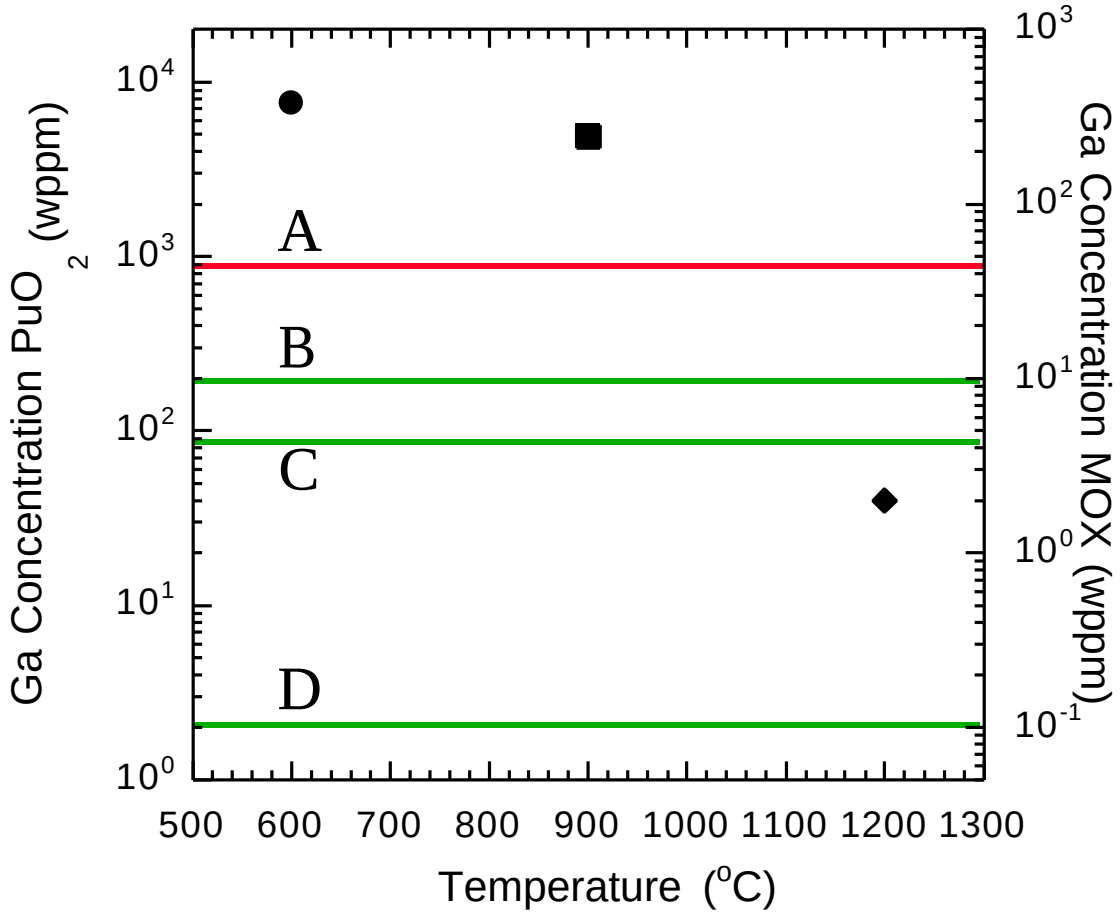

Fig. 5-11. Drawing of sample positions for short-term materials compatibility tests. The boat is shown without Ga_2O_3 powder for clarity.

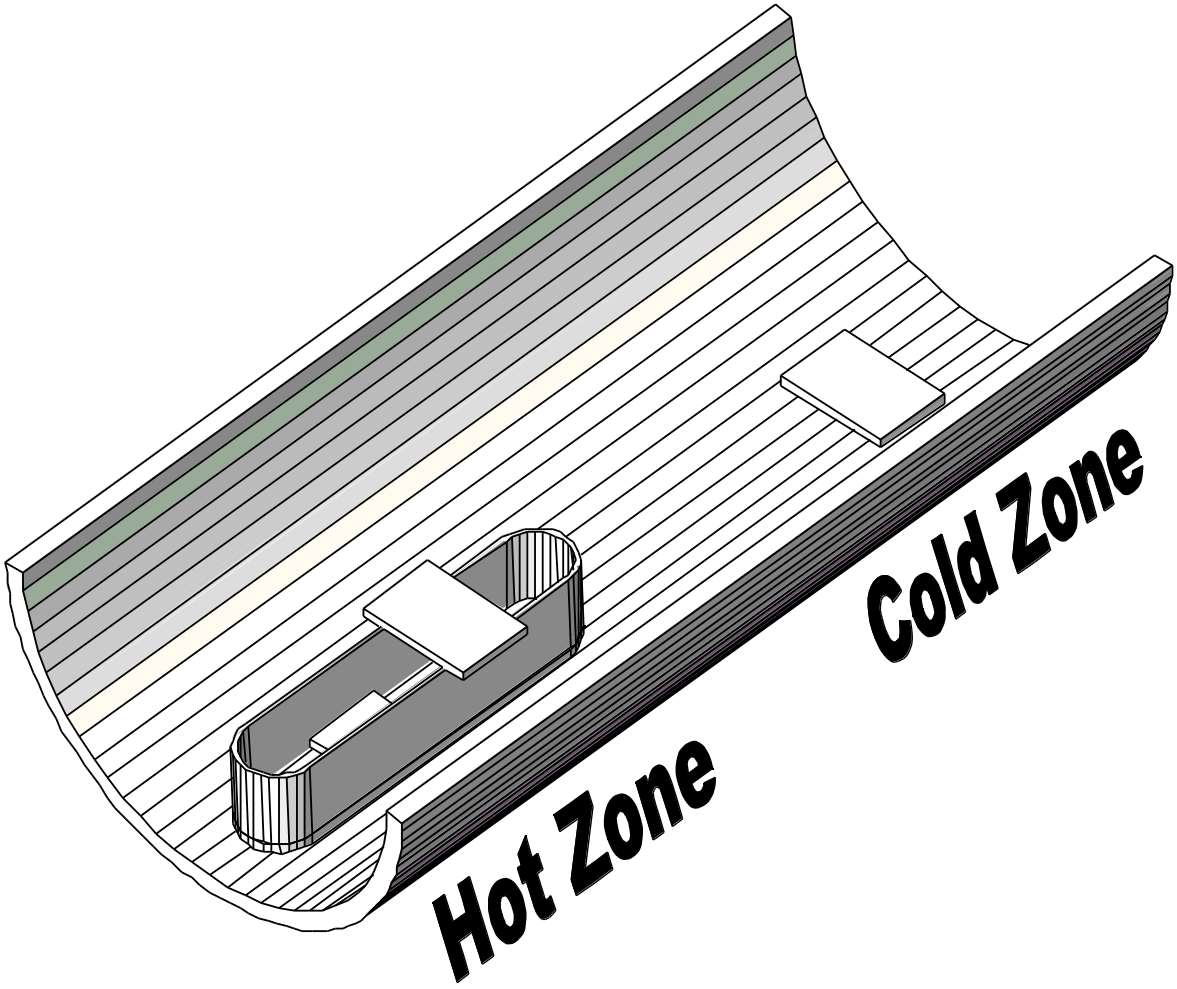

Fig. 5-12. Exploded view of a long-term compatibility test sample. The entire assembly is sealed and placed in a furnace at 1100°C for 2 months.

5.5. Cold Prototype Testing

This task included TIGR studies in the cold laboratory involving surrogate (CeO_2) fuel. Results from these studies are included in this section.

Various studies were performed in FY98 on the CeO_2 surrogate MOX feedstock material to assess the kinetics of gallium removal. The work lays the foundation for development and understanding of a thermal process for removing gallium from PuO_{2-x}. Plutonium and cerium are similar; thus, cerium oxides are good surrogates for plutonium oxides and provide a rapid, relatively cheap, and safe means of understanding the fundamentals of gallium removal, as well as a means of collecting the evolved gallium from plutonium. In addition, a well-characterized surrogate that can be used outside of the glovebox environment aids evaluations for pilot or full-scale production equipment that could be used in setting up a large-scale system. In FY98, a

variety of parametric studies on the kinetics of gallium removal were performed on surrogate feedstock by thermally induced processes. The resulting data are being used to design a full-scale system for gallium removal from WPu.

5.5.1. Experimental Procedure

CeO_2-based MOX surrogates were prepared by a similar route to conventional MOX fuel by blending, sintering, and milling CeO_2 and Ga_2O_3 powders. Details of material preparation and equipment, as well as other related information, have been reported previously (Refs. 5-5 to 5-10). The primary MOX surrogate used was a CeO_2-2 wt % Ga_2O_3 (herein referred to simply as the surrogate).

The process of removing gallium from the surrogate used a reducing atmosphere of Ar–6% H_2. Studies were done at 600°C to 1200°C as a function of time, sample lot size, gas flow rate, and particle size. The surrogate pellets and three powder-lot sizes, 0.3, 0.9, and 2.5 g, were used for most tests. The desired amounts of surrogate powders/pellets were placed side by side into a controlled-heat furnace with alumina crucibles. Surrogate powder and pellet samples were heated to the desired temperature (600°C to 1200°C) at 20°C/min and held for 0.5 to 12 h. The weight of the surrogate was monitored before and after exposure and the change determined. Samples were analyzed using Joel 6300 FVX SEM/energy dispersive spectroscopy (EDS), x-ray photoelectron spectroscopy (XPS), Rutherford backscattering spectrometry (RBS), proton-induced x-ray emission (PIXE), direct current plasma emission spectroscopy (DCP), and a LECO TC-136 oxygen/nitrogen analyzer.

5.5.2. MOX Surrogate Sample Characterization

As illustrated in Fig. 5-13, the pressing and sintering steps produced pellets with fairly consistent relative densities. The final average density of pellets for about 600 surrogates was ~95% of the theoretical density. Figure 5-14 shows the measured gallium content of the surrogate before and after sintering compared with 1 wt % Ga_2O_3–PuO_2 and Pu–1wt % Ga samples after sintering. The amount of Ga in the CeO_2–2 wt % Ga_2O_3 surrogate was reduced ~50% during sintering (from ~14,000 to ~7500 ppm), which is comparable to the amount of gallium from PuO_2–1 wt % Ga_2O_3 (7400 ppm) and Pu–1 wt % Ga fuel (8700 ppm). The exact gallium amount (14,314 ppm) measured from a green pellet essentially agreed with the calculated value (14,878 ppm) from CeO_2–2 wt % Ga_2O_3 mixture. From this figure, it is apparent that the gallium loss during sintering provided a surrogate with a gallium content comparable to that achieved under similar conditions with WPu. Most of these samples were the same as the specimens used for the gallium sintering studies, so the range of conditions is the same as discussed in Section 3.2.

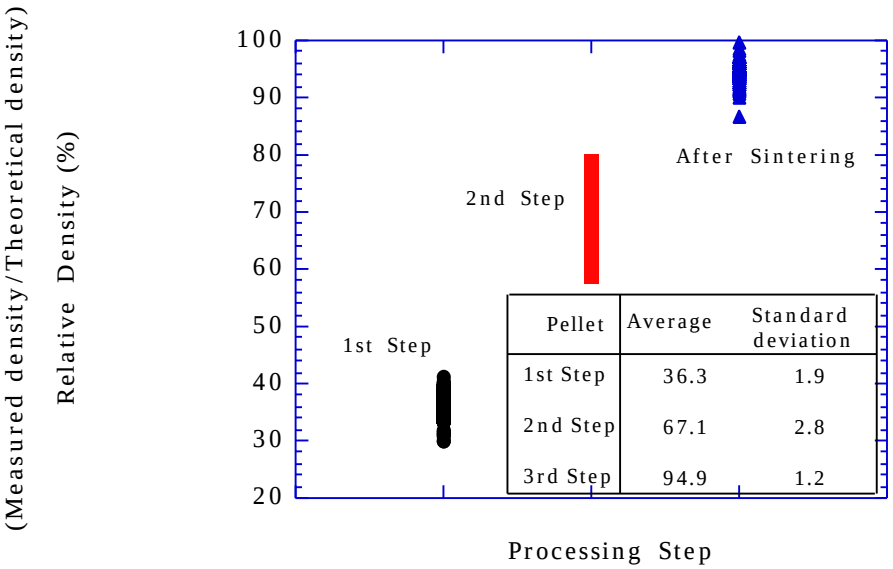

Fig. 5-13. Plot of green and fired densities of CeO_2–2 wt % Ga_2O_3 pellets after pressing and sintering.

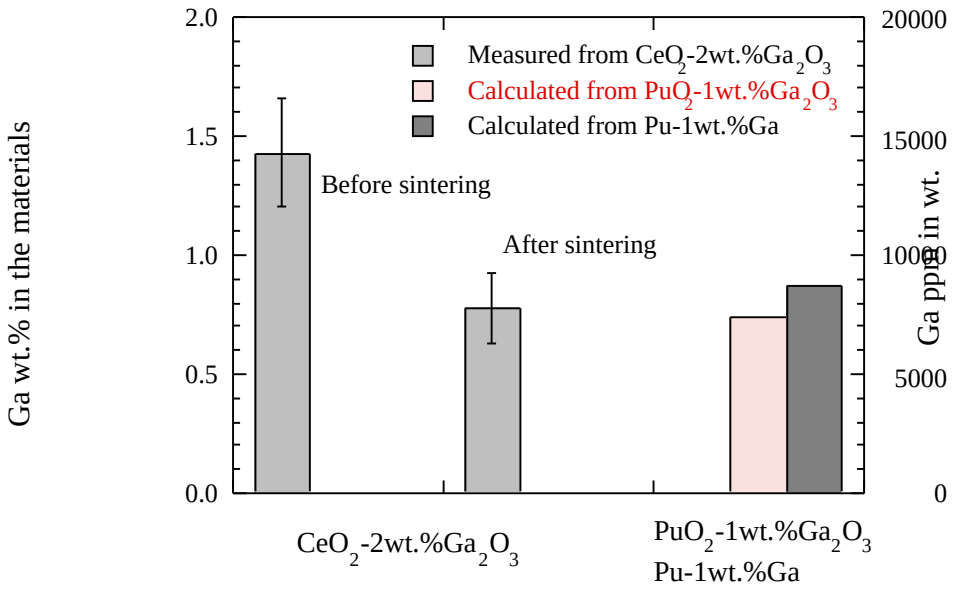

Fig. 5-14. Residual gallium amount in CeO_2–2 wt % Ga_2O_3 surrogate powders before and after sintering and calculated gallium concentrations for PuO_2–2 wt % Ga_2O_3 MOX fuel after sintering.

SEM and EDS analyses indicated a uniform distribution of gallium in the surrogate. Figure 5-15 displays the corresponding morphology from the cross section of the sintered surrogate pellet, showing agglomerated grains and pores obtained during

sintering. The x-ray elemental map on the bottom associated with the SEM image in Fig. 5-15 shows strong gallium intensities at grain boundaries through the sintered surrogate. EDS patterns in the middle row show differences from the regions between the gallium segregated grain boundaries and the CeO_2 matrix. EDS quantitative analysis verifies the possible presence of a Ce–Ga–O mixture in the grain boundaries. However, the segregated Ce–Ga–O compounds rarely were observed in the CeO_2 grains from the surrogate. Nonetheless, because the solubility of gallium in both cerium and plutonium is similar, the gallium segregated compound also should be expected in the PuO_2 grain boundaries, as seen in CeO_2.

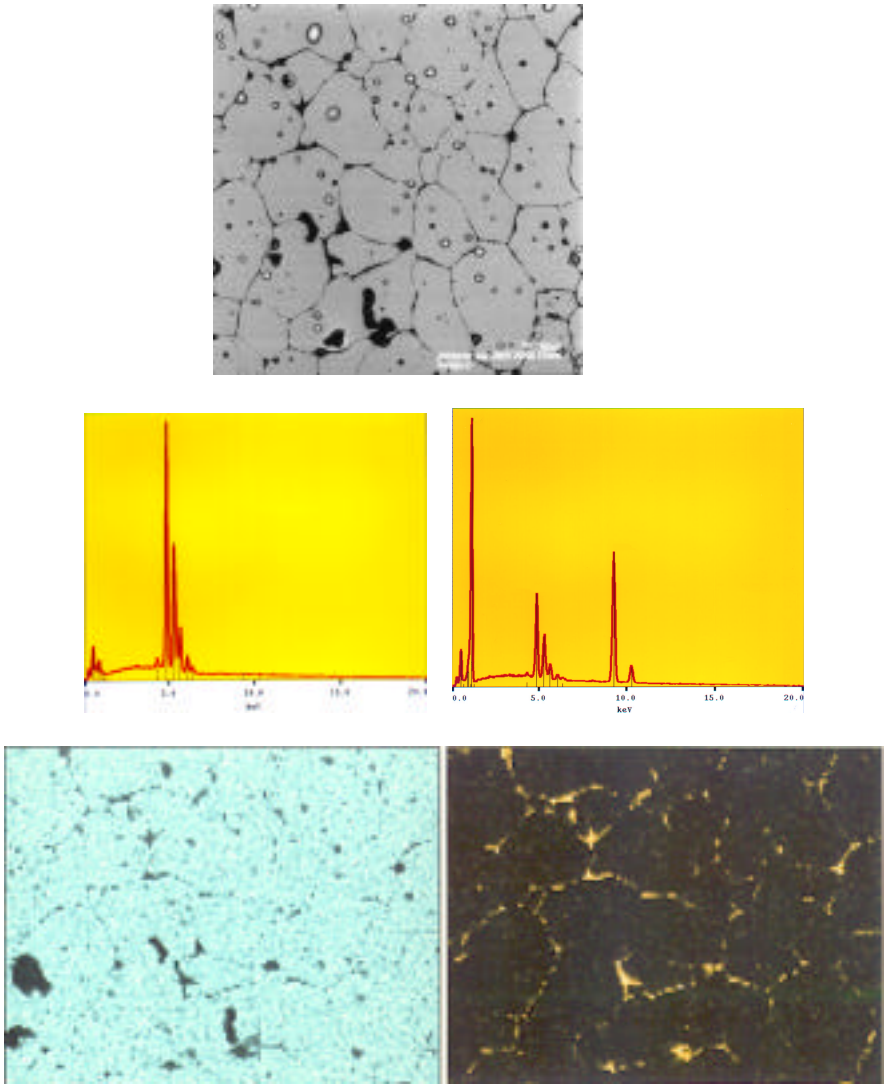

Fig. 5-15. SEM morphologies from the cross section of the sintered pellet showing grain boundaries and pores through cross section (top), EDS pattern from CeO_2 matrix (left on the middle row), and a gallium-rich area in the grain boundary (middle right). The x-ray map shows the gallium intensity in the grain boundaries (bottom).

5.5.3. Thermally Induced Gallium Removal from MOX Surrogate

These studies were performed either in Ar–6% H_2 or pure argon. Four sample loading morphologies were used, as illustrated in Fig. 5-16, which included a single uncrushed pellet and flat boats filled with 0.3, 0.9, and 2.5 g of surrogate powder. The photos on the left-hand side show the materials before exposure, and those on the right show the materials after exposure. The color of the surrogate powder and pellet changed to gray and metallic when exposed to the Ar–6% H_2 environment (top). This is probably because in this reducing environment, there are additional reactions, such as the vaporization of Ga_2O_3 to other gallium species, ceria reduction, and stoichiometry changes; however, the change to gray indicates that gallium suboxide is the predominant reaction. No color changes (yellow-white) on exposure to a pure argon environment implies no pronounced removal of Ga_2O from the surrogate in the absence of hydrogen.

Starting feedstock. 1 cm After 1100°C, 0.5 h in Ar–6% H_2.

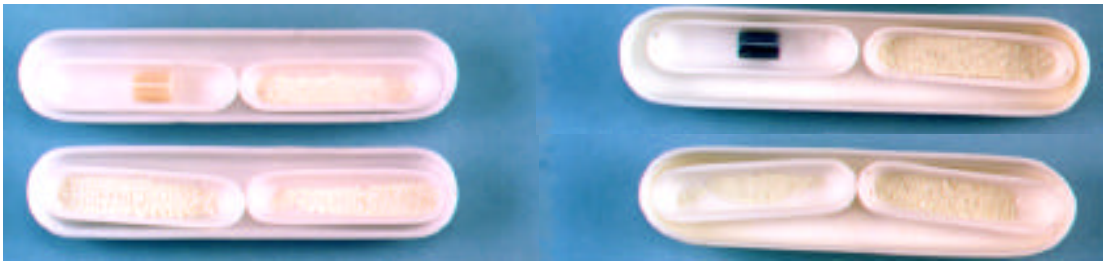

Starting feedstock. After 1100°C, 0.5 h in pure argon.

Fig. 5-16. Photographs of surrogate pellets and powders shown as they were placed in alumina boats for gallium evolution testing. The photos show the materials before (left) and after (right) exposure to Ar–6% H_2 (top) and pure argon (bottom) at 1100°C for 30 min. Three powder-lot sizes were used for the 0.3-, 0.9-, 2.5-g and pellet tests.

Figures 5-17 and 5-18 demonstrate that the kinetics of gallium removal is affected strongly by the reducing atmosphere and temperature; that is, gallium removal can most effectively be achieved at 1000°C and in an Ar–6% H_2 environment (compared to a pure argon environment). The O / M (O / Ga+Ce) ratio calculated from chemical analyses was observed for surrogates exposed to Ar–6% H_2 and then cooled in air, as shown in Fig. 5-19. There was no difference in the O / M ratio either before or after exposure. Surrogate samples exposed to argon also showed no difference in the O / M ratio either before or after exposure. This is probably because CeO_2 regained oxygen rather rapidly after being tested in hydrogen, and the losses of Ga_2O_3 (maximum 2 wt %) in the surrogate did not affect the O / M ratio.

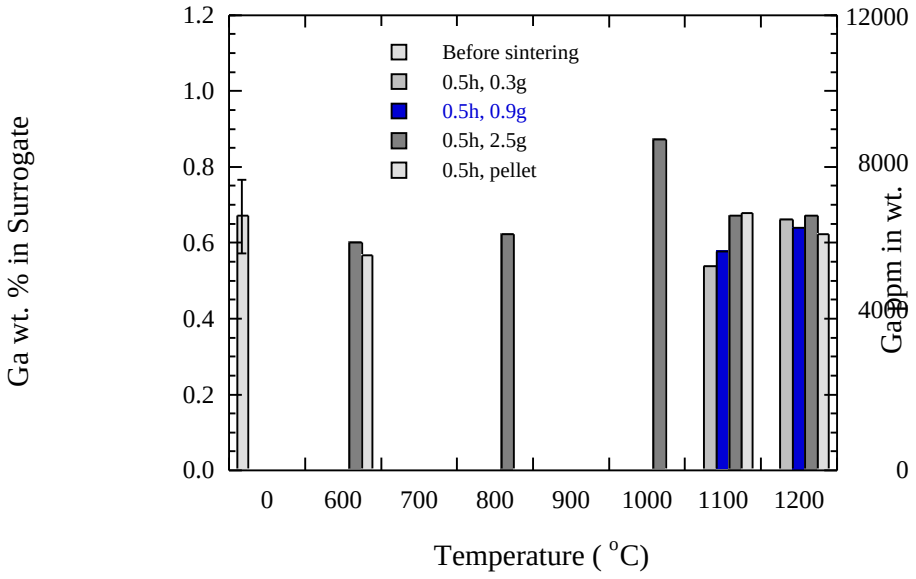

Fig. 5-17. Plot of residual gallium vs temperature for CeO_2–2 wt % Ga_2O_3 samples exposed to argon for 30 min.

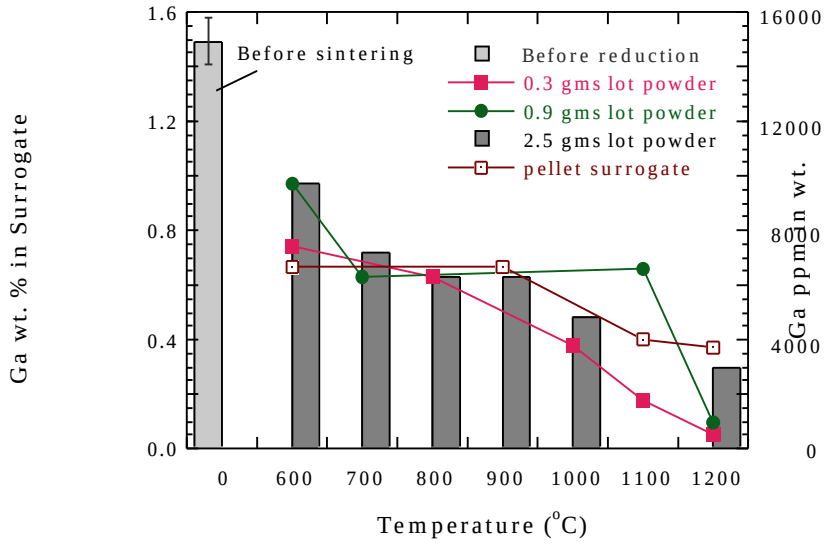

Fig. 5-18. Plot of residual gallium vs temperature for CeO_2–2 wt % Ga_2O_3 samples exposed to Ar–6% H_2 for 30 min. The 0.3- and 0.9-g powder lots and pellets are plotted by a line graph, and the 2.5-g powder lot is plotted as a bar graph.

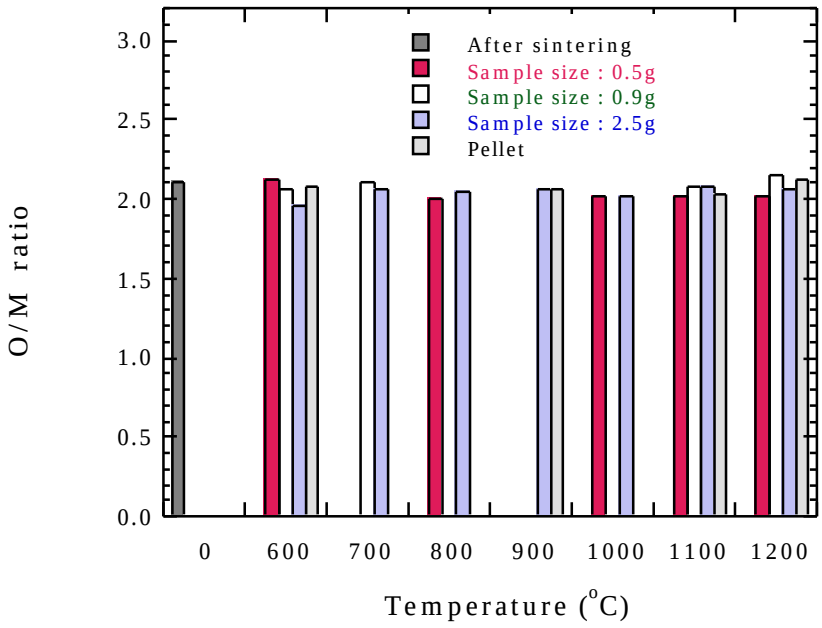

Fig. 5-19. O/M ratios in the MOX surrogate showing no obvious differences when exposed in Ar–6% H_2 vs air.

Next, the effect of sample size on gallium removal observed by DCP analyses was studied. The results of PIXE, XPS, MXRF, and neutron activation analysis were reported in Ref. 3-3 for FY97 and showed that the efficiency of gallium removal improved with decreasing sample lot size. In FY98, experiments were performed that considered the effects of large sample sizes on gallium removal. These experiments involved investigations of a large sample (100 g) at 1200°C for 12 h in a 3-cm/s Ar–6% H_2 environment. Small samples were taken from various locations in the bed for chemical analyses. Following the first exposure, the sample was exposed a second time, and samples were taken again for analyses from identical regions of the bed. Figure 5-20 summarizes the results of these studies. These results, combined with results of previous studies of gas flow rates and sample sizes in particular, lead to the conclusion that in the system used for these studies, the vaporization of gallium from the surrogate is rate limited by the gaseous transport of Ga_2O and limited solid diffusion. Thus, in designing the TIGR, the kinetics of gallium removal can be improved by flowing through, rather than over, a powder bed or by using a rotating system. However, it was also determined that temperature has an even stronger effect (as previously discussed).

Figure 5-21 shows the effect of time on residual gallium in the surrogates exposed to an Ar–6% H_2 environment for 0.5 to 12 h at 600°C, 900°C, and 1200°C. The plot shows that no significant gallium removal was achieved up to 900°C. As the exposure time increased, gallium removal was increased to 1200°C, as shown by the bar graph. The residual gallium was diminished to 60 to 130 ppm after 12 h at 1200°C. In the meantime, the pellets showed higher gallium residue than the powders. This larger residue amount from pellets was due to the longer diffusion distance for segregated gallium species in the grain boundaries of pellets, showing that removal of gallium from a pellet can be improved with longer process times than required for powders. The plot indicates that the kinetics of gallium removal strongly depend on the temperature at which removal occurs within 1 h. It can be explained that in the early stages, residual gallium species at the surface are reduced. However, as time passes, the removal depends on the diffusion of gallium species from the Ga–Ce–O compound in the surrogate, resulting in the slower reduction of gallium than in the earlier stages.

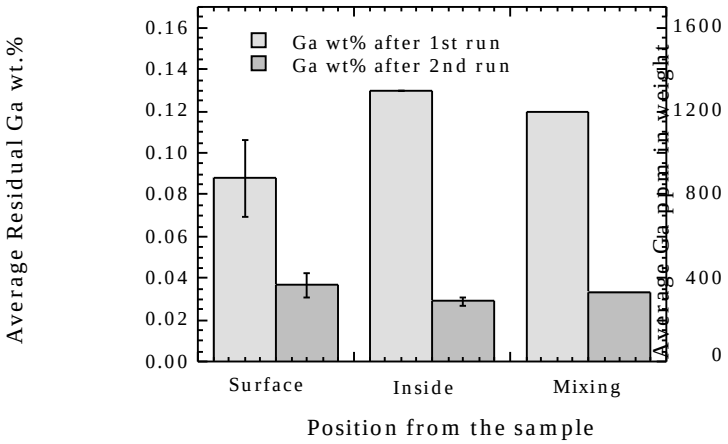

Fig. 5-20. Residual gallium amount from a 100-g lot-size powder sample after testing at 1200°C for 12 h in Ar–6% H_2.

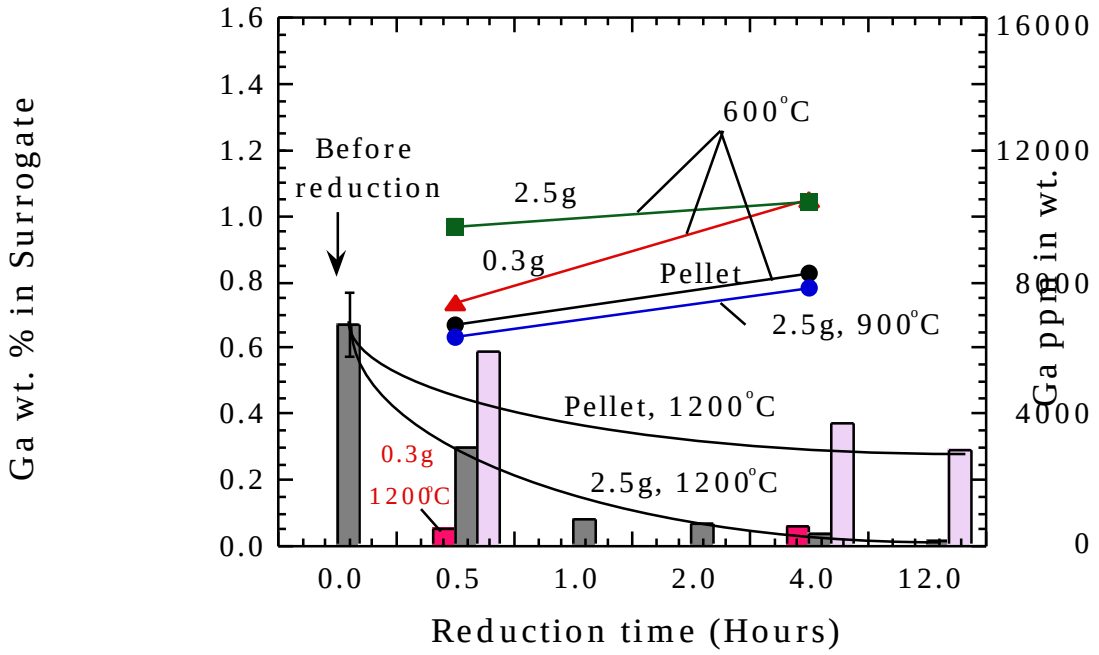

Fig. 5-21. Plot of and residual gallium vs time for the CeO_2–2 wt % Ga_2O_3 sample exposed to Ar–6% H_2 at 600°C, 900°C, and 1200°C. Lines represent the gallium residual.

Figure 5-22 (a) shows the effect of the gas flow rate on gallium removal for flow rates of 1.5 and 3.0 cm/s for 30 min. Again, gallium removal was affected by temperature, not by flow rate. To confirm the flow rate effect, the flow rate was increased to 6.0 cm/s at 1200°C in Ar–6% H_2 for 30 min. None of the sample lots exhibited any variations with increasing gas velocity. This implies that the kinetics is not limited by mass transport between input hydrogen and surrogate surface boundaries in the range of a 0- to 6.0-cm/s flow rate, but it does not rule out the possibility that the kinetics is limited by $Ga_2O(g)$ transport. Another series of experiments is being planned in which the gas flow rate will be ~20 cm/s. Figure 5-23 shows the effect of particle size on weight loss and gallium removal. Again, the amount of residual gallium was affected strongly by temperature.

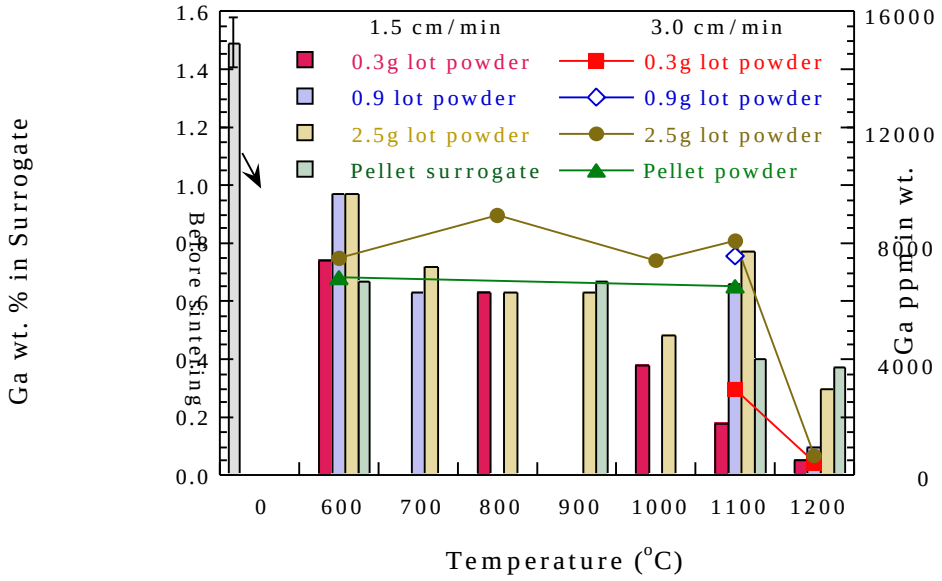

(a)

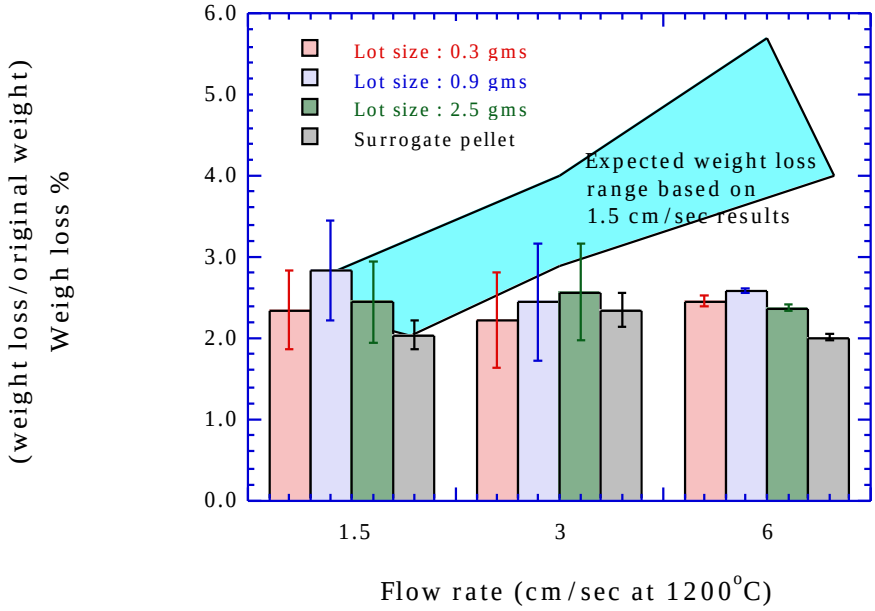

(b)

Fig. 5-22. Plot of flow rates: (a) residual gallium (top) vs temperature for CeO_2–2 wt % Ga_2O_3 sample exposed to Ar–6% H_2 at a 1.5- and 3.0-cm/s flow rate and (b) weight loss vs flow rates for the CeO_2–2 wt % Ga_2O_3 sample exposed to Ar–6% H_2 at a flow rate of 1.5, 3.0, and 6.0 cm/s.

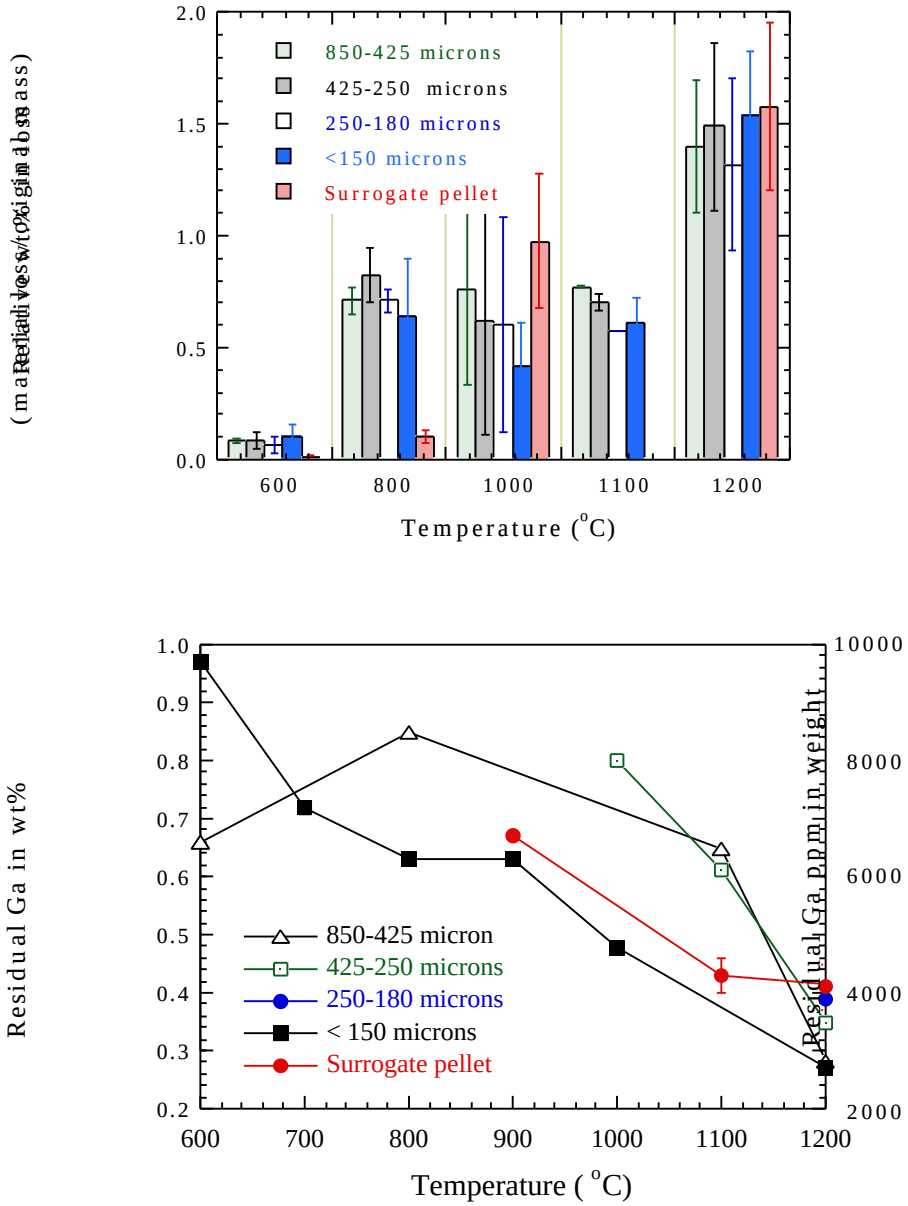

Fig. 5-23. Plot of grain size effect on weight loss (above) and residual gallium (bottom) vs temperature for the CeO_2–2 wt % Ga_2O_3 sample exposed to Ar–6% H_2 for 0.5 h at a flow rate of 1.5 cm / s.

5.5.4. Kinetics and Mechanism of Gallium Removal

The possible kinetics and mechanisms of gallium removal from MOX feedstock are considered, as shown in Fig. 5-24. This diagram shows grains and possible Ga–Ce–O compounds based on observations. Though Ga_2O_3 decomposes possibly into Ga(l), GaO(g), and Ga_2O(g), the main evaporation phase is considered to be Ga_2O(g) in the hydrogen environment. Therefore, the possible rate-controlling steps for gallium

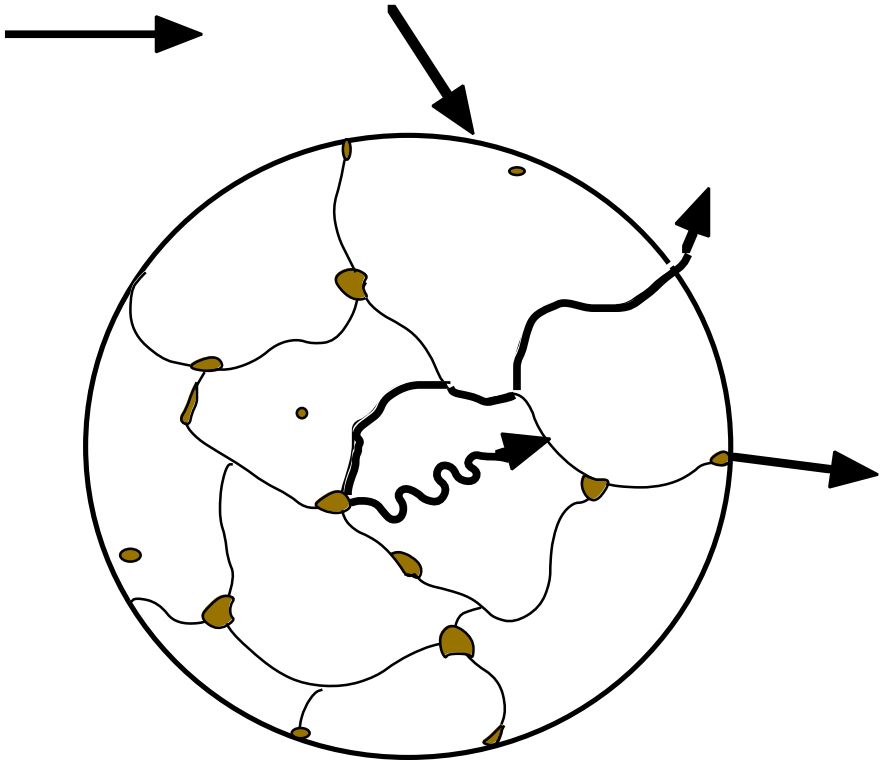

Fig. 5-24. The possible kinetics and mechanism of gallium species transport in the MOX surrogate.

removal could be (1) flow of reactant gases (Ar–6% H_2) into the system, (2) mass transport of reactant gases to the MOX fuel surface, (3) diffusion within the particles of either hydrogen or gallium species, and (4) transport of product gases away from the fuel.

If the amount of hydrogen gas supplied in the experiment is less than the amount needed to form $Ga_2O(g)$ in Eq. (2), then it may not be necessary to consider the rate-controlling steps (steps 2 through 4) in Fig. 5-24. The amount of $H_2(g)$ supplied can be calculated by the amount of Ar–6% H_2 required during each experimental run. The amount of $Ga_2O_3(s)$ in Eq. (2) is obtained by the composition of MOX surrogate feedstock starting materials. Equation (2) illustrates that 2 moles of $H_2(g)$ was needed to vaporize 1 mole of $Ga_2O_3(s)$. Thus, the amount of $H_2(g)$ supplied was calculated as being enough to achieve the vaporization of $Ga_2O(g)$. Therefore, step 1 cannot be the rate-controlling step for current experimental conditions.

To determine the rate-controlling step in the MOX system, mass transfer through the boundary layer by gaseous diffusion between the surrogate phase and the input gas stream was considered as boundary-layer diffusion, as shown in Eq. (4).

$$Ga_2O_3(s) + 2H_2(g) \rightarrow Ga_2O(g) + 2H_2O(g), \quad (2)$$

$$\text{Mass flux} = \delta m h \frac{\delta P}{RT}, \text{ and} \quad (3)$$

$$h \quad D^{\frac{2}{3}} \gamma^{-\frac{1}{6}} \left(\frac{v}{L}\right)^{\frac{1}{2}}, \quad (4)$$

where δm represents the weight changes, h is the mass-transfer coefficient, D is the diffusion coefficient, γ is the kinematic viscosity of mixed gases, ν is the velocity of the gas flow, L is the length of the specimen, and δP is the difference in the partial pressure of the species between the bulk gas and that at the surface of the specimen. Because the same geometry and conditions were used in all of the surrogates samples, the kinematic viscosity of mixed gases and the length of the specimen were constant. Thus, the mass flux should be proportional to the square root of the flow gas velocity for the rate-controlling step (step 2). Neither the weight loss nor the gallium residue in the surrogate depends on the flow rate, ν. Thus, step 2 cannot be a rate-controlling step in the gallium removal from the MOX surrogate below flow rate conditions of 6 cm/s.

Statistical experimental data still are being collected to explore the rate-controlling step between steps 3 and 4. However, based on results to date, in the initial stage of gallium removal or in the case of homogeneous distribution of gallium through the surrogate, step 4 is important because the partial pressure of $Ga_2O(g)$ at the boundary layer will be the driving force for the removal of gallium species from the surface of the surrogate. As removal proceeds, or in the case where gallium segregation is dominate at the grain boundaries (or in the grains), such as a large particle size containing numerous grains, the rate-controlling step is likely to be step 3. The diffusion of gallium species located at the grain boundary of feedstock surrogate/powder to the surface of the sample will be important for the removal of gallium. Therefore, gallium removal is achieved effectively within an hour and then slows down with time. It has been reported that the solubility of cerium and plutonium are similar. Thus, plutonium-based MOX fuel is expected to have the same rate-controlling behavior as discussed above for the CeO_2-based surrogate. If PuO_2 is expected to have the same behavior as CeO_2, then step 3 becomes important, in addition to step 4. This is because the gallium species in the surrogate is more likely to segregate in the grain boundaries, or the gallium species in the powder is more likely to form Ce–Ga–O compounds. Results also indicate that enhancing gallium diffusion through the sample effectively can enhance removal of residual gallium from MOX fuels. Thus, it was observed that weight loss and residual gallium after reduction in Ar–6% H_2 showed a strong dependence on temperature. Temperatures >1200°C may facilitate gallium removal by enhancing the diffusivity and possible decomposition of gallium species in the MOX fuel.

The removal of gallium from PuO_2 and CeO_2 is a matter of not only $Ga_2O(g)$ transport, but also of Ce(Pu)–Ga–O. For more information, see Section 3.2.2 of this report regarding the identification and significance of the perovskite phase.

6.0. CONCLUSIONS

In conclusion, most of the tasks described in the R&D test plan (Ref. 3-1) for FY98 were accomplished. In the area of feed qualification/supply, a feed characterization database was developed, a report was issued detailing the database structure, and efforts to fill the database began. The AUC UO_2 feed material was successfully purchased, although later than planned. PuO_2 inventory requirements were identified, and available sources of PuO_2 feed materials were used when possible. Several new sources of PuO_2 also were identified for future acquisition, including directly oxidized and aqueously purified sources. A draft MD PuO_2 feed specification also was issued. In addition, a characterization plan was developed, sampling was begun, and an initial characterization report was issued for the sampling of various pits and plutonium oxides from stockpiles.

In the area of fuel fabrication development, several studies involving the AUC UO_2 feed material were conducted to provide density and shrinkage data for process development purposes, and a summary report was issued. PuO_2 variability studies were performed, and comparisons were made of the MOX fabricability of several sources of PuO_2 feed material. Additionally, gallium sintering studies took place with surrogate materials to determine the effect gallium has on the sintering process.

Analytical methods were developed in FY98 to provide more accurate analyses for the detection of gallium and to determine the O/M ratio of powders and pellets. Gallium detection studies were enhanced by refining both the MXRF (spatial distribution) technique for bulk gallium concentration in surrogate and prototypic MOX fuel and LIBS, an on-line method for determining trace gallium concentrations in PuO_2 fuel.

Finally, several studies were performed regarding the TIGR system. General studies included the determination of chemistry/physical characteristics and the on-line measurement of gallium. Additionally, process development and prototypic design and testing studies were performed involving parameters such as temperature, time, sample mass, and flow rate. Furnace material compatibility evaluations also were initiated. Cold prototype testing studies involved determining the behavior of gallium in surrogate material.

The results of these studies will provide important technical information for the use of surplus weapons plutonium in fabricating MOX fuel for reactor-based disposition. They will support PuO_2 preparation and analytical improvements directly, as will the procurement process for MOX fuel fabrication and irradiation services and the selected commercial fuel fabricator for implementation of the entire mission. A summary of the FY98 R&D Nuclear Fuels Technologies activities and the status of each are displayed in Table 6-1.

TABLE 6-1. FISCAL YEAR 1998 R&D MILESTONE SUMMARY

Section	Milestone	Scheduled Completion Date	Status
2.2	Complete MD MOX Feed Database Architecture	November 1997	Completed November 1997
2.3	Obtain PuO_2 for R&D and Test Fuel Fabrication	January 1998	Completed; continued as needed
2.3	Obtain AUC UO_2	January 1998	Completed March 1998
2.4	Issue Draft MD PuO_2 Feed Specification	June 1998	Completed January 1998
3.1	Complete AUC UO_2 Baseline Development Plan	November 1997	Completed November 1997
3.1	Complete Baseline Process Development Report	August 1998	Completed September 1998
3.2	Complete Alternate PuO_2 Feed Test Plan	November 1997	Completed November 1997 (included in Baseline Development Plan)
3.3	Issue Gallium Sintering Study Test Plan	December 1997	Completed December 1997
3.3	Issue Gallium Sintering Study Test Report	September 1998	Completed October 1998
4.1	Complete Installation of High-Power X-Ray Tube	May 1998	Completed February 1998
4.1	Complete Installation of Monolithic Capillary	May 1998	Completed March 1998
4.1	Demonstrate MXRF Method for Gallium Detection	September 1998	Completed May 1998
4.3	Complete On-Line LIBS Assessment	December 1997	Completed December 1997
4.3	Demonstrate LIBS in TA-55	July 1998	Completed May 1998
4.3	Calibrate LIBS for Gallium in PuO_2	September 1998	Initial Curve Completed August 1998; work ongoing
4.4	Complete Autoradiography Implementation	September 1998	Completed; Not yet reported

TABLE 6-1. FISCAL YEAR 1998 R&D MILESTONE SUMMARY (cont)

5.0	Issue TIGR R&D Test Plan	January 1998	Completed January 1998
5.1	Issue Surrogate Validity Report	July 1998	Rescheduled to January 1999
5.2	Issue Final Systems Requirement Document	April 1998	Completed April 1998
5.2	Conduct System Design Review	July 1998	Rescheduled to February 1999
6.0	Issue FY97 R&D Summary Report	October 1997	Completed November 1997
6.0	Issue FY98 R&D Test Plan	November 1997	Completed June 1998

7.0. REFERENCES

1-1. D. Alberstein et al., "Nuclear Fuels Technologies Fiscal Year 1998 Research and Development Test Plan," Los Alamos National Laboratory report LA-13461-MS (June 1998).

2-1. P. Chodak III, H. R. Trellue, et al., "Mixed-Oxide Database Architecture (FY98, Task 2.1)," Los Alamos National Laboratory report LA-UR-97-4496 (November 1997).

2-2. D. Alberstein, letter NMD98-064, to Mr. James V. Johnson (October 2, 1998).

3-1. S. L. Eaton et al., "Nuclear Fuels Technologies Fiscal Year 1998 Feed Materials Baseline Development Summary Report," Los Alamos National Laboratory report LA-UR-98-3990 (September 1998).

3-2. R. J. Hanrahan et al., "Nuclear Fuels Technologies Fiscal Year 1998 Fuel Fabrication Development Gallium Sintering Summary Report," Los Alamos National Laboratory report LA-UR-98-4932 (October 1998).

3-3. H. R. Trellue, T. Baros, H.T. Blair, J. J. Buksa, D. P. Butt, K. Chidester, S. F. DeMuth, S. L. Eaton, G. L. Havrilla, R. J. Hanrahan, Jr., C. A. James, D. G. Kolman, R. E. Mason, Y. Park, M. Stan, J. H. Steele, Jr., S. S. Voss, T. C. Wallace Sr., and C. G. Worley, "Nuclear Fuels Technologies Fiscal Year 1997 Research and Development Test Results," Los Alamos National Laboratory report LA-UR-97-4423 (November 1997).

3-4. Y. Park and D. Butt, "The Kinetics of and Atmospheric Effects on Gallium Removal from a CeO_2-Based Surrogate," presented at the 100th Annual Meeting of the American Ceramic Society, Cincinnati, Ohio (1998).

3-5. T. Shishido, Y. Zheng, A. Saito, H. Horiuchi, K. Kudou, S. Okada, and T. Fukuda, *J. Alloys Comp.* **260**, p.88–92 (1997).

4-1. George J. Havrilla, Christopher G. Worley, Jon Schoonover, Roland Schulze, Donald Carpenter, and Patrick Treado, "Spectroscopic Characterization of a MOX Feed Surrogate," Third Topical Meeting on DOE Spent Fuel and Fissile Materials Management, Charleston, South Carolina, September 8, 1998.

4-2. James Rubin, "Evaluation of Analytical Methods for the Determination of the Oxygen-to-Metal Ratio in Mixed Oxide (MOX) Fuels," Los Alamos National Laboratory report LA-UR-98-4199 (September 1998).

4-3. Jean Blaise, Mark Fred (Argonne), and Ralph G. Gutmacher, "The Atomic Spectrum of Plutonium," Argonne National Laboratory report ANL-83-95 (August 1984).

4-4. *The Handbook of Chemistry and Physics*, 79th Ed. (CRC Press, 1998).

4-5. K. Chidester et al., "Nuclear Fuels Technologies Fiscal Year 1999 Research and Development Test Plan," Los Alamos National Laboratory report LA-UR-98-5354, November 1998.

5-1. S. DeMuth, "Nuclear Fuels Technologies Thermally Induced Gallium Removal System (TIGRS) Fiscal Year 1998 Research and Development Test Plan," Los Alamos National Laboratory report LA-UR-98-2023 (June 1998).

5-2. S. DeMuth, "Functional Requirements for Thermally Induced Gallium Removal (TIGR)," Los Alamos National Laboratory report LA-UR-98-2024 (April 1998).

5-3. R. R. Hart et al., "Gallium Interactions with Ga Zircaloy Cladding," Amarillo National Resource Center for Plutonium report ANRCP-1998-5 (1998).

5-4. D. F. Wilson et al., "Interactions of Zircaloy Cladding with Ga: 1998 Midyear Status," Oak Ridge National Laboratory report ORNL/TM-13625 (1998).

5-5. D. P. Butt, Y. S. Park, and T. N. Taylor, "Thermal Vaporization and Deposition of Gallium Oxide in Hydrogen," Los Alamos National Laboratory report LA-UR-98-1868 (1998).

5-6. Y. S. Park, T. N. Taylor, A. Arlette, and D. P. Butt, "The Kinetics of and Atmospheric Effects on Gallium Removal from a CeO_2-Based Mixed Oxide Surrogate," Los Alamos National Laboratory report LA-UR-98-2735 (1998).

5.7. Y. S. Park, D. G. Kolman, C. L. Haertling, and D. P. Butt, "Thermal Removal of Gallium from Weapons Grade Plutonium and Cerium Oxide Surrogate by Thermal Technique," presented at the Materials Research Society Fall meeting, Boston, Massachusetts (September 1998).

5-8. Y. S. Park, D. P. Butt, R. J. Hanrahan, M. S. Stan, T. Wallace Sr., J. C. Huling, C. L. Haertling, D. G. Kolman, and C. A. James, "Thermal Removal of Gallium from Weapons Grade Plutonium Oxide," presented at the American Nuclear Society Third Topical Meeting, DOE Spent Nuclear Fuel and Fissile Materials Management, Charleston, South Carolina (September 1998).

5-9. D. G. Kolman, C. A. James, D. P. Butt, Y. S. Park, M. Stan, B. S. Bender, M. E. Griego, and D. J. Lujan, "Thermally-Induced Gallium Removal from Plutonium Dioxide for MOX Fuel Production," presented at the American Nuclear Society Third Topical Meeting, DOE Spent Nuclear Fuel and Fissile Materials Management, Charleston, South Carolina (September 1998).

5-10. Y. S. Park and D. P. Butt, "The Kinetics of and Atmospheric Effects on Gallium Removal from a CeO_2-Based Surrogate," Los Alamos National Laboratory report LA-UR-98-2018 (1998).

5-11. *The ASM Handbook, Vol. 3, Alloy Phase Diagrams* (ASM International, Materials Park, Ohio, 1992).